UNIVERSITÀ DEGLI STUDI DI GENOVA

SCUOLA POLITECNICA

DIME

Dipartimento di Ingegneria Meccanica, Energetica, Gestionale e dei Trasporti

TESI DI LAUREA MAGISTRALE

IN

INGEGNERIA MECCANICA

Experimental characterization and numerical modelling of leakage flow through heavy-duty gas turbine strip seals

Relatore:

Chiar.^{mo} Prof. Ing. Alessandro Bottaro

Correlatore:

Dott. Ing. Francesco Bavassano

Allievo:

Simone Tubino

Marzo 2023

Caratterizzazione sperimentale e modellazione numerica dei flussi di leakage attraverso strip seal di turbina a gas heavy-duty

Sommario

Nell'ambito della transizione energetica, la tecnologia turbogas assume un'importanza strategica, permettendo di mantenere la stabilità della rete nonostante l'aleatorietà delle fonti energetiche rinnovabili, grazie alla sua flessibilità. Per ottimizzare i consumi e ridurre le emissioni legate a questa tecnologia è fondamentale il suo sviluppo per cercare di migliorarne l'efficienza. Una via possibile consiste nel cercare di ridurre il consumo di Aria Secondaria spillata dalla sezione compressore, senza pregiudicarne gli scopi di raffreddamento delle parti calde. L'oggetto di questa tesi è il miglioramento di un sistema di tenuta tra le singole pale turbina statoriche adiacenti, il quale permette di ridurre i trafilamenti (leakage) dal Sistema Aria Secondaria ai gas caldi che espandono nel canale principale della sezione turbina. Tali trafilamenti causano un calo di potenza ed efficienza della macchina, in quanto quelle portate d'aria ad alta entalpìa non espandono completamente in turbina e non partecipano alla combustione. Inoltre, essi non hanno una funzione specifica di raffreddamento ma sono, appunto, flussi parassiti, inevitabili tra parti metalliche ove siano presenti giochi seppur minimi e anche in presenza di contatto stretto tra esse; ciò a causa, ad esempio, della rugosità superficiale e della non perfetta planarità del contatto. Questi leakage sono quindi i perfetti candidati ad essere ridotti e da decenni lo sviluppo dei turbogas si dedica anche a tale scopo. Per questa tesi, svolta in collaborazione con Ansaldo Energia, è stata effettuata una campagna sperimentale in laboratorio su una nuova tipologia di tenuta a lamina per le pale statoriche in associazione a estensivi calcoli svolti con una rete fluida monodimensionale a parametri concentrati nell'ottica dello sviluppo tecnologico della turbina a gas AE94.3A. Sono poi discussi i risultati in termini di caratteristiche di flusso e di benefici prestazionali.

Experimental characterization and numerical modelling of leakage flow through heavy duty gas turbine strip seals

Abstract

In the context of energy transition, gas-turbine technology assumes a strategic relevance, allowing to keep grid stability nevertheless renewables sources randomness, thanks to its flexibility. In order to optimize fuel consumption and reduce the emissions related to the present technology it is crucial to develop it to improve its efficiency. A possible way consists on Secondary Air consumption reduction spilled from compressor section without affect the hot-gas parts cooling purpose. The present thesis object is the improvement of a sealing system between each contiguous turbine stator blades, which allows to reduce leakages from Secondary Air System to hot-gas which expand in turbine section main channel. Mentioned leakages produce power and efficiency drop of the engine, because that mass flows with high enthalpy do not expand completely in the turbine and do not participate to combustion. Moreover, they do not have any particular function but they are, as said, parasitic fluxed, unavoidable between metallic parts where clearances, even minimum, are detected, also when a close contact between them is verified; this can be ascribed, for example, to surface roughness and not perfect contact planarity. These leakages are the perfect candidates to be reduced and for decades gas-turbine development dedicates also to this aim. For the present thesis, made in collaboration with Ansaldo Energia, a laboratory test campaign has been made on a new foil between stator blades, together to extensive calculus made with a one-dimensional fluid network with concentrated parameters in the context of AE94.3A technological development. Results in terms of flux characteristic and performance benefits are then discussed.

Ringraziamenti

Ci tengo a ringraziare innanzitutto il Prof. Alessandro Bottaro, che mi ha seguito per cercare di darmi la migliore opportunità possibile per svolgere la presente tesi in un'azienda d'alto profilo quale Ansaldo Energia.

Ringrazio poi Francesco Bavassano, team leader del Sistema Aria Secondaria, che è stato di grande ispirazione e supporto grazie alla sua notevole conoscenza nell'ambito di Aria Secondaria delle turbine a gas. Ci tengo a specificare il suo notevole sostegno ed aiuto nonostante gli innumerevoli impegni e progetti che richiedono la sua assistenza.

Ringrazio Elena Pestelli, l'altro membro del team, che mi ha aiutato ad entrare nel merito di dettagli che non sarei mai riuscito a cogliere e capire senza la sua guida. Ringrazio entrambi poi per la pazienza avuta nei miei confronti, in particolare nel formarmi per un lungo periodo e risolvere i mei dubbi e curiosità legati a questo interessante ambito, oltre che avermi fatto sentire parte del team.

Ringrazio Matteo, un'amicizia ritrovata con l'università, con cui abbiamo condiviso molteplici attività incluso il tirocinio nella medesima compagnia, per l'appoggio che mi ha dato in merito ai miei dubbi in un po' tutti gli ambiti, anche esulanti da quelli prettamente universitari.

Ringrazio Sebastian e Gian Mario, con cui ho condiviso il percorso universitario e che mi hanno sempre supportato e spronato anche nei momenti di maggiori incertezze e difficoltà e che si dimostrano sempre più presenti nonostante le difficoltà che ci sono nel tenersi in contatto.

Ringrazio poi tutti Denise, Riccardo, Alessio, Noemi, Andrea e Luca, che sono sempre stati presenti e che mi hanno spronato sempre a fare scelte ponderate e a staccare nei momenti di necessità.

Ringrazio infine la mia famiglia, che nonostante le difficoltà affrontate, non hanno mai avuto dubbi nel non farmi mancare niente per potermi permettere di inseguire i miei sogni e sono sempre stati pronti a supportami in ogni modo possibile.

Index

1 Introduction

The present thesis is made in collaboration with Ansaldo Energia, a company leader in power generation technologies. Ansaldo Energia Group can supply components (gas turbines, steam turbines, generators), turnkey plants and the most innovative support service solutions to the electricity generation market. It is also active in the nuclear sector - from fusion to waste management - and supports its customers in the delicate phase of energy transition with green products and innovative storage solutions.
For what concerns the gas turbine sector, Ansaldo Energia offers E-, F- and H-class heavy-duty gas turbines with output ranging from 80 to 538 MW (ISO Power) for Open Cycle, from 120 to 760 MW for Combined Cycle and Combined Heat and Power applications.
The present thesis is focused the "AE94.3A", which is the biggest Ansaldo Energia's gas turbine from former Siemens' license derivation, which is an F- class with about 300 MW output power with high efficiency.
The core argument of the present document is the Secondary Air System (SAS) analysis with a particular focus on the sealing technology which will be discussed in the next chapters. The current seal strips which are adopted to seal the stator interfaces will be compared with an upgraded version with thinner and more flexible elements than the ones nowadays adopted.
The Secondary Air System has the objective to preserve the integrity of gas turbine's components, which are operated at high temperature and pressure. It can happen because of two reasons: if they are not cooled enough or if the hot-gas exits from the main channel and it goes where it is not prevented. The air saving is fundamental because it means that more air can go in the combustion chamber; in addition, it has to be ensured the fast start-up and high temperature to reach high efficiency and output power. If Secondary Air consumption rises too much, it can generate combustion instability, because not enough air enters in the combustion chamber. A lower air quantity available for the combustion induces high flame and turbine inlet temperature, producing a high level of NO_X. With this brief discussion, it is evident that the main objective of the Secondary Air System upgrades is to reduce the air consumption, without renounce to cooling and sealing. In order catch the presented objectives, it is crucial to gain effectiveness on the cavities (to avoid hot-gas ingestions), improve sealing performance (to avoid the Secondary Air leakages) and the coolant effect on the hot-parts.
The main sealing technology analyzed in the present document consists of many seals positioned in different axial and radial locations, named "*strip seal*". This kind of seal is a particular component that separates the plenum that contains the cooling and sealing air from the turbine main flow channel, and they are positioned to grant the sealing between stator-stator parts. Their performance will be analyzed in the present document with an experimental test campaign.
In order to make calculus easier, Ansaldo Energia implemented a property 1D tool, named SiX_o. The presented software is calibrated with CFD results, field data and experimental results. The Secondary Air savings for each SAS upgrade will be estimated in the initial analysis with this simplified model, in order to understand its benefits.

1.1 Thesis scope

The scope of this thesis is summarized in the present section.

- New and worn, thick (actual) and thin (upgrade) *strip seals* characterization in different conditions via experimental campaign.
- Construction of correlations which mathematically describe the strip seals behavior.
- Ansaldo Energia's 1D fluid network tool calibration with experimental results.
- Ansaldo Energia's 1D fluid network tool improvement via finer modelling.
- Evaluation of the improvement brought by thin strip seal adoption as compared to thick ones.

1.2 Ansaldo Energia

Ansaldo Energia is a company leader on the energy systems' sector. Its mission is to be always committed to a sustainable and innovative power generation with the aim to ensure a lower environmental impact and a high flexibility in energy production.

The Ansaldo Energia's history starts a long time ago, when Giovanni Ansaldo & Co. was born, in 1863; initially it was a locomotive producer but in 1923, it built its first power plant. The company changed the name in 1991, and it began producing gas turbines under Siemens' license, by which derives the current AE engine series; since 2005 the company gained its technological independence and started to design its own machines. In 2016, with the acquisition of Alstom Power, Ansaldo gained extended its product portfolio and know-how and, in 2020 the first GT36 engine, the most powerful and efficient gas turbine ever produced in Italy, was sold.

In its portfolio it has heavy-duty gas turbines, steam turbines and generators; moreover, it provides to its customer entire power plants, and it ensures also the maintenance with the service offer. The company has headquarters in Italy, but also it has an international presence: in China with the two joint ventures Ansaldo Gas Turbine Technology and Shanghai Electric Gas Turbine, in Switzerland, in the United Kingdom with Ansaldo Nuclear Ltd, and in the United Arab Emirates (Abu Dhabi). The broad-based presence allows the group to quickly react to customers' needs and to better offer them its rich value proposition.

Heavy-duty gas turbines represent the company's core business, and it is committed to ensure to the customers the best solution in terms of performance, flexibility and reliability with low environmental impact. Ansaldo Energia also designs and supplies full Power Plants with all the components needed and a full set of advanced, sustainable technical solutions that include the ability to burn hydrogen in the fuel mix. Once the plant is in operation, Ansaldo Energia can ensure all maintenance and repair activities; the existing power plants can be upgraded with the latest technologies to improve sustainability and efficiency.

The company has included in its priority goals a leading role in the green revolution, even going so far as to create a new company dedicated to it (Ansaldo Energia Green Tech) that is already working to help energy producers and users to integrate hydrogen and energy storage into existing facilities [1].

1.2.1 The AE94.3A

The present document is focused on the Ansaldo Energia's AE engines, in particular the main focus in on the AE94.3A (F-class, shown in Figure 1.1). This gas turbine is able to operate in both the typical GT configurations: simple or combined cycle.

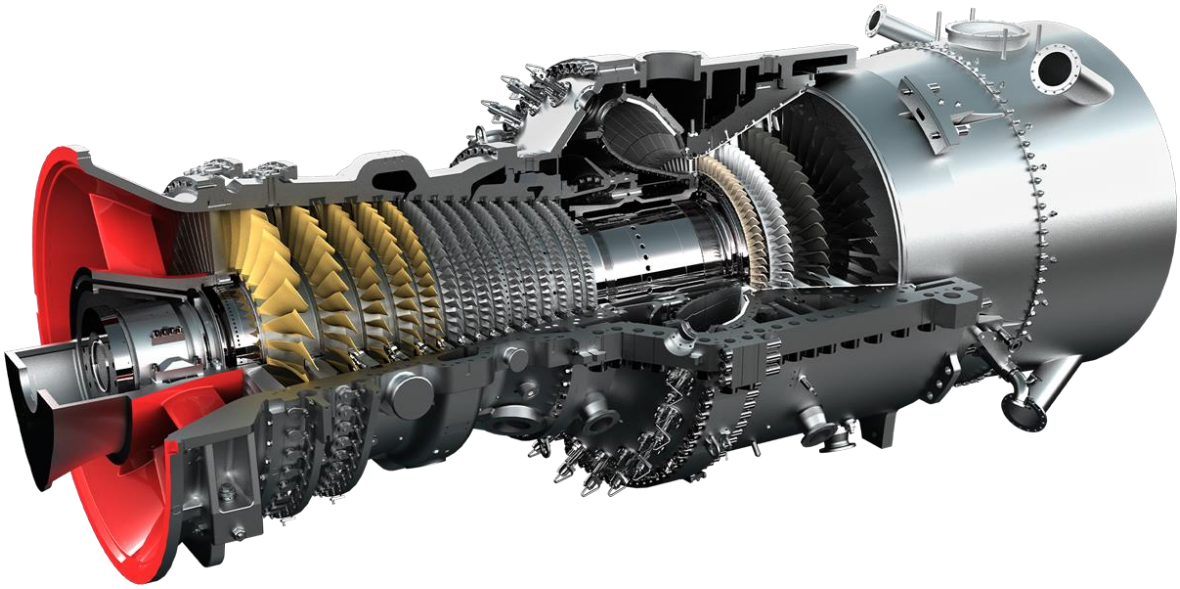

Figure 1.1 - Gas Turbine: AE94.3A [1]

The engine is characterized by a high flexibility thanks to the reduced MEL and the high design net power; the MEL reduction is currently one of the most important objectives for the gas turbine because it permits to the engine to stay on the grid with a very low load, thus the engine is ready to rapidly cover a larger peak request without spending too much fuel in the waiting. This kind of operation is rewarded by the electricity market.

In the AE series, the engine does not use a "one piece" shaft, but the rotor is composed by many disks which are connected each other with a particular configuration of contact surfaces between those components to be coupled and the *tie-rod* ensures the stacking. Inside the rotor there are secondary air paths that cool (or warm at the start-up) the rotor parts and the turbine blades, the stator parts are cooled with the stator lines, which pass via pipelines outside the engine casings, connecting the compressor to the turbine section

Thanks to the annular combustion chamber a good temperature distribution at the turbine inlet is there. This combustion chamber is also able to burn different fuels: natural gas, oil or a blend of natural gas and hydrogen in dry premixed mode. Thanks to the flame technology adopted, which is dry premixed, the emissions are very low, and they get reduced even more thanks to recent updates. Nowadays NO_X levels are down to 15 ppm for dry gas mode and 60 ppm for dry oil mode. To reach out to the customers the engine maintenance strategies were changed to make this kind of operations easier and cheaper with extended time between the major overhauls, high durability of hot gas path parts and on-site activities.

In addition, this GT has also some advanced control systems which grant self-adjustment capability, by adapting itself to the natural gas composition also with hydrogen percentage variation (up to 40%); this means that quick and reliable fuel change over between liquid and gaseous fuels and vice versa are available as well. There are also systems that can pre-

heat or cool the inlet air in order to reduce the minimum environmental load and keep the engine ready to support the grid.

These precautions and updates gave as results a high level of reliability and high cycling capability; more over the engine is almost always ready to ensure power to the grid since the start up time is approximatively 20 minutes [1].

In the following part the performance levels will be resumed. First of all, below the simple cycle performance are reported.

Table 1.1 - AE94.3A plate data

Gross GT power output	340	[MW]
Gross GT efficiency	40.3	[%]
GT exhaust mass flow	755	[kg/s]
GT exhaust temperature	593	[°C]
GT minimum load	40	[%]

Instead, for the optimized combined cycle the performances are reported in the table below.

Table 1.2 - AE94.3A combined power plant plate data

Power plant configuration	**1+1**	**2+1**	
Net power plant output	495	992	[MW]
Net power plant efficiency	60	60.3	[%]
Net power plant heat rate	5995	5970	[kJ/kWh]
Power plant turndown minimum load	45	25	[%]

1.3 Gas turbines for energy production

The gas turbines are machines that can produce power by using the Brayton-Joule cycle and their working fluid is air. The power produced can be used in different ways, in fact it can be made a distinction between different classifications of this kind of engine: heavy-duty, aero-derivative and aeronautical [2]. The first two are land-based and used to produce power for the electricity grid, in a classic power plant, the third one is used on the planes to generate the thrust for the plane flight. The design criteria are different between the different machines, in function of the aim of the project:

- Heavy-duty turbines: they are the most common and, in general, the biggest gas turbines because the main focus is to get high power and efficiency to feed the energy market requests.
- Aeronautical turbines: in this kind of engines a nozzle to increase the air's momentum is installed, moreover they are smaller than the previous ones, this is due to the different objective of the project, in fact the principal focus in this kind of engines is to reduce their weight and improve their efficiency, objective that can match with a higher pay-load in the flight business.
- Aero-derivates turbines: they are engines that have the same structure of the previous ones, but instead the nozzle which generates the thrust it is substituted with the "*power turbine*": this component converts the pressure into work at the shaft of air momentum. The advantage of this kind of gas turbine is that the "core" can run at

different rotational velocity with respect to the power turbine, which must rotate at the same frequency of the grid.

The gas turbines used "on land" (heavy duty and aero-derivative) are often equipped with a heat recovery system, named "*Heat Recovery Steam Generator (HRSG)*", to save the residual heat, at a too low pressure to be expanded, but hot enough to generate steam and expand it in a bottoming cycle to generate more power. With the mentioned component (HRSG) it is possible to generate steam as a classic steam cycle. For this kind of engine more than one category exists, in fact the gas turbines can be classified in function of the technology level and engine size; the most relevant classes with their most well-known commercial classification are reported as follow:

- E-class: this class is the less efficient on the market and it is characterized by the smaller output power, but it usually ensures more robustness and flexibility than other engines.
- F-class: this gas turbines' class identify high performance engines, with the aim to grant a good balance between the power production and the flexibility; this class is characterized by engines with a high output power combined with high flexibility and reliability.
- H-class: this is the highest class, the gas turbines which are part of it are the most powerful and efficient, but it is characterized by higher costs and more complex technical solutions; the engine in this case reach an output power over 500 MW.

The main advantage of the gas turbines is the flexibility with which they can be operated, and this aspect is now more important than ever; in fact, nowadays the energy power production can vary a lot, since the renewable sources have the priority of dispatching on the grid. Because of this consideration, the gas turbines production varies a lot during the day, in according with the daytime and the weather, which affect the renewables production. With their high flexibility the gas turbines can cover the energy request in matter of minutes, with a fast start-up and ramp-up, thus they grant the grid stability with a minimum grid frequency variation. Moreover, as wide is the power range where the engine can work, as greater is the flexibility that characterizes the engine: the minimum power level granted by the gas turbine is the MEL (Minimum Environmental Load), related to the law emissions limits, and the maximum is commonly named BL (Base Load). To ensure a faster start-up and ramp-up it is crucial to develop the Secondary Air System to avoid high stresses due to the fast deformations during the power rise. In fact, during the start-up the temperature is low, and it rise rapidly as consequence of that higher stresses are detected in this moment because of temperature gradient in the engine components. The start-up can be faster if the thermal stresses are low, so if the engine can be heated uniformly. This can be obtained with SAS, which drives the air along the whole engine and contributes to warming as uniformly as possible the stator and rotor components. If SAS does not provide it the same start-up time affects significantly its operating life.
Since in the future there will be, expectably, more renewables power plants, this kind of engine need to gain more flexibility hopefully without engine usage increase.

This kind of engines produce a certain quantity of pollutant emissions (carbon monoxide, Nitrogen oxides, …), and CO2 but a significant reduction can be obtained by using improved combustor technologies and other fuels such as hydrogen (potentially zero emissions in the future), but also, they can keep the stability and avoid the black-out risk. At the moment the

gas turbines already have low emissions if compared with other technologies and this is thanks to the fuel adopted and to the high efficiency too. In fact, an efficiency improvement can reduce fuel consumption and still grant the same power. In addition, particular type of burning flame is utilized in order to try to also reduce the other particles, such as NO_X and CO; in particular, the flame adopted in this kind of engines is typically dry premixed. Dry means that the flame does not consume water in the combustion chamber, premixed means that the reagents are premixed before the combustion chamber inlet.
With the objective to use the gas turbine to stabilize the grid in the next future, it is vital to avoid the emissions that still there are at the moment, thus it is necessary that the new fuels will be produced with renewables sources. The main focus at the moment is condensed on the hydrogen and the capability of the engines to burn this particular molecule at the moment is significantly high, more than what the system can provide. To confirm this, at the moment the most of gas turbines are able to burn natural gas mixed with a certain percentage of hydrogen, up to 40% if the AE94.3A is considered, with the objective to burn the 100% in the next future. Despite the ambitions, there are some complications, related to the difficulties control the flame: in fact, because of its low molar mass, the flame is really fast. As consequence of what just said, the fuel has to entry in the combustion chamber faster than now to ensure that the flame velocity is equal to the reagents' velocity with the objective to keep the flame fixed in the space and thus to avoid the flashback risk; the velocity increase generates a pressure losses increase and to keep the flame fixed the air has to be faster than ever in the gas turbines, thus it can be difficult to keep the flame alive .
One more reason which make more over important this technology is the high efficiency, especially on combined cycles, which can reach an efficiency around 64% nowadays.
Standing the current technology development, it is hard to increase even by a fraction of a percentage point; this difficulty is due to the Carnot cycle efficiency limit, in fact the technology is remarkably close to it and to improve a fraction of efficiency percentage the attention has to be focused on the details.

1.3.1 Basic gas turbine cycle

The Brayton-Joule cycle is composed by 4 thermodynamic transformations:

- compression,
- combustion,
- expansion,
- atmospheric discharge.

The ideal-cycle is reported below:

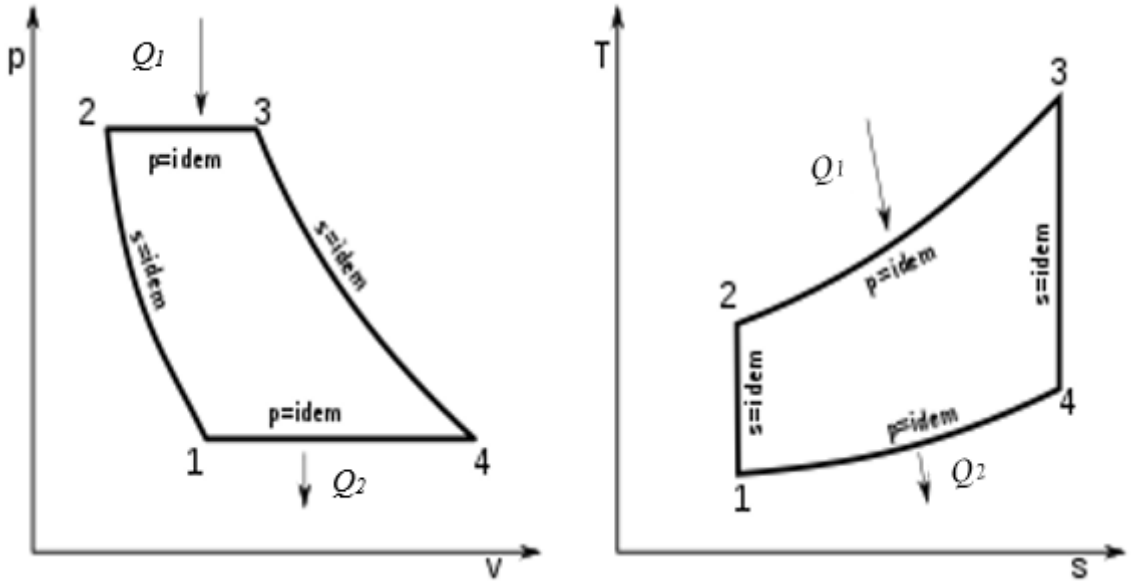

Figure 1.2 - Joule-Brayton ideal cycle [2]

In the figure above the four thermodynamic transformations which describes the Joule-Brayton cycle are represented:

- 1-2: adiabatic compression.
- 2-3: isobaric combustion.
- 3-4: adiabatic expansion.
- 4-1: isobaric discharge.

In the reality the latter transformation mentioned is not detectable in the engine since the operative cycle isn't closed, but the working fluid is captured constantly from the ambient and it doesn't come from the expansion exit; for this reason, it can be said that the transformation 4-1 is an isobaric discharge of the working fluid in the atmosphere. To save the remaining heat at the point 4 often it's introduced the steam bottoming cycle already cited some lines above [2].

The cycle's components are reported in the picture below:

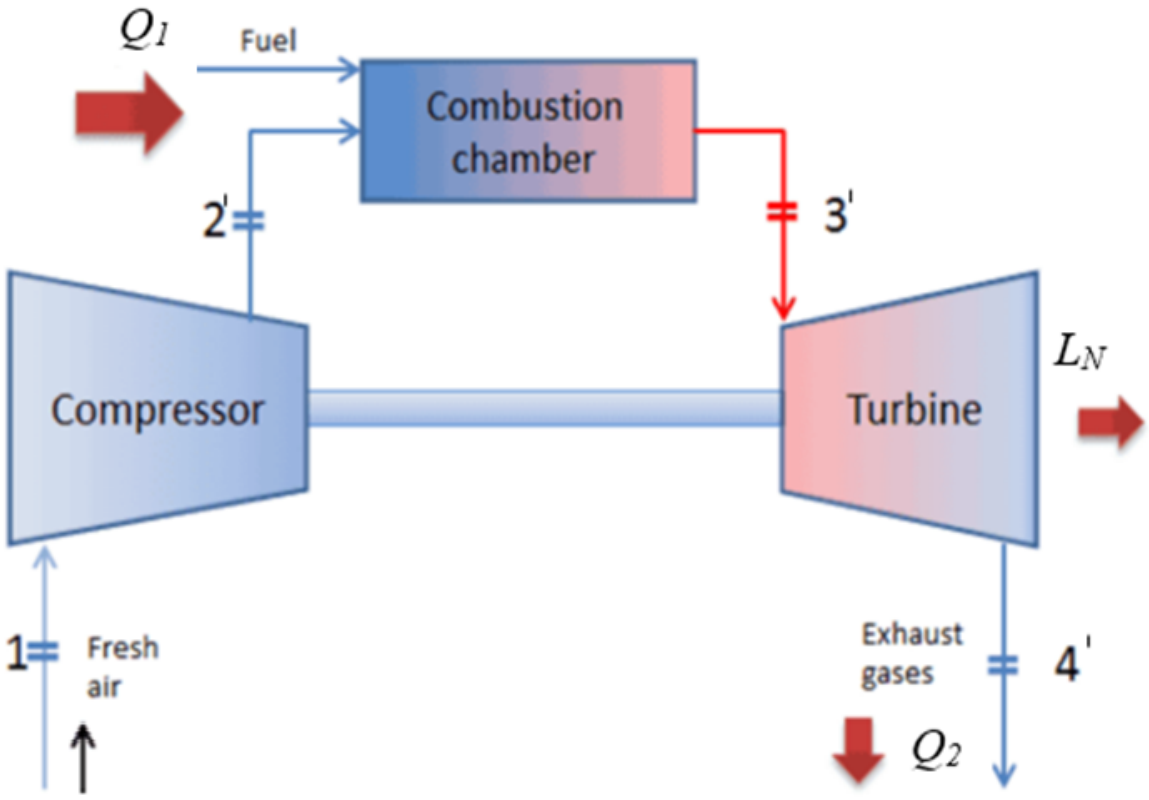

Figure 1.3 – Joule-Brayton cycle's components

The transformations that can be seen in the Figure 1.2 are achieved by the components shown in the Figure 1.3 and below they are reported:

- Compressor.
- Combustor.
- Turbine.

The air flow entries at point 1 and then it will be compressed with a specified pressure ratio, following there is the combustion chamber, where the temperature increase until the maximum admitted by the cooling technology adopted. Finally, there is the turbine which is connected with the shaft at the compressor; a portion of the work extract from the turbine goes at the compressor, the remaining part is named "*network*" (L_N) and it is the output of the system. To convert the work at the shaft into power to feed the grid the shaft is connected to a generator. As it is requested from the grid, whole the gas turbines have to rotate at 3000 [rpm] to keep the grid approximatively at 50 [Hz].

First of all, let us determine the efficiency of the ideal cycle and it can be derived from the first principle, so it can be write as below reported:

$$\eta = \frac{L_N}{Q_1} \tag{1.1}$$

$$= \frac{Q_1 - Q_2}{Q_1} = \frac{C_p(T_3 - T_2) - c_p(T_4 - T_1)}{c_p(T_3 - T_2)} =$$

$$= \frac{(T_3 - T_2) - (T_4 - T_1)}{T_3 - T_2} = 1 - \frac{T_4 - T_1}{T_3 - T_2} =$$

$$\eta = 1 - \frac{T_1\left(\frac{T_4}{T_1} - 1\right)}{T_2\left(\frac{T_3}{T_2} - 1\right)} \tag{1.2}$$

Then, noted the adiabatic transformations 1-2 and 3-4, the temperature ratio may be written as:

$$\frac{T_4}{T_3} = \left(\frac{p_4}{p_3}\right)^{\frac{k-1}{k}} \tag{1.3}$$

$$\frac{T_1}{T_2} = \left(\frac{p_1}{p_2}\right)^{\frac{k-1}{k}} \tag{1.4}$$

Now, by defining the pressure ratio as β and φ the exponent of the (1.2) and (1.3), and by supposing neglectable the pressure losses in the combustion chamber, we can write the relations below reported:

$$\beta := \frac{p_2}{p_1} = \frac{p_3}{p_4} \tag{1.5}$$

$$\varphi := \frac{k-1}{k} \tag{1.6}$$

$$\beta^{\varphi} = \frac{T_2}{T_1} = \frac{T_3}{T_4} \tag{1.7}$$

Then, by the (1.7) we can immediately see the following relation:

$$\frac{T_4}{T_1} = \frac{T_3}{T_2} \tag{1.8}$$

Now, by using the previous described relations, the ideal cycle efficiency will be:

$$\eta = 1 - \frac{T_1}{T_2} = 1 - \frac{1}{\beta^{\varphi}} \tag{1.9}$$

The last relation shows that the ideal efficiency η strikes 1 when the pressure ratio β strives ∞. Now to understand what is the output of the system let us calculate the net work L_N by starting from the (1.1):

$$\eta = \frac{L_N}{Q_1} \tag{1.1}$$

$$L_N = \eta * Q_1 =$$

$$= \left(1 - \frac{1}{\beta^{\varphi}}\right) * C_p * (T_3 - T_2)$$

$$= \left(1 - \frac{1}{\beta^{\varphi}}\right) * C_p * T_1 * \left(\frac{T_3}{T_1} - \frac{T_2}{T_1}\right)$$

$$L_N = \left(1 - \frac{1}{\beta^{\varphi}}\right) * C_p * T_1 * \left(\frac{T_3}{T_1} - \beta^{\varphi}\right) \tag{1.10}$$

From the (1.10) it can be seen that for a fixed T_1 the net work depends by the maximum temperature T_3 and the pressure ratio β: if the maximum temperature increases the net work also increases for the linear dependence with T_3 but something different happens if the pressure ratio is considered, in fact L_N is 0 when $\beta = 1$ or $\beta^{\varphi} = \frac{T_3}{T_1}$ and, since $\beta = \left(\frac{T_2}{T_1}\right)^{-\varphi}$, this means that there isn't any heating contribution in the transformation 2-3. In addition, it can be found the pressure value which ensures the maximum net work by deriving the (1.10); the passages are shown following:

$$\frac{\partial L_N}{\partial \beta} = 0 \tag{1.12}$$

$$-\varphi * (-\beta^{-\varphi-1}) * \left(\frac{T_3}{T_1} - \beta^{\varphi}\right) + (1 - \beta^{-\varphi}) * \varphi * (-\beta^{\varphi-1}) = 0$$

$$\frac{T_3}{T_1} * \beta^{-\varphi-1} - \beta^{-1} - \beta^{\varphi-1} + \beta^{-1} = 0$$

$$\frac{T_3}{T_1} * \beta^{-\varphi} = \beta^{\varphi}$$

$$\beta_{opt}^{\varphi} = \sqrt{\frac{T_3}{T_1}} \tag{1.13}$$

Thus, remembering the (1.8), the maximum work condition is:

$$T_2 = T_4 = \sqrt{T_3 * T_1} \tag{1.14}$$

These three work conditions analyzed are reported in the picture below:

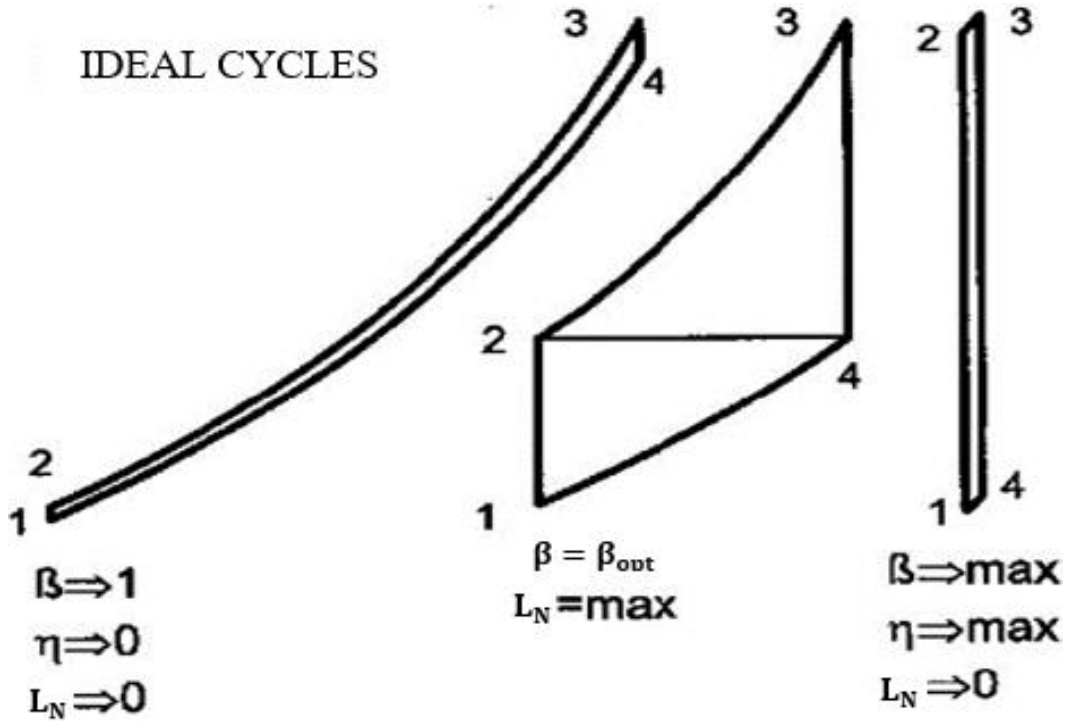

Figure 1.4 – Ideal Joule-Brayton cycles [20]

As in can be seen in the picture above the two conditions in which the net work is neglectable are characterized by an infinitesimal cycle's area, instead the maximum net work condition is characterized by the biggest cycle's area as possible, condition which is verified when the pressure ratio is optimal ($\beta = \beta_{opt}$). Below a picture with the efficiency and net work behavior is reported.

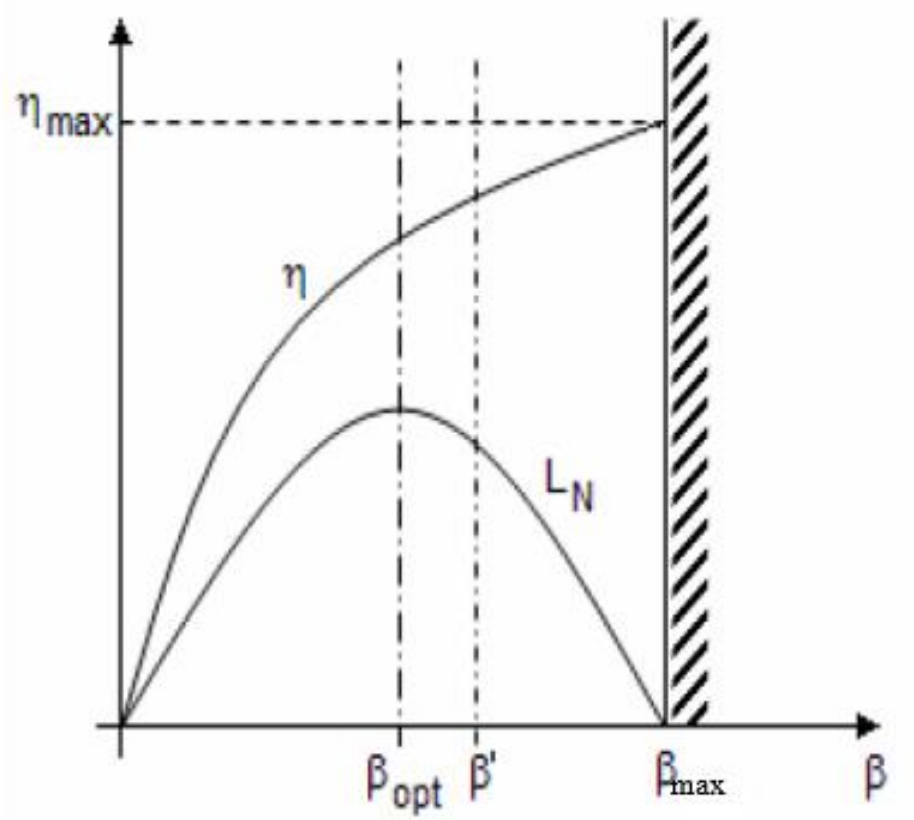

Figure 1.5 – net work and efficiency behavior [20]

In Figure 1.5 it is shown the behavior of the mentioned quantities versus β, as it was previously described.

The whole discussion just reported refers to the ideal cycle, but if the real cycle is considered the efficiency formulation changes. The engine's components are not able to make an ideal transformation, instead they increase also the entropy because of the irreversibility that the air experiments; thus, in the real case, the compression and expansion transformations won't be considered iso-entropic, and it will be introduced the iso-entropic efficiency for each element. In addition, there are pressure losses the combustion chamber that are not neglectable, but this particular will not be faced in the present document. The real cycle is reported in the picture below.

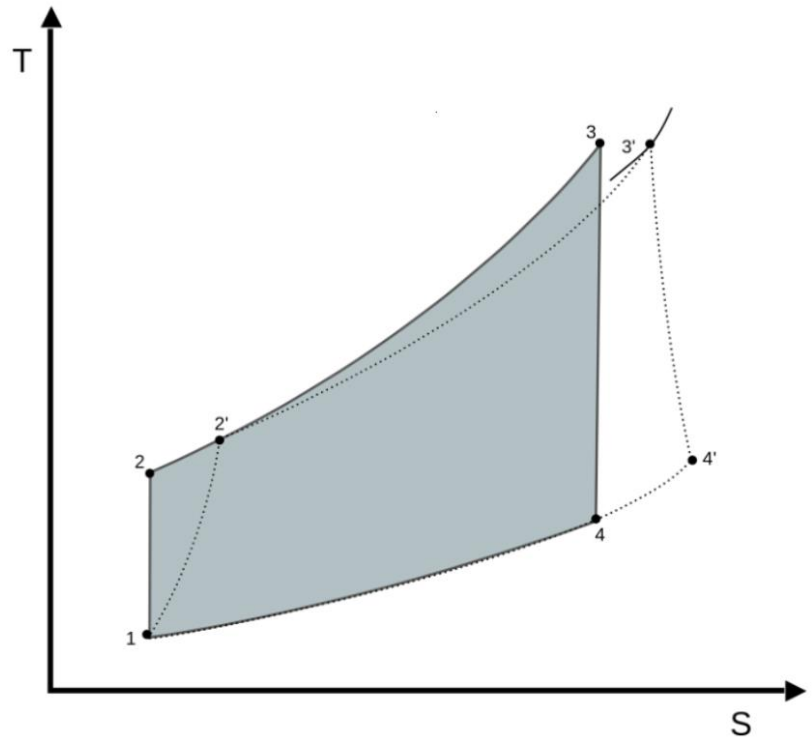

Figure 1.6 – Real Joule-Brayton cycle [21]

Figure 1.6 shows that the transformations in the real case change a little bit, in fact many irreversibilities are detected:

- The compression (1-2') is characterized by an increase of entropy and temperature compared to the ideal case, problems such as the friction generate an additional temperature jump, thus $T_{2'} > T_2$;
- The combustion (2'-3') shows the temperature increase but also a pressure reduction, due to the hot and cold losses. The pressure reduction ensures that with the same fuel mass flow the temperature reached is lower than the ideal case, consequently, to reach the same temperature $T_3 = T_{3'}$ more fuel is needed, even if the combustion starts at a higher temperature
- The expansion (3'-4') has the pressure constrained because the inlet pressure is the pressure at the outlet of the combustion chamber and the ambient constrains $p_4 = p_{4'} = p_{amb}$. Because of this, pressure jump is smaller and real outlet temperature is higher than the ideal cycle.

After this brief introduction to the real cycle let us consider the iso-entropic efficiency, this kind of efficiency is defined in two different ways, one for the turbine and one for the compressor. To define them it was made a hypothesis which consists of the neglect pressure losses in the combustion chamber: this means that the point *three* coincides with *3'*.

$$\eta_c = \frac{h_2 - h_1}{h_{2'} - h_1} = \frac{L_{c,ideal}}{L_{c,real}} \tag{1.15}$$

$$\eta_t = \frac{h_3 - h_{4'}}{h_3 - h_4} = \frac{L_{t,real}}{L_{t,ideal}} \tag{1.16}$$

Now it can be written the net work as $L_N = L_{t,real} - L_{c,real}$ and thus the (1.1) can be re-written for the real cycle and the passages are following reported.

$$\eta_{real} = \frac{L_N}{Q_1} \tag{1.1}$$

$$\eta_{real} = \frac{\eta_t * (h_3 - h_4) - \frac{h_2 - h_1}{\eta_c}}{h_3 - h_{2\prime}}$$

Now if it is considered $h = C_p * T$ it can be written and supposing C_p constant:

$$\eta_{real} = \frac{\eta_t * C_p * (T_3 - T_4) - c_P * \frac{T_2 - T_1}{\eta_c}}{C_p * (T_3 - T_{2\prime})}$$

$$\eta_{real} = \frac{\eta_t * T_3 * \left(1 - \frac{T_4}{T_3}\right) - T_1 * \frac{\frac{T_2}{T_1} - 1}{\eta_c}}{T_1 * (\frac{T_3}{T_1} - \frac{T_{2\prime}}{T_1})} \tag{1.18}$$

If the (1.7) is replaced in the (1.18) and if the term $\frac{T_{2\prime}}{T_1}$ is re-written in function of the compressor efficiency with the following passages:

$$\eta_c = \frac{h_2 - h_1}{h_{2\prime} - h_1} = \frac{C_p * (T_2 - T_1)}{C_p * (T_{2\prime} - T_1)} = \frac{\frac{T_2}{T_1} - 1}{\frac{T_{2\prime}}{T_1} - 1}$$

$$\frac{T_{2\prime}}{T_1} = \frac{\frac{T_2}{T_1} - 1}{\eta_c} + 1 \tag{1.19}$$

Thus the (1.18) can be written as follow:

$$\eta_{real} = \frac{\eta_t * \frac{T_3}{T_1} * \left(1 - \frac{T_4}{T_3}\right) - \frac{\frac{T_2}{T_1} - 1}{\eta_c}}{\frac{T_3}{T_1} - \frac{\frac{T_2}{T_1} - 1}{\eta_c} - 1}$$

$$\eta_{real} = \frac{\eta_t * \frac{T_3}{T_1} * (1 - \beta^{-\varphi}) - \frac{\beta^{\varphi} - 1}{\eta_c}}{\frac{T_3}{T_1} - \frac{\beta^{\varphi} - 1}{\eta_c} - 1} \tag{1.20}$$

The last formulation describes the efficiency that characterizes the real Joule-Brayton cycle, and it depends by the pressure ratio β, the temperature ratio $\frac{T_3}{T_1}$ and the compressor and turbine's iso-entropic efficiency η_c and η_t. In particular the (1.20) is a function characterized by a maximum for a specific β: the pressure ratio value that maximizes the efficiency is

related to the temperature ratio $\frac{T_3}{T_1}$, in fact if it increases the pressure ratio for which η_{real} is maximum is higher and also the maximum value of η_{real}; in addition also if the iso-entropic efficiencies increase also the η_{real} and β increase. Following a chart that explains this discussion is reported.

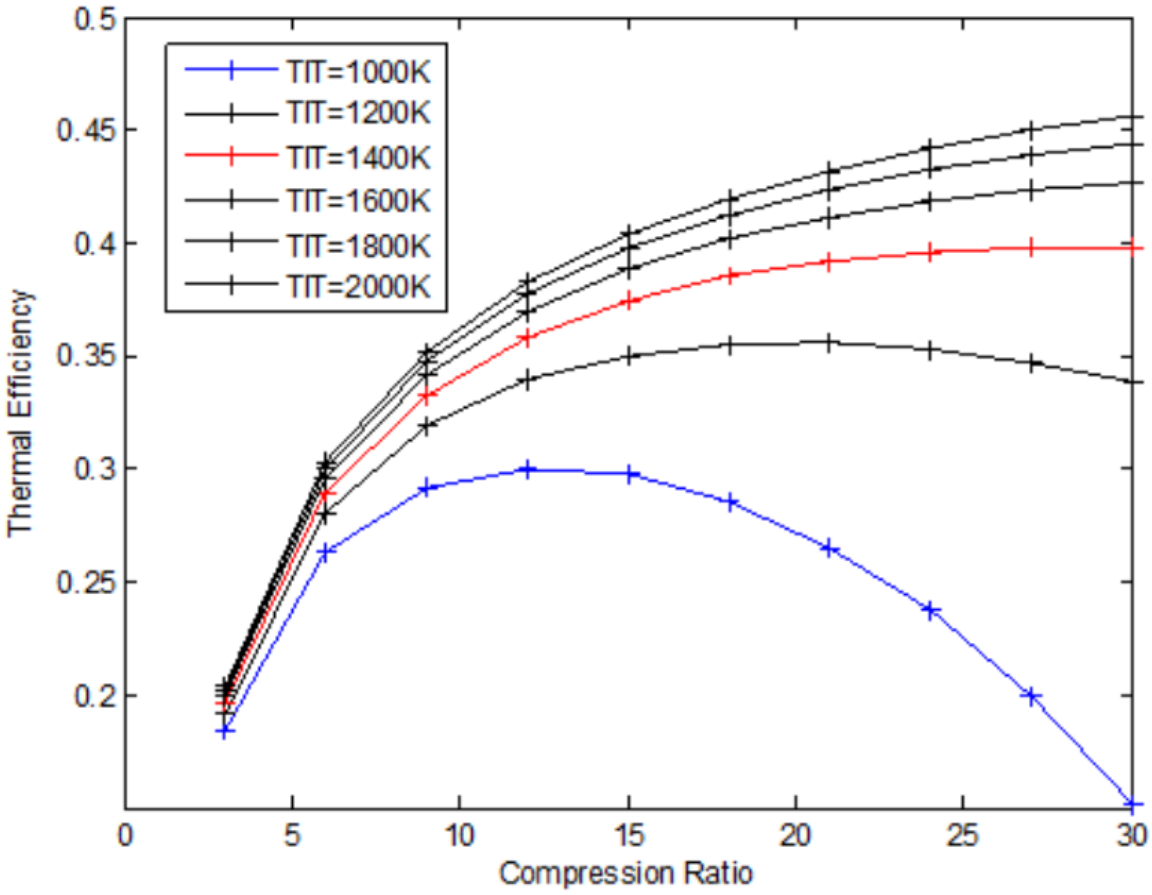

Figure 1.7 - η_{real} vs β with different temperature [22]

In Figure 1.7 the η_{real} is reported as function of the β, with fixed ambient temperature T_1; in the chart the temperature ratio increase is shown with the turbine inlet temperature (TIT). As it was said about the equation (1.20) the maximum value of η_{real} increases if the temperature ratio increases too and to catch the maximum η_{real} it is needed a higher pressure ratio β. An important observation consists of the asymptotic trend which describes the η_{real} curves for high TIT (or temperature ratio) values, in fact, for high temperature ratio when it strives ∞ the formulation (1.20) will be simplified, and it will correspond with the (1.9).

With what was just obtained it is possible to estimate the net work in the real case, in fact it was only introduced in the previous discussion, but it was not analyzed, thus let us consider the equations (1.15) and (1.16) to determine it.

$$L_N = \eta_t * (h_3 - h_4) - \frac{h_2 - h_1}{\eta_c} \qquad (1.21)$$

$$L_N = C_p * \left[\eta_t(T_3 - T_4) - \frac{T_2 - T_1}{\eta_c}\right]$$

$$L_N = C_p * \left[\eta_t * T_3 * \left(1 - \frac{T_4}{T_3}\right) - T_1 * \frac{\frac{T_2}{T_1} - 1}{\eta_c}\right]$$

$$L_N = C_p * T_1 * \left[\eta_t * \frac{T_3}{T_1} * \left(1 - \frac{T_4}{T_3}\right) - \frac{\frac{T_2}{T_1} - 1}{\eta_c}\right]$$

$$L_N = C_p * T_1 * \left[\eta_t * \frac{T_3}{T_1} * \left(1 - \frac{1}{\beta^{\varphi}}\right) - \frac{\beta^{\varphi} - 1}{\eta_c}\right] \qquad (1.22)$$

The equation (1.22) has the same dependencies of the (1.20), but with different exponents, in fact there is not the denominator. Following a chart is reported and it represent the efficiency and work with different pressure ratio and temperature ratio.

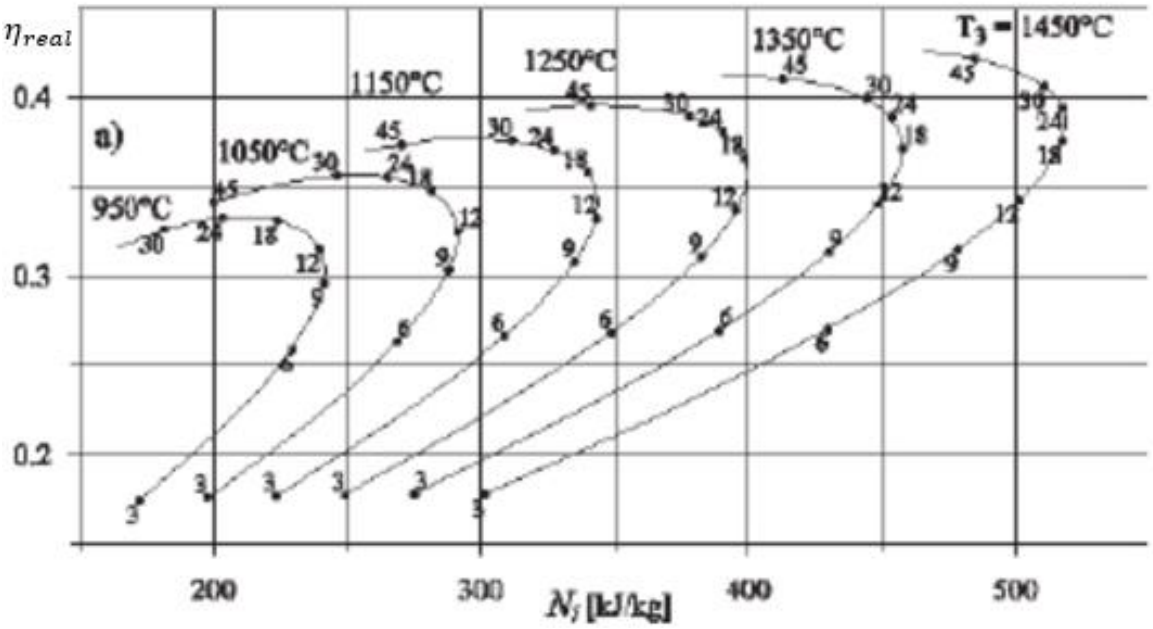

Figure 1.8 – efficiency vs specific work with β and T_3 as parameters [20]

The picture above shows in which way the efficiency and the net work change with the pressure ratio and the temperature ratio, which is shown as T_3 since T_1 is fixed and constant. It is possible to see that the pressure ratio that ensure the maximum specific work is always lower than which is needed to catch the maximum efficiency and if the temperature ratio rises the pressure ratio to catch both the maximum values also increases. To conclude, it is possible to say that the design pressure ratio has to be chosen in function of the cycle's temperature ratio and in function of the objective of the engine, maximize the efficiency, typically in the areo-engines, or the specific work, typically in the heavy-duty engines. It is from this discussion that it is possible to understand to importance of the Secondary Air

System, in fact if it is more efficient less air will be loss and more mass flow can go where it is needed and this can improve the cooling efficiency, thus it is possible to increase the turbine inlet temperature (T_3) [2].

1.4 Secondary Air System

Not all the compressed air expands in turbine to produce the useful work, but a certain quote is taken for other uses; this mass flow which do not participate to the combustion is extracted from the compressor section at various locations and transported along the engine by the Secondary Air System (SAS) towards the turbine section. The bled air is taken from the compressor at different pressure levels in function of the different objectives that the air has to satisfy. In the following, the secondary air will be named "*Turbine Cooling and Leakage Air*", TCLA is the acronym.

It is essential that the SAS is more efficient as possible, basically because if less air is needed to cool down the engine's components much air can participate to the combustion process and expand in the whole turbine. Thanks to this, the output power and efficiency rise without reducing the operative life of the engine. Moreover, an efficient SAS ensure, thanks to relatively hot gases which flows in the ducts which warms the components, the high turn-down during engine operation. Nowadays it is usual for the gas turbines operating in off-design conditions and the SAS flows prediction is vital to ensure a fast ramp-up and down and preserve the life cycle. Objectives of SAS consist of gain flexibility to follow the grid requirements [23]. Since TCLA, as said above, does not participate to combustion and it does not expand in the whole turbine, but only from where it is introduced by different ducts, it is crucial to use in an effective way this expensive air. Moreover, higher turbine inlet temperature matches with higher net work and efficiency (as it was seen in the paragraph 1.3.1).
In function of where the TCLA is needed different air circuits are available, in fact two main typologies exist: the internal compressor bleeds (*ICN*, with N that indicates the bleed number) to seal and cool the rotor parts and the external compressor bleeds (*ECM*, with M that indicates the bleed number) to seal and cool the stator parts. Secondary air fluxes ensure the best thermal condition as possible for the engine; moreover, they affect also the radial gaps between blades and external stator parts, with performance rising if they increase.
Below an image with the SAS circuits typical of AE94.3A engine is reported:

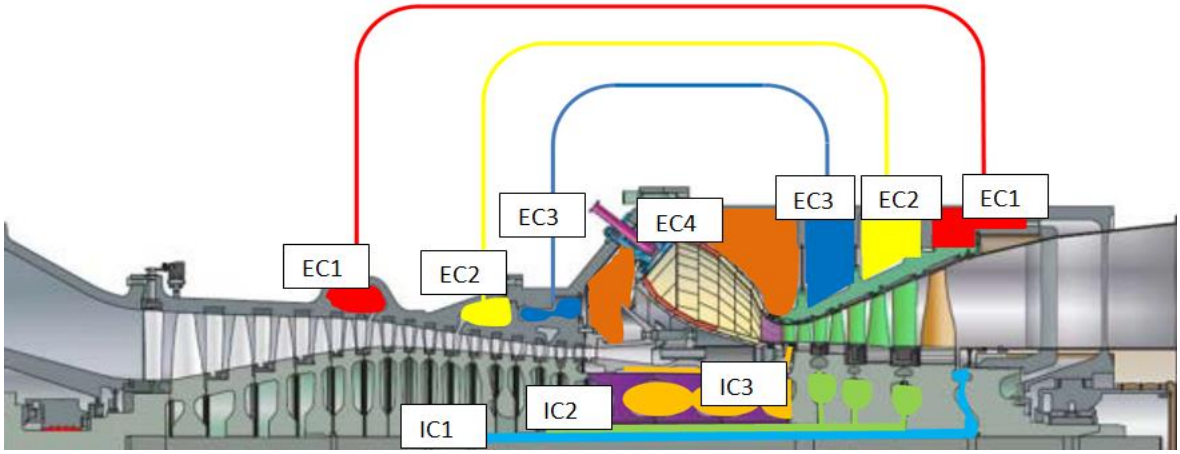

Figure 1.9 - GT Secondary Air System lines [20]

The spillage locations are chosen in function of what the bleed has to do, in fact it is vital that the spillage air has a greater pressure than the location where it will be discharged, with a certain safety range, to avoid the risk of hot-gas ingestion in the SAS lines. It is also important to keep the safety range as little as possible, in according to avoid the hot-gas ingestion risk, to save more energy, and thus to obtain the maximum output work and efficiency, as possible. As conclusion of the presented discussion, critical choice in SAS design is the optimal spillage position for a specific objective.

The main objectives of the Secondary Air System are summarized in the following:

- Cooling rotor and stator components.
- Sealing the open cavities where the hot-gas can enter.
- Clearance control by proper thermalization of casings and rotor
- Rotor axial thrust control.
- Reducing the parasitic leakages.

1.4.1 Turbine cooling system

The first SAS objective is to cool the hot parts to improve the engine life cycle. In function of the stage temperature a different cooling technique can be chosen. In general, as high is the hot-gas temperature as big will be the ΔT between the metal and the hot-gas to preserve the component since the maximum metal temperature is mostly fixed by the material limits; in addition, if higher gas temperatures are there, higher and higher performance materials are needed. For this reason, much more air is spent in the first stages of a turbine section due to higher temperatures involved. The cooling techniques change in function of the stage because of what just said, and the main ones are here reported:

- Film cooling
- Impingement cooling
- Convection cooling

The first mentioned consists of cool air that flows out from blade and vane's holes and protects the airfoil with a low temperature air film. As consequence of this film, the airfoil's aerodynamic gets worse, but the primary objective is to keep the integrity of the blades and

vanes. In certain engines in the first stages the platform cooling is also introduced, which is basically a film cooling that protects the airfoil's platforms.

The second method reported is the impingement cooling, this cooling technique consists of the air that is blown in jets against the blade or vane's internal walls to improve the heat exchange from the metal walls and the cooling air. First of all, below the relations which describe the heat exchange are reported as follow.

$$Nu = \frac{\dot{Q}_{conv}}{\dot{Q}_{cond}} = \frac{h \cdot \Delta T}{k \cdot \frac{\Delta T}{L}} = \frac{h \cdot L}{k} \tag{1.23}$$

$$Re = \frac{\rho \cdot V \cdot L}{\mu} \tag{1.24}$$

$$Pr = \frac{\mu \cdot C_p}{k} \tag{1.25}$$

$$Nu = 0.0296 \cdot Re^{0.8} \cdot Pr^{\frac{1}{3}} \tag{1.26}$$

Where:

- h is the convective heat exchange factor
- L is the characteristic length
- k is the conductive heat exchange factor
- ρ is the fluid density
- V is the fluid velocity
- μ is the fluid dynamic viscosity
- C_p is the specific heat at constant pressure.

Locally the air jet, which is pushed against the airfoil's wall, increases its turbulence intensity thus the Reynolds number (defined in (1.24)) rises and, by remembering that the Nusselt number can be expressed as function of Reynolds as shown in (1.26), Nusselt rises too, and this grants a bigger heat exchange due to convection as it can be seen in the (1.23) between the airfoil and the cooling air [26].

Finally, the convection cooling is analyzed. This kind of cooling technique is the less effective but also the simplest. The air passes through the blade or vane and the heat passes from the metal to the low temperature air. It can be possible that in the airfoil's internal ducts there is some object (as "*pin fins*" or "*rib fins*") which can increase the TCLA's turbulence intensity, thus, by remembering the relations (1.23), (1.24) and (1.26), this increases the convective heat exchange.

As conclusion of the cooling methodologies, the blades and vanes' cooling system usually is not the same since the temperature that they see is quite different and different cooling choices can optimize the TCLA savings and the metal temperature reduction. More than only one cooling strategy is often adopted for each airfoil. Following a picture with an internal airfoil's cooling system is shown:

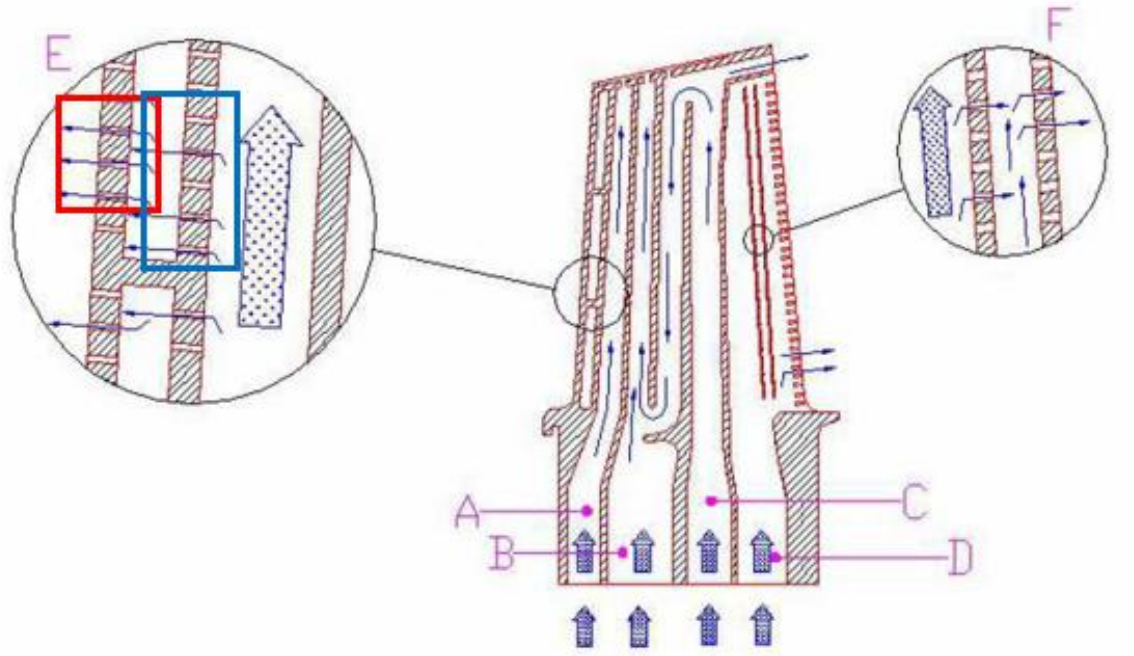

Figure 1.10 - Airfoil cooling system [23]

In the picture above a blade's cooling system is shown; it can be seen the film and impingement cooling holes in the circles "*E*" and "*F*." In "*E*" the film cooling is located at the left wall (red square) and the impingement cooling pushes the air against the wall and is identified by the blue square. In "*F*" only internal impingement is shown and the convection cooling is ensured by the blade's internal ducts [23].

1.4.2 Turbine sealing system

The gas turbines are composed by many components, some of these are rotating and some others are not; between the different components there can be a gap, which depends on the design parameters and the admitted tolerances. The sealing system is crucial to reduce the leakages from the high pressurized SAS lines in order to save as much TCLA as possible. Secondly, the closure of such gaps to the maximum extent, prevents or reduces the risk of hot gas ingestion from the main channel into stator casings or rotor discs which could not sustain the related temperatures.

To reduce the air leakages and hot gas ingress there are essentially three main sealing typologies: the "*strip seals*", the "*rim seals*" and the "*labyrinth seals*", which deal with different technical challenges The first one is adopted to seal the stator-stator or rotor-rotor gaps between SAS circuits and hot-gas path, the second one is usually utilized to prevent the hot-gas ingress between the vanes and blades platforms into stator-rotor cavities and the last one is usually adopted to seal the rotor-stator parts to control the flow through them, such as the gap at the inner diameter between vanes and the rotor.

The *strip seals*, which will be described with more detail in the present document, are narrow and thin metal sheets with an opportune design and they are lodged in opportune housings/grooves and thanks to the pressure gradient between SAS and hot-gas path they are pushed against the sits with high forces; what just described grants a better sealing and

reduces the cooling air leakages. In order to prevent the hot-gas ingress the TCLA pressure must be greater than the hot-gas one.

The *rim seals* consist of cavity between rotor and stator parts, in particular between the blades and vanes foot, where there is a gap to ensure the rotation possibility to the blades without contact with stator parts. This kind of seals are less efficient than the previous one, in fact a gap is usually left open in this case, and the sealing capability depends on the seal geometry (that is the cavity plus the rim protrusion geometry).

The *labyrinth seals* are components which are located between the vanes/stator and the rotor disks, with the aim to avoid the contact between the two components while controlling/keeping the air flow through them to a minimum. As the *rim seal*, this one is located between rotor and stator parts, but this time is usually adopted at the vane foot, more generally not too near to the main hot gas channel [4] [5] [6] [7].

The three sealing techniques are shown in the pictures below:

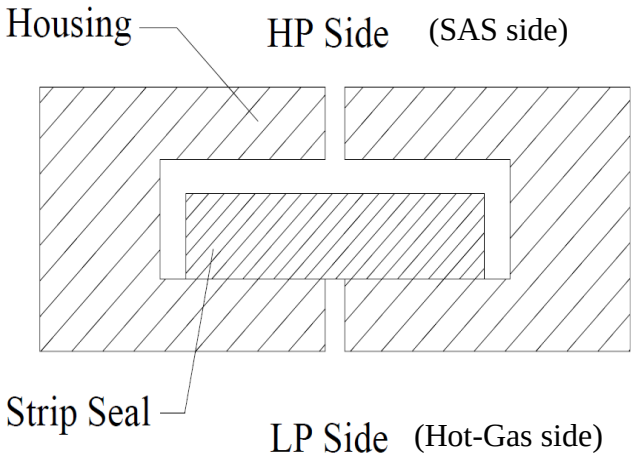

Figure 1.11 - Strip seal [7]

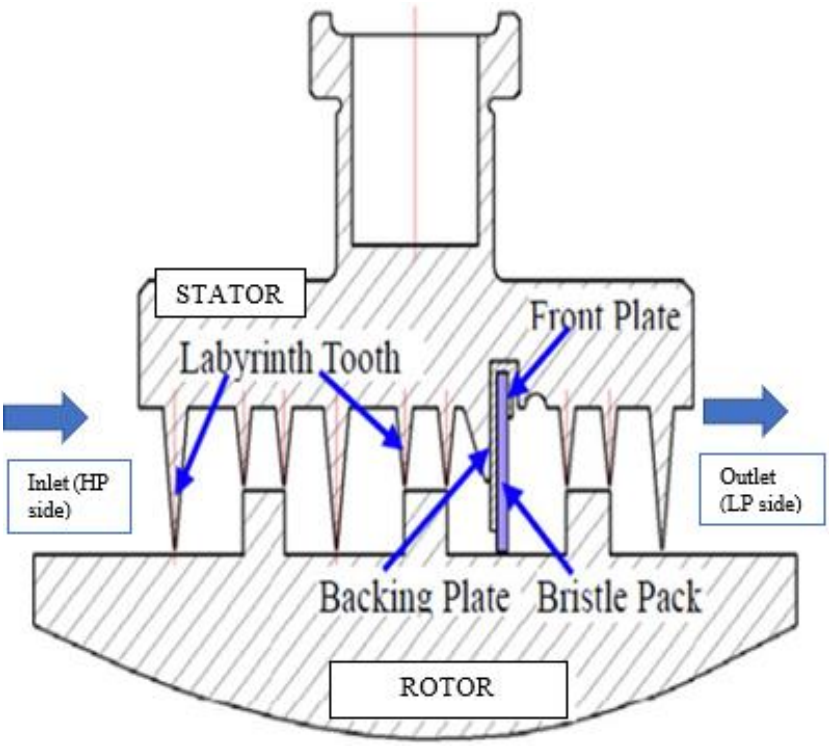

Figure 1.12 – Labyrinth seal (including brush seal) [18]

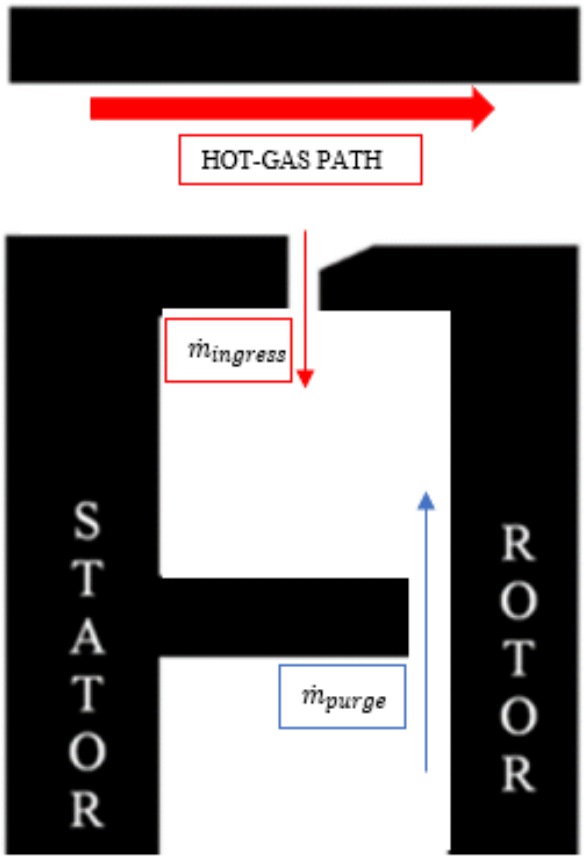

Figure 1.13 – Rim seal geometry [24]

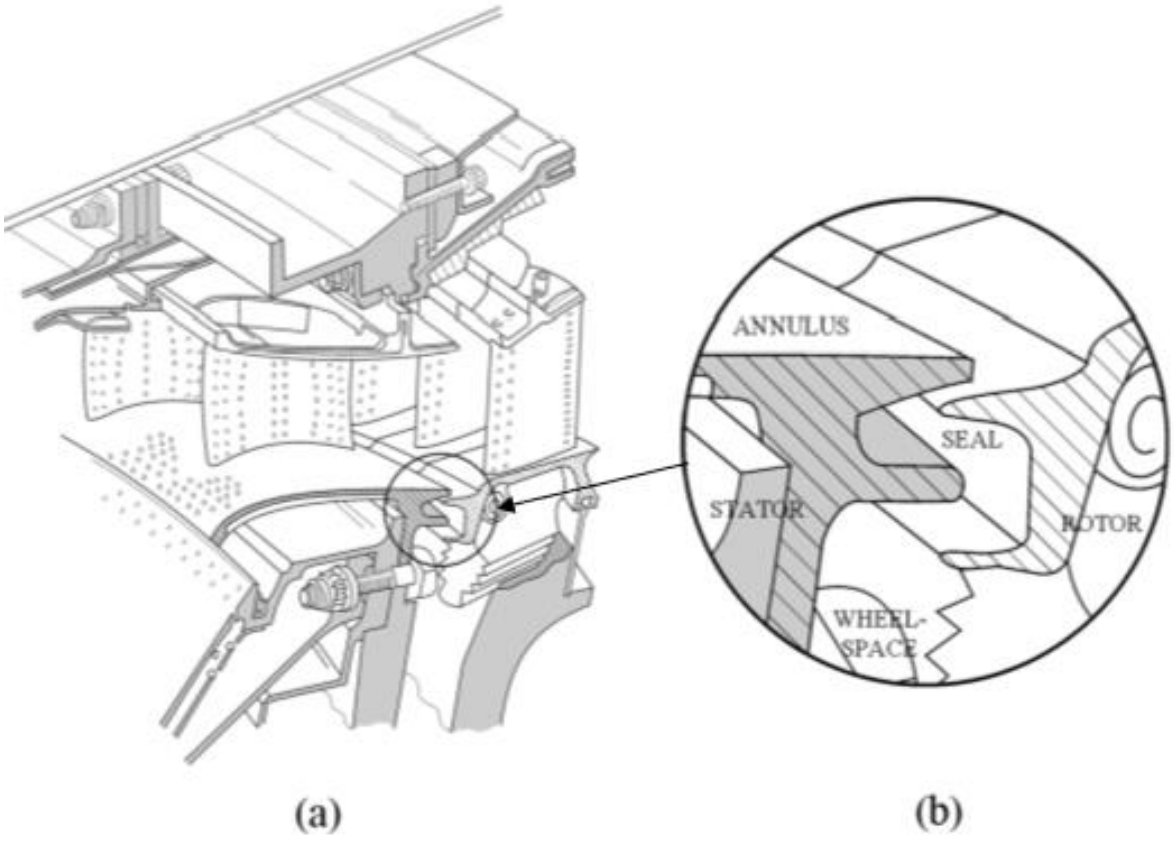

Figure 1.14 - Rim seal position [25]

In Figure 1.11, *strip seal* is reported with the seal's sit (that in this particular case are stator components); the space where the seal is lodged is commonly named "*groove*" and strip seal is pushed from the high pressure plenum (*HP side*), that is the SAS side, against the low pressure side (*LP side*), which is the hot-gas one.

In Figure 1.12, the *labyrinth seal* is shown; this kind of seal is adopted to seal the gap between the vane and rotor with a little play. The hot-gases pass where they suffer less resistance as possible, thus they tend to pass not across the vane channel but through the gap between rotor and stator parts. If what just described happens, they hot-gases expand less than expected, thus lower output power can be found, and they risk ruining the parts that are not designed to resist to high temperature. In order to avoid these consequences, the seal analyzed generates high pressure drops between HP and LP side and it impedes the hot-gases passage.

Last two pictures reported are Figure 1.13 and Figure 1.14; the first one represents the simplified rim seal geometry. This kind of seal is positioned between the stator and rotor parts as it is shown in the Figure 1.14 and its aim consists of reducing much as possible the inflow from the hot gas path. For these particular seals it is possible to define the seal effectiveness (ε), that is the seal's capability to prevent the hot-gas ingress. The mentioned quantity is defined as follow [23]:

$$\varepsilon = 1 - \frac{\dot{m}_{ingress}}{\dot{m}_{purge}} \tag{1.27}$$

By observing the relation above it is evident that the effectiveness is as higher as higher is the $\dot{m}_{purge}$ and as lower is the $\dot{m}_{ingress}$; since the main objective is to reduce the TCLA it's crucial to try to reduce the purge mass flow, even if the ingress mass flow has not to rise to inhibit the components degradation and this can be obtained with an improved and more complex seal geometry.

1.4.3 Axial thrust control

The axial thrust control is a mechanism which permits to generate the thrust along the engine's axis to keep the GT in place.

In gas turbines, stator and rotor blades and vanes are subjected to an aerodynamic force, which acts mainly tangentially; the output work is strictly related to this mentioned force. The axial component of this force is unbalanced in favor of the turbine, because of the higher mechanical power generated from the turbine compared with the compressor. The presented forces unbalance between compressor and turbine is absorbed by a thrust bearing, usually an oil-dynamic one. If the rotor axial thrust generated by the engine is high, the only thrust bearing solution can be expensive, thus part of the turbine is designed as balancing piston. In this case the SAS pressurizes some cavities, which are properly the "*balancing piston*"; thanks to this solution the net thrust that acts on the thrust bearing is smaller.

As follow the resultant axial thrust to balance is shown: as just said the turbine generates higher thrust than compressor and if it is not balanced the engine risks to dismount itself.

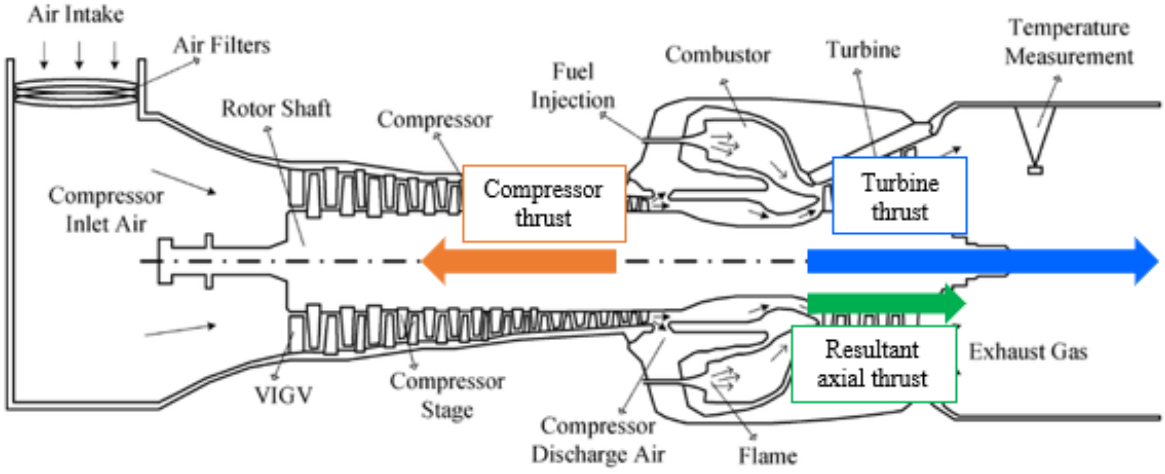

Figure 1.15 - Axial thrust estimation

As results of the vectors sum the resultant vector is shown in green, thus the bleed air IC1 has to be carry to the turbine outlet in a balancing chamber to use the pressurized air to keep in place the engine axis with an opposite axial force.

1.4.4 Passive clearance control

The most critical phase in the engine life cycle is the warmup. If the temperature variations are not controlled, problems related to the fatigue mechanism can be detected and they can determine the engine failure. TCLA, when it passes through the ducts, heats and cools the gas turbine's components guaranteeing more uniform and gradual temperature variations

compared to the only conductive heat transfer. The presented mechanism ensures lower thermal stress, so a faster start-up with the same equivalent operative hour cost. The rotor characteristics influence the engine's temperature variations. Depending by the rotor configuration, the warmup can be more or less efficient, such as in a stacked discs-rotor configuration were the TCLA flows surround most of the discs or the welded discs where the TCLA flows are only passing through small portions of the rotor.

1.4.5 Air leakages: impact and management

In this section the SAS leakages are analyzed with the aim to understand what their impact on the engine is. Leakages induce TCLA increase, thus the reduction of the air in the combustion chamber. The presented condition, at same engine power would tend to increase flame temperature, to reduce the flame stability and to generate an emissions rise.

As direct consequence of the working fluid reduction the output power decreases if the same T_3 is kept, because of lower working fluid which can expand in the turbine. To keep the same output power, T_3 needs to rise and it can be obtained with higher turbine inlet temperature, thus with much fuel mass flow. What just described leads to a *specific fuel consumption* increase. Because of this, it is crucial to control and minimize leakages with the opportune sealing technologies. The reason of undesired leakages is to be imputed to the geometrical tolerances and unavoidable small gaps even in presence of interposed sealing elements.

In general, as high is the sealing capability of each sealing component as low the TCLA can be because it is not wasted; obviously, there will always be leakages due to the non-perfect components' sealing capability. Moreover, the sealing capability for each seal can vary with the operating point, due to the different pressure conditions. To reduce the leakages, it is possible to use the sealing techniques mentioned in the paragraph 1.4.2. The impact of leakages bigger than expected/wanted can also be that the pressure in some SAS plenum drops also be and, as consequence, there could be hot-gas ingestion somewhere in the SAS circuits.

2 Strip seals

The modern gas turbine's blades and vanes are built independent from each other, in order to ensure an easier maintenance and a greater reliability. This choice imposes the presence of gaps between the blades and vanes' platforms. The mentioned gaps affect the engine performance and a study conducted by Reid et al. [4] confirms that this kind of gap can affect the GT's stage efficiency, with a reduction from about 0.5% up to 1.5%. Thus, it is crucial to design these gaps in order to minimize their effect on the main channel in order to reduce the mentioned efficiency losses. To reduce the ingestion from these gaps it is possible to use a sealant flow and the coolant effect of this mass flow was analyzed in a linear cascade by Ranson et al. [6]; the results that were found show that an increasing of the sealant flow did not improve the vane and blade platform coolant effect. In the next studies new sealing techniques are analyzed, in particular a certain airflow is not the only mean of sealing this kind of gap, but rather an interposed mechanical element is chosen in order to close (even if not perfectly) the inter-platform openings. The gaps that will be analyzed in the present chapter affect in a significant way sealing and cooling effects that the TCLA can potentially ensure and it can also generate a *specific fuel consumption* increase; moreover, as result of the sealant flow outlets, there will be undesired interactions between the cooling and sealing flow with the hot-gas path. The focus of all the sealing technologies that will be shown consists of reducing the amount of leakages at the inter-platform gaps, this because an advanced sealing system can improve the engine performance. The *strip seals* represent the current most used sealing technology for the mentioned gaps and they are classified as static seals since they are positioned between two stator elements which, ideally, do not have relative movement one to each other [7]. A simplified picture is reported below:

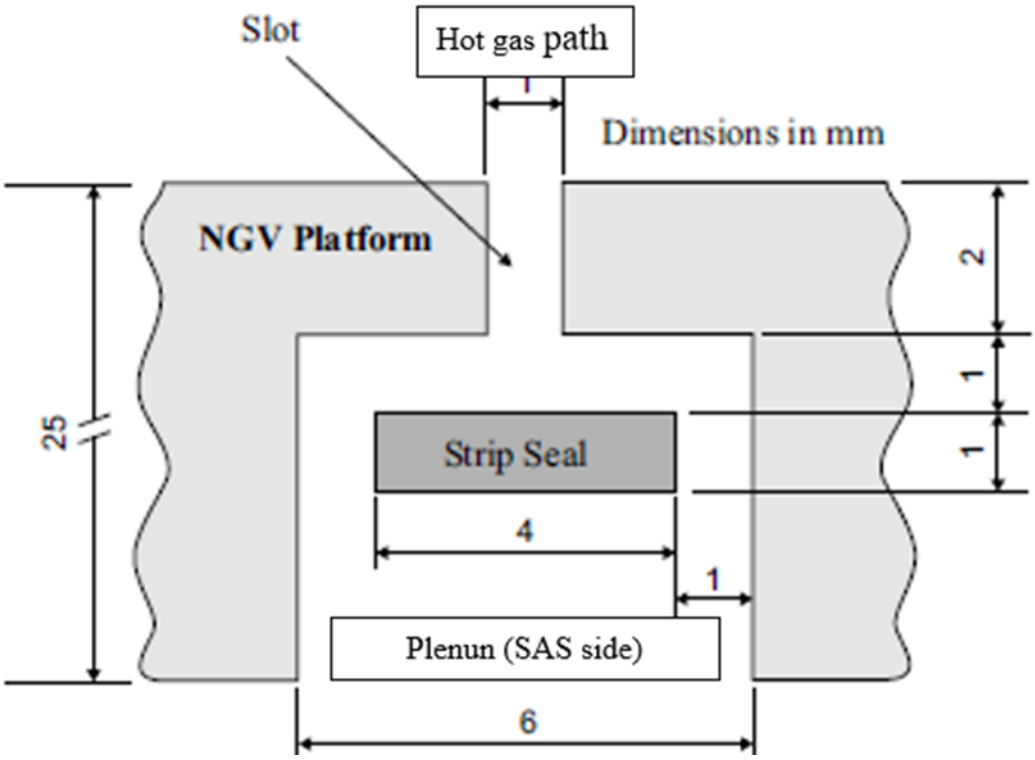

Figure 2.1 - Strip seal conceptual [5]

In Figure 2.1 a sketch of a strip seal is reported; as it can be seen the strip seal separates two plenums: the low temperature side (SAS) and the high temperature side (engine's main channel). Usually, at the SAS side the strips are interfaced with an air plenum which feeds the cooling and sealing system and since the gap between the two stationary parts (NGV Platforms in the picture) is difficult to reduce because of constructive limits, the mentioned seal grants substantially a gap reduction [5].

Ideally, the strip seals are positioned between elements which do not move relatively each other, as it was already said, but in reality, all the engine components will move respectively to each other because of thermomechanical displacements and existing clearances which allow for it. This can make the performance reduce; thus, if the engine gaps between stator parts will be reduced the sealing effect of this kind of components would increase [8]; in addition, it is possible that the seals get worn faster than expected because of this relative movement, especially during the transient conditions. To easily accommodate the seals in this geometrical environment the strips should be flexible to adapt themselves to the different engine's conditions [9] or it is possible to use strip seals which are composed by more than one part as said by Farahani et al. [7].

This kind of element changes its sealing capability with the different engine conditions, such as thermal expansion, the engine's components misalignment, due to the just mentioned constructive tolerances and thermomechanical displacement, and the operating condition, because the hot-gas path and TCLA's pressure can vary a lot between the MEL and the BL. The "*narrow path*" is the geometrical parameter which affect in a considerable way the sealing, especially its height; a sketch is reported below [8].

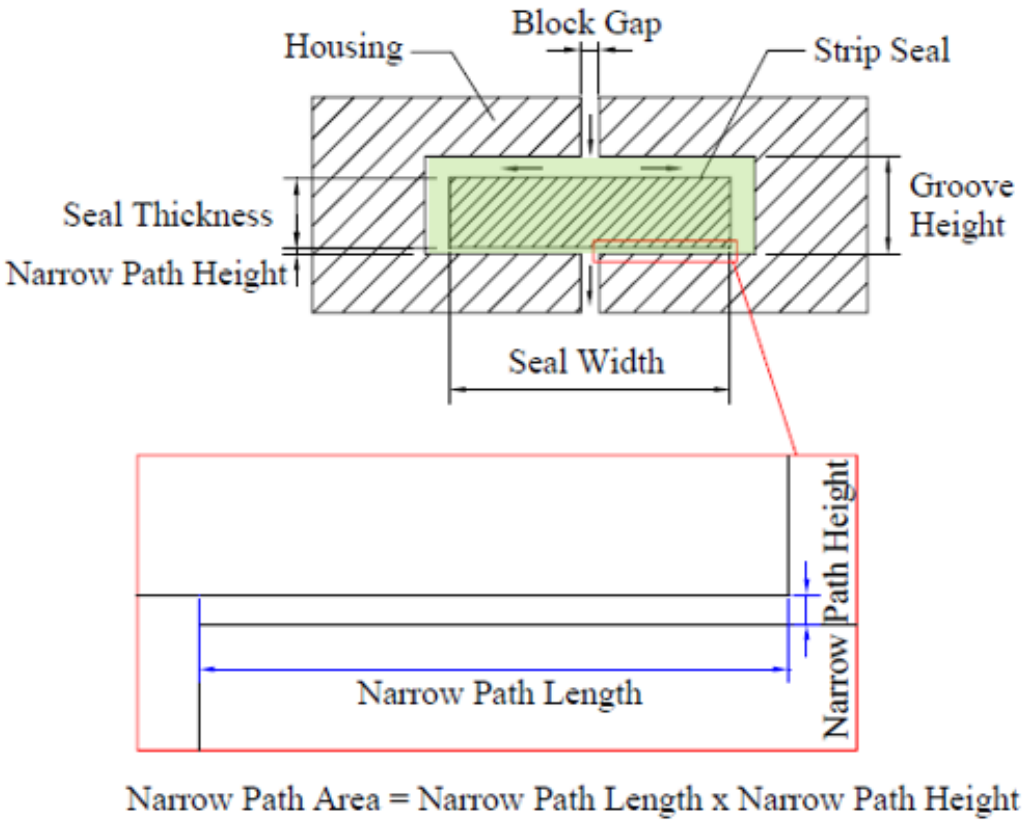

Figure 2.2 - Strip seal detail [8]

It can be easily concluded by observing Figure 2.2 that, if the delta pressure between the SAS and hot-gas side will rise, the narrow path height would reduce thus the sealing effect should increase. It is crucial to always ensure a SAS side pressure greater than the hot-gas side to avoid ingestion problems. The groove is the ambient where the strip seal is lodged, so it is the portion in light green in Figure 2.2.

The pictures reported in the present section show only a type of strip seal, with a rectangular shape from both the front and upper views, but there are more than one types, such as curved or more complex. The most famous kind of strip seal will be analyzed in a separate paragraph.

2.1 Strip seals characterization

The following paragraph has the aim to individuate the typical strip seal behavior and the main parameters which affect the sealing performance; it is crucial to understand the sealing element behavior because the flow which pass through the strip seal contributes almost to $1/3$ of the TCLA. In general, it is plausible to expect that the sealing capability is function of the sealing typology, the groove curvature and the groove and seal roughness; moreover, the sealing quality should depend by the geometrical tolerances, thus it is related to the deviation between the design conceptual and the real geometry and the movements between the two groove's sides [9].

The strip seals can be characterized with experimental campaigns with mass flow, temperature and pressure measurements; typically, mass flow is taken on the strip seal feeding line, pressure is taken in a plenum upstream the seal and in the ambient and the temperature is taken upstream the seal, near to the plenum pressure sensor. Following is reported a classic test rig adopted for this kind of seals.

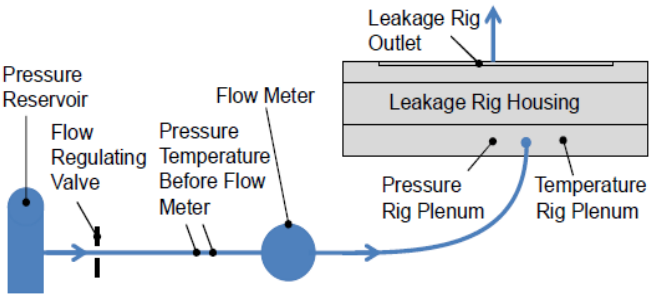

Figure 2.3 - strip seal test line [9]

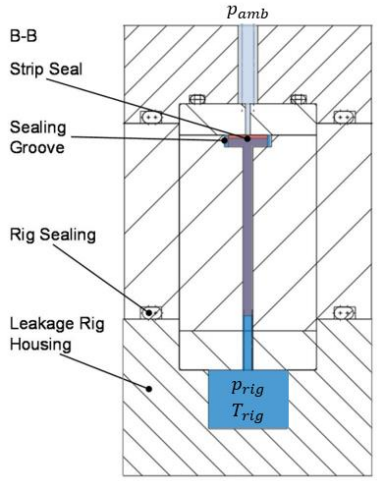

Figure 2.4 - strip seal test rig [9]

With these measurements it is possible to define an equivalent gap J_{eq} which simplifies the leakage calculus. The leakage mass flow across a strip seal can be written as:

$$\dot{m} = \rho \cdot L_{seal} \cdot J_{eq} \tag{2.2}$$

In literature it is possible to find out the correlations to determine the equivalent gap and Hubert et al. [9] use the following definition:

$$J_{eq} = \dot{m}_{rig} \cdot \frac{\sqrt{R \cdot T_{rig}}}{p_{rig} \cdot L_{seal} \cdot \Psi} \tag{2.3}$$

By considering the formulation above, it is evident that the leakage (thus the equivalent gap) is strictly related the thermodynamic flow conditions, in fact temperature and pressure inside the rig's plenum are needed. In equation (2.3) is also reported a term: Ψ. It can be defined in two different ways, depending by the pressure ratio between the rig's plenum and the ambient. In order to do that, critical pressure ratio which identifies the sonic condition is defined:

$$\Psi_{crit} = \left(\frac{k+1}{2}\right)^{\frac{k}{k-1}} \tag{2.4}$$

In case of subsonic condition ($\frac{p_{rig}}{p_{amb}} < \Psi_{crit}$) Ψ is given by:

$$\Psi = \sqrt{\frac{2k}{k-1}\left[\left(\frac{p_{amb}}{p_{rig}}\right)^{\frac{2}{k}} - \left(\frac{p_{amb}}{p_{rig}}\right)^{\frac{k+1}{k}}\right]} \tag{2.5}$$

Instead, for the supersonic condition when the mass flow is chocked ($\frac{p_{rig}}{p_{amb}} > \Psi_{crit}$):

$$\Psi = \sqrt{k \cdot \left(\frac{2}{k+1}\right)^{\frac{k+1}{k-1}}} \tag{2.6}$$

From this discussion it can be extracted that the sealing performance (strictly related to J_{eq}) depends by two plenums' pressures that the strip seal sees, of the air temperature and its length.

For some kind of seals, pressure gradient is not the only factor which influences the leakages, it is also needed to consider the stress generated by the seal geometry [17]. In this case the researchers had found a relation to estimate the equivalent gap and it is reported as follow:

$$J_{eq} = \left[1 - \frac{9\pi^2}{16} \cdot \left(\frac{\sigma}{E}\right)^2\right] \cdot R_z \tag{2.7}$$

Quantities described above are not the only ones which affect the leakages, and other dependences are known. Rathbun [10] found that J_{eq} depends by the pressure gradient across the seal, but also the contact force, the surface roughness and finishing (referring to the micro-structure and micro-asperities and also macro-structure) and the seal material. The analysis was implemented by Armand et al. [11] who found that the by rising the contact force, the leakages can be reduced. This is due to plastic deformations of the seal's seat. Unfortunately, contact force effect cannot be investigated alone, in fact it generates deformations which are related to the material type and the surface roughness; this relation was investigated also by Roth and Inbar [12] and Roth [13] in a de-pressurized ambient and they showed how the leakage got reduced with the rising of the contact force because of the flattering of the asperities which characterize the surface roughness. Moreover Roth [13] had found a relation to estimate the leakage mass flow in function of the peak-to-valley height (R_z) of the roughness and of the contact stress (σ); the mentioned relation is reported as follow:

$$\dot{V} \propto R_z \cdot e^{3 \cdot \frac{\sigma}{K}} \tag{2.8}$$

The term "*K*", named *sealing factor*, is related to the material and it is tabulated; if *K* rises the leakage mass flow reduces. Successively, it was found also dependences by the direction of the roughness profile, hardness, tensile strength [14]. A successive study [15] had found one another interesting parameter which influence the leakage: the tightening force history. It was observed that there is a hysteresis cycle in the leakage mass flow, with lower leakages for decreasing the applied force; this particular behavior is due to the local plastic deformations of the roughness peaks.

Since the leakages are strictly related to deformations and stresses, as said few lines above, it is probable that they can be influenced by the contact area. For the same load applied, stress can vary as function of the contact area, thus if it would be a line, the stress contact will increase, and it should reduce the leakages. The relation between these parameters is analyzed by Bricaud et al. [16], who investigate the seal leakages by varying the seal roughness and the shape of the sealing surface. For both the analysis, two values were compared: for what concerns the roughness, the conditions compared are one *fine* and one *coarse*, instead, regarding the shape of the sealing surface, *cylindrical-flat* and *flat-flat* contacts were investigated. It was found that, for the same force applied, *cylindrical-flat* contact ensures a leakage reduction (thus smaller J_{eq}) if compared to *flat-flat* contact; this is due to higher local stress generated by the first contact type which helps to seal in a most effective way. Any noteworthy evidence was not found, instead, for the different roughness tested, even if the asperities suffer plastic deformations due to the maximum load applied (in the engine it is typically the BL condition). Highest leakage reduction is attributable to the load applied as consequence of the pressure gradient across the seal and, if the contact surface is smaller, local stress is higher and also after the seal de-loading a leakage reduction remains, because of the plastic deformations. In this case high stress compensates the small contact surface area. As fundamental result, it can be said that the linear contact ensures a better sealing because of the high stress due to the small contact surface.

Leakage related to this kind of seal depends also by strip seal's slot location between the blades or vanes as it was demonstrated by Reid et al. [5]. Four different slot positions were tested, and they're shown below:

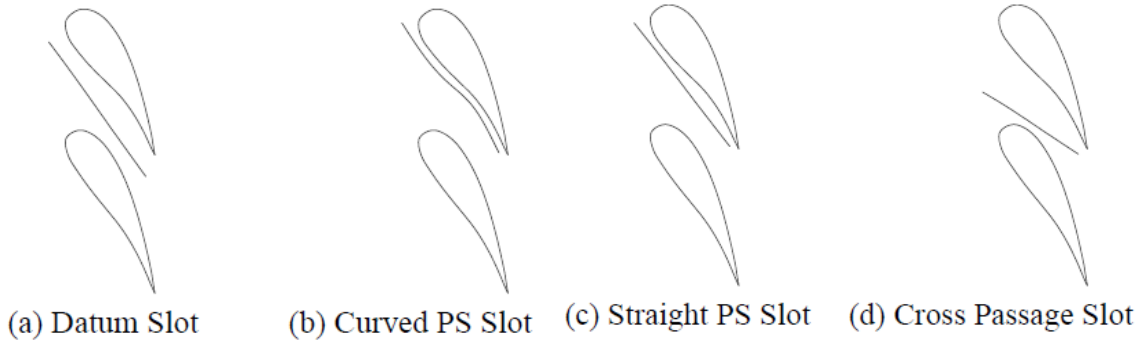

Figure 2.5 - Strip seal's slots positions [5]

Different slot positions shown in Figure 2.5 are characterized by different local static pressure gradient; the presented study shows the importance of the slot position choice, and by considering the picture below the authors conclusions can be reported.

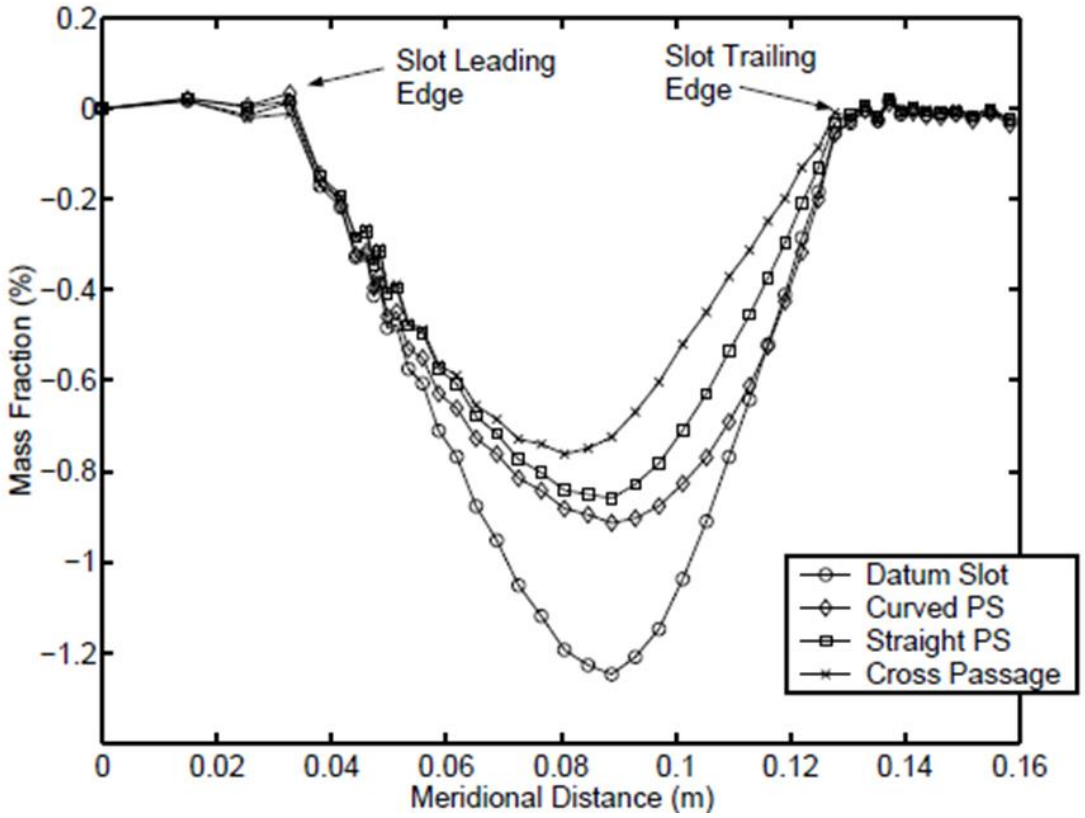

Figure 2.6 - Mass flow fraction variations between hot-gas path and seal's plenum [5]

In the picture above, negative slope represents the mass flow which exits from the main channel and positive slope indicates that the flow is entering in the mainstream annulus. By seeing the results reported it is evident that the "*cross-passage*" ensures a lower leakage, and, thanks to CFD analysis, it is demonstrated that this condition is related to the slot location with a relatively constant static pressure. Moreover, researchers had shown how the slot radial angle can affect the leakages across the strips; the comparison reported in the paper is between two slots directed respectively to the vane pressure side and suction side, but only for the "*datum slot*". A synthetic scheme is reported below:

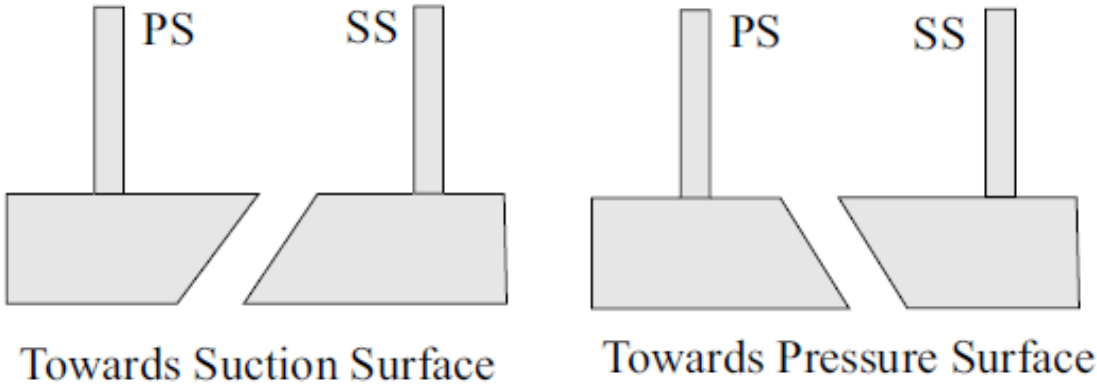

Figure 2.7 - Angled slots tested [5]

Two configurations shown in Figure 2.7 are compared to the straight *datum slot*. Results are shown as follow.

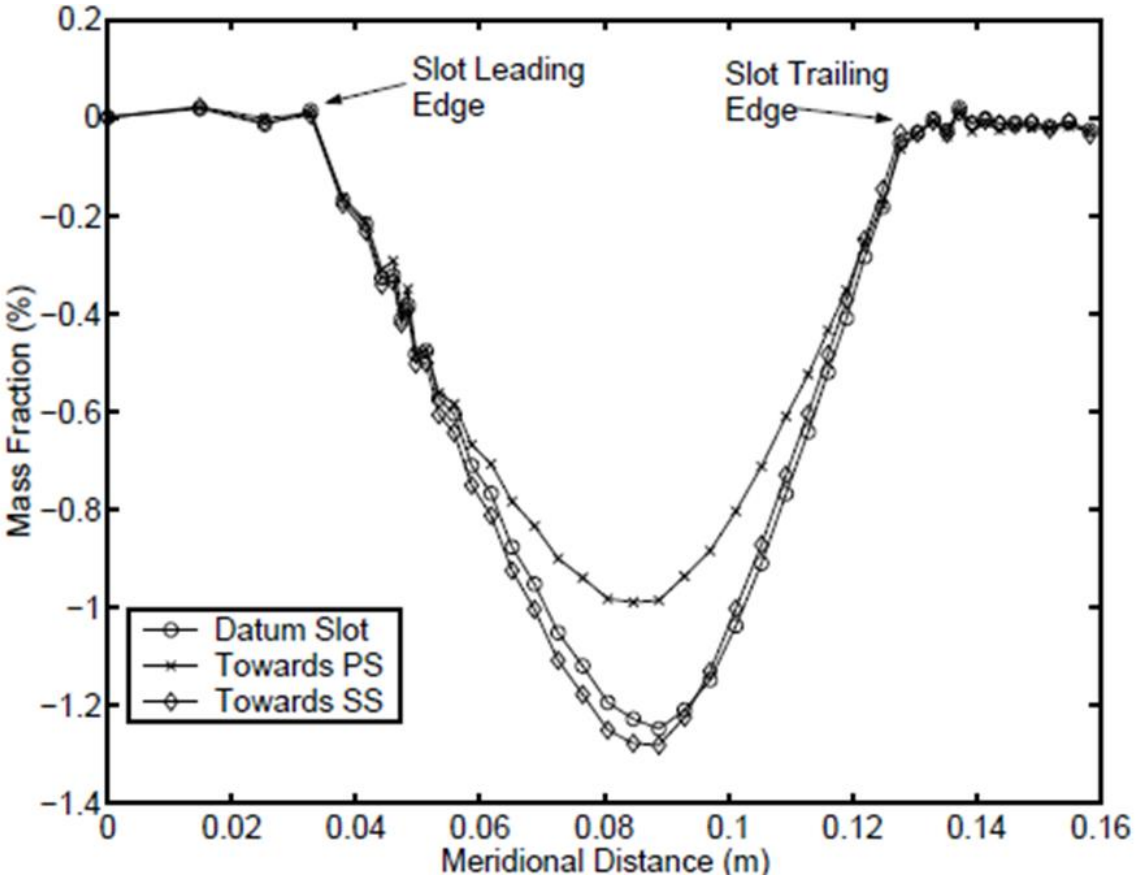

Figure 2.8 – Mass flow fraction variation: comparison between towards SS, towards PS and datum slot [5]

Figure 2.8 shows that the slot "towards PS" is the most effective on the leakage reduction, in fact in this particular condition the slot is leaned towards the pressure side, thus there is less flow which can pass through the slot if compared the standard datum slot.

2.2 Different kind of strip seals

A lot of types of strip seals exist depending by the different aim and position where they are lodged. In the present document the ones that will be described as follow are the a the most relevant by a technological point of view [7].

2.2.1 Flat strip seals

The most common and easy to build strip seals are the "*flat*" (or "*straight*") strip seals (the section is shown in Figure 2.1 and Figure 2.2). Typically, if they are thin, their upper and bottomer faces are characterized by smooth surfaces; instead if their thickness rise a face is rugged (at the SAS side) to grant a better deformability and avoid the seal failure. The seals' thickness affects in a significant way the sealing performance and it is expected that in the ideal engine condition the thinner strip seals should grant better sealing between the cooling air and the high enthalpy flow which expands in turbine. In general, for this particular geometry there could be some problem in case of misalignment as said in paragraph 2.1; a simple sketch which describes the two possible conditions is shown below.

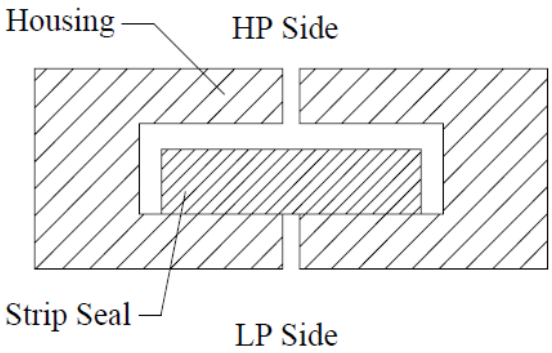

Figure 2.9 - Flat strip seal – aligned [7]

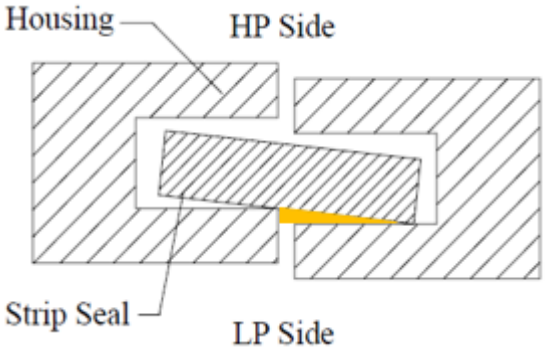

Figure 2.10 - Flat strip seal – misaligned [7]

Figure 2.10 shows that if radial misalignment is detected, the seal does not ensure a perfect contact and a triangular shaped gap area (highlighted in orange) is introduced.

2.2.2 Curved strip seals

One another possible geometry is the "*curved*" one; this configuration can be built with two different materials with different thermal expansion coefficient α. If the formulation related to stresses and thermal deformations, below reported, is considered it is possible to generate a curved shape.

$$\sigma = E \cdot \Delta\alpha \cdot (T - T_{amb}) \tag{2.9}$$

A possible problem related to this kind of seal is the stress generated by the contact between the two materials but, since for the most metal-materials the α has almost the same order of magnitude (tens of $[\frac{\mu m}{m\,^{\circ}C}]$), stress due to the contact in general is low. In fact, by imposing an high T compared to the ambient ($T - T_{amb} = 400\,^{\circ}C$) and taking as a typical $\Delta\alpha = 1.5 \cdot 10^{-5}\,[\frac{1}{^{\circ}C}]$ the strain $\frac{\sigma}{E}$ is about 0.4% that is really small and it doesn't justify a sealing performance improvement as it can be verified by seeing the equation (2.7).

The main disadvantage of this kind of seal is related to the seal-groove contact; even if the stress between metal interface is low, the stress associate to the contact between the seal and the groove is really high, without sealing improvement as said. A scheme related to this strip seal geometry is show as follow.

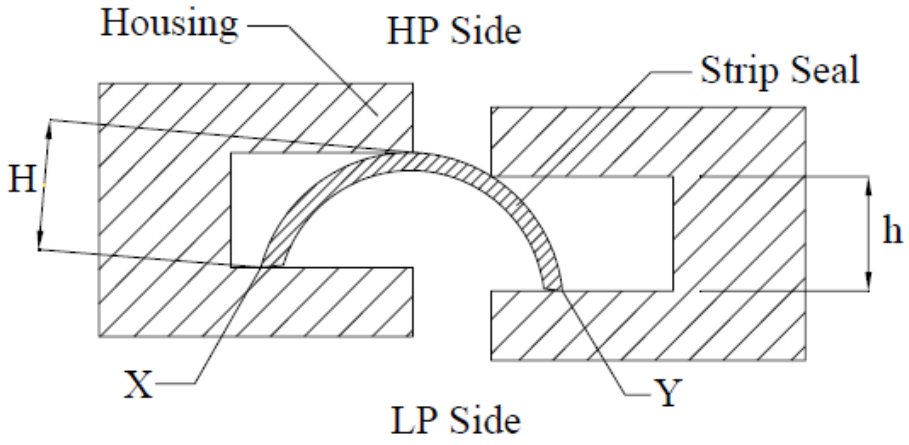

Figure 2.11 - Curved strip seal [7]

2.2.3 Spring-like seals

The seals that will be described in this section have the aim to generate a clamping force with a mechanism that increases the contact force and stress, with particular configuration [18]. This shouldn't affect strip's sealing capability in misaligned groove. This kind of seal can be realized with different geometries and each company has its own patent. Typically, they are generated with thin and curved surfaces, but (as it was explained in paragraph 2.2.2) curved seals do not ensure the best sealing capability as possible. Main reason can be summarized as follow:

- Stress rising due to the clamping force and low contact area will never be enough to reduce significantly the equivalent gap, J_{eq} is strictly related to the ratio $\frac{\sigma}{E}$ that cannot be significantly high for metal-metal contacts - equation (2.7).
- Curved surfaces induce non-perfect contact that the straight strip seals improve. The absence of performance decay in misaligned case can be ascribed to the already low sealing performance in aligned configuration (due to bad contact type).
- Huge gaps are introduced with this strip seals between the strip's bottom surface and the lower surface of the groove because of non-planar surfaces, thus the air can pass easily.
- Small contact surface together to low thickness generate high stress that can lead to failure.
- Complex manufacturability.

Two seals examples are reported as follow:

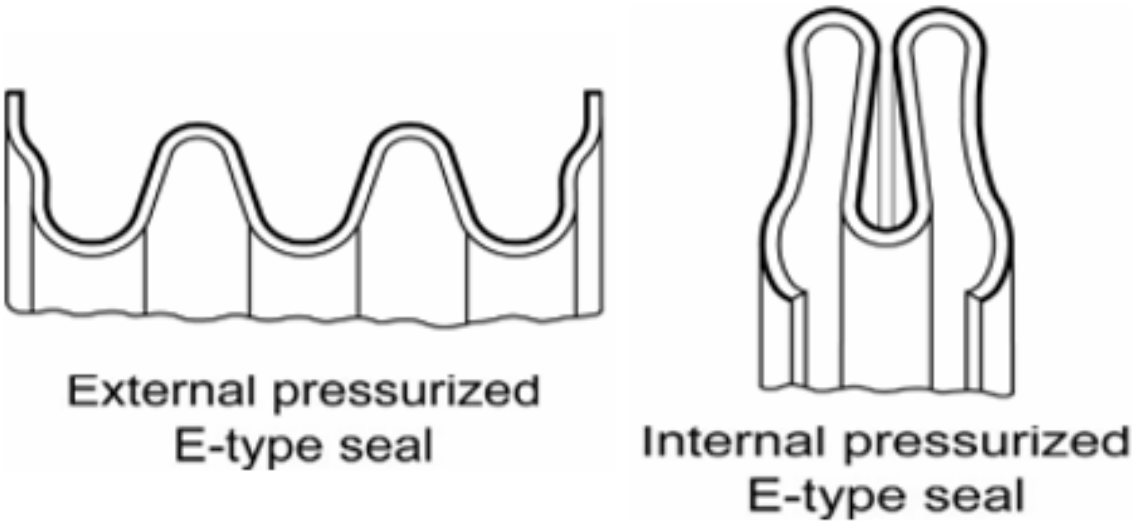

Figure 2.12 - E-type strip seals

2.2.4 Jaw-shaped strip seals

Strip seal, in this case, is composed by two parts, first thicker than the second one and they are welded together. Thicker one has to be thick enough to avoid buckling of both the seals and thinner one has to ensure the opportune deformability when the pressure gradient is

applied. The great deformability obtained allows to follow the groove misalignment. Seal's cross section is shown below.

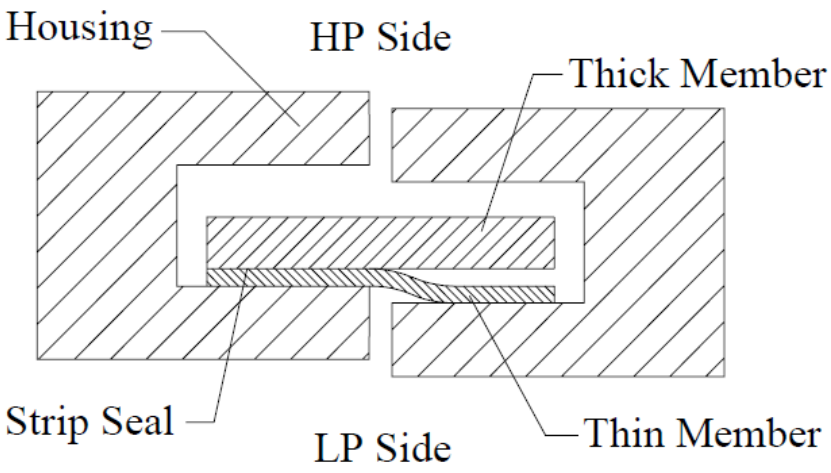

Figure 2.13 - Jaw-shaped strip seal [7]

Figure 2.13 shows that, in case of mismatching between the two housing sides, thinner component is able to follow the slot platforms thus it is possible to reduce the leakage in the misaligned configuration. To do that, two components get separated in one side. To ensure the presented adaptability the components thickness has to be chosen carefully.

2.2.5 Cloth seals

As typical design approach, straight strip seals are commonly adopted for large interface gaps. Even stator parts move relatively each other and, if this movement is relevant, straight strips cannot adapt themselves to different geometrical configurations. As consequence of this, sealing performance decays and consumption rises [18]. Strip seals can adapt more effectively if thickness reduces, but also mechanical integrity reduces. To comply the presented necessities (life cycle and sealing performance) "*cloth seals*" are developed. A simplified scheme is shown as follow.

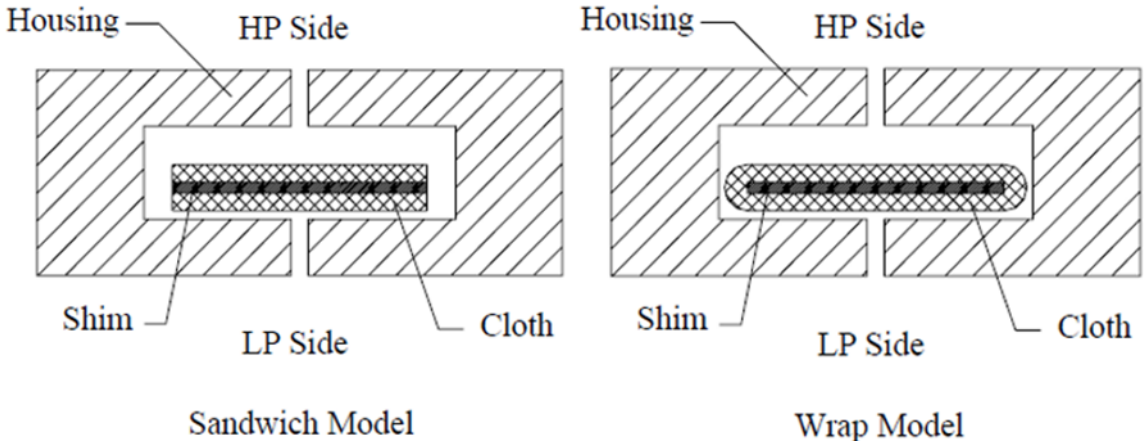

Figure 2.14 - Cloth seal [7]

This kind of seals have two main components: a variable number of thin metal sheets (*shims*), and a coating of a metal woven cloth. Cloth layer is sacrificial material that protect the shims

and it increase seal's thickness but not the stiffness. Shims ensure the mechanical strength and seal flexibility. Cloth layer is wrapped around shims and some spot welds along the center line lock up all (as it is shown in Figure 2.14).

2.3 AE94.3A strip seals

AE94.3A's strip seals are located along the whole turbine. Strip seals, object of the next analysis, are characterized by a not neglectable thickness that for convenience in the next chapters will be named as "*current-thick*". A simplified scheme is reported below (Figure 2.15) with the aim to show where this kind of seal is lodged. *Current-thick* strip seals are located at the outer diameter, between the plenum (orange portion - Figure 2.15 - is composed by many plenums) and the related vane (red squares - Figure 2.15); they are also positioned at inner diameter in some specific location.

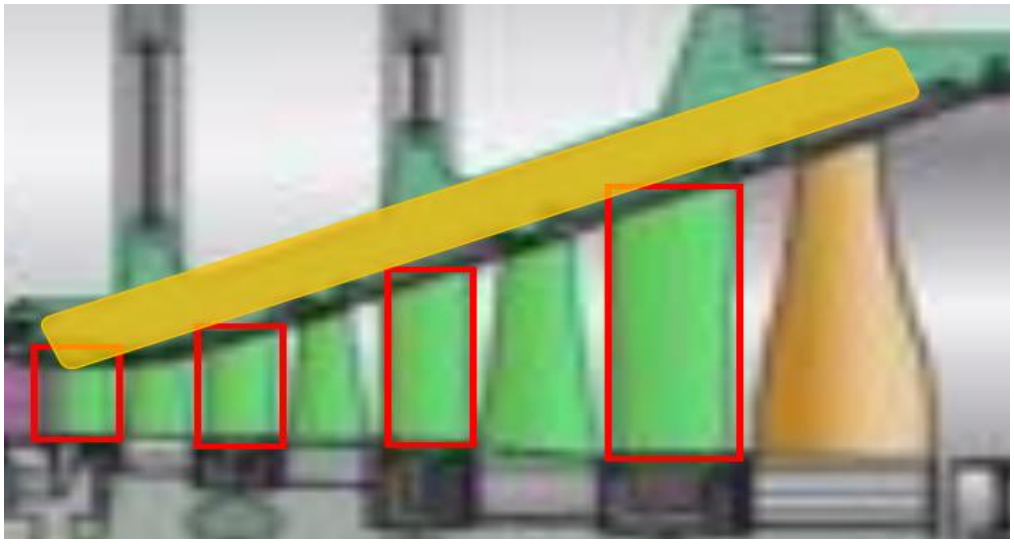

Figure 2.15 – strip seals positions – vanes: red squares; orange: shroud plenums

2.3.1 Strip seals working Δp

Strip seals are located in various axial positions of the turbine thus, they are characterized by different pressure gradients. Pressure along the turbine decreases, so each seal, that faces to only one plenum and hot-gas, is subjected to different pressure gradient along its axis. Accordingly to turbine pressure reduction, also SAS pressure can be reduced (as explained in paragraph 1.4), but plenum's pressure is constant. As consequence of this, each strip seal is subject to a rising pressure gradient from vane's leading to trailing edge. Pressure gradient variation along seal's axis has as consequence J_{eq} variation for the same seal and a different movement of the seal, that can be fixed in single position by the pressure or not (in this case it moves and vibrates thus it wears quickly).

Pressure gradient range to which a seal can be subjected is shown below.

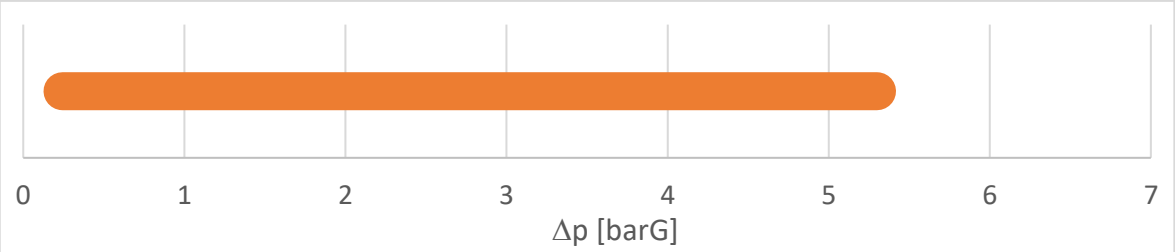

Figure 2.16 - strip seals possible working Δp

2.3.2 Current geometry

Strip seals that will be discussed in the present document are already named "*current-thick*" and they are characterized by a multitude of linear corrugations parallel to the seal's axis. These mentioned corrugations are represented by periodic peaks in the seal's cross section. They grant the seal deformability and avoid the failure; thanks to them, the seal is able to follow the engine displacement and groove misalignment. For what concerns the seals analyzed, the strips have a nominal height almost equal to the grooves' height; because of design tolerances, the grooves can be slightly bigger (order of magnitude of $[\mu m]$). An example is shown as follow.

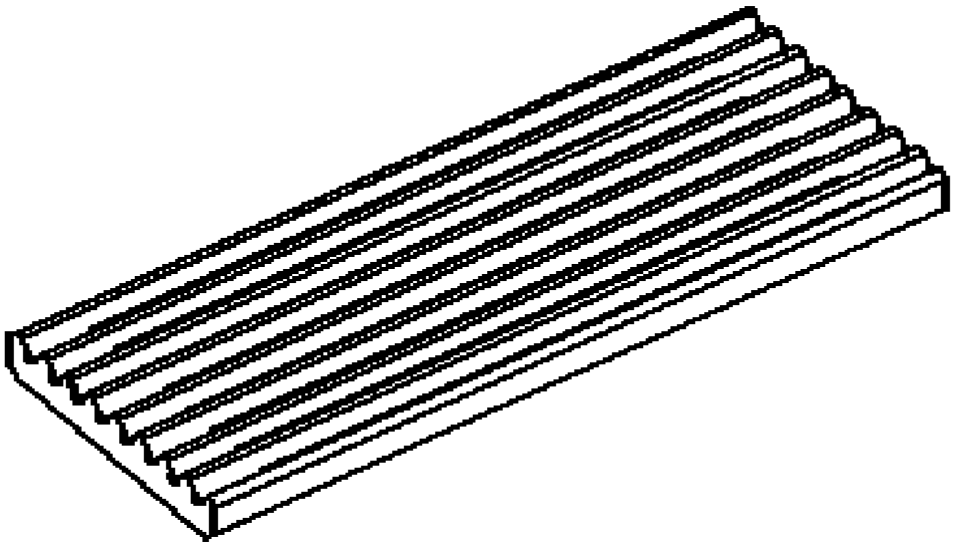

Figure 2.17 – 3D sketch of a strip seal - example

3 Test set-up

In the present chapter, test rig and test specimens will be described. The set-up parts adopted are chosen with the aim to characterize and then better quantify the leakage in the real engine. Different apparatus layouts are adopted in order to characterize in the best way as possible the strip seals behavior at different pressures and therefore mass flow rates. Moreover, different instruments are adopted in some test repetitions in order to measure with the proper sensitivity the whole tested range. Two different rig's geometry are tested to mimic an aligned and a misaligned status of the facing sides of the housing grooves which accommodate the strip.

3.1 Experimental apparatus

In the present section the laboratory equipment and the test rig will be described with a simplified scheme. The experimental apparatus was adopted in three different configurations. For each layout, a simplified scheme is reported below.

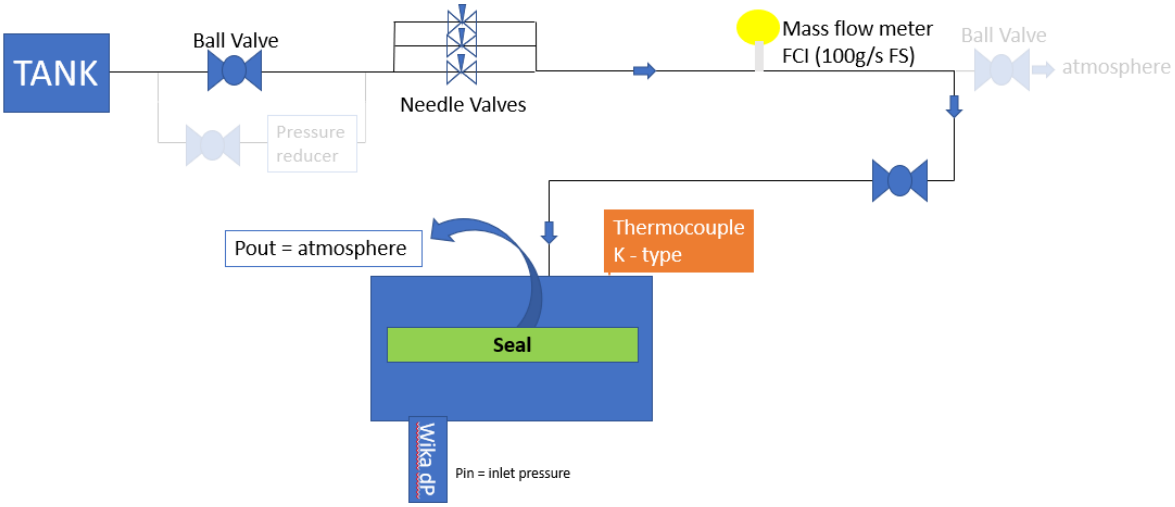

Figure 3.1 - Test rig - Air line scheme – Layout 1

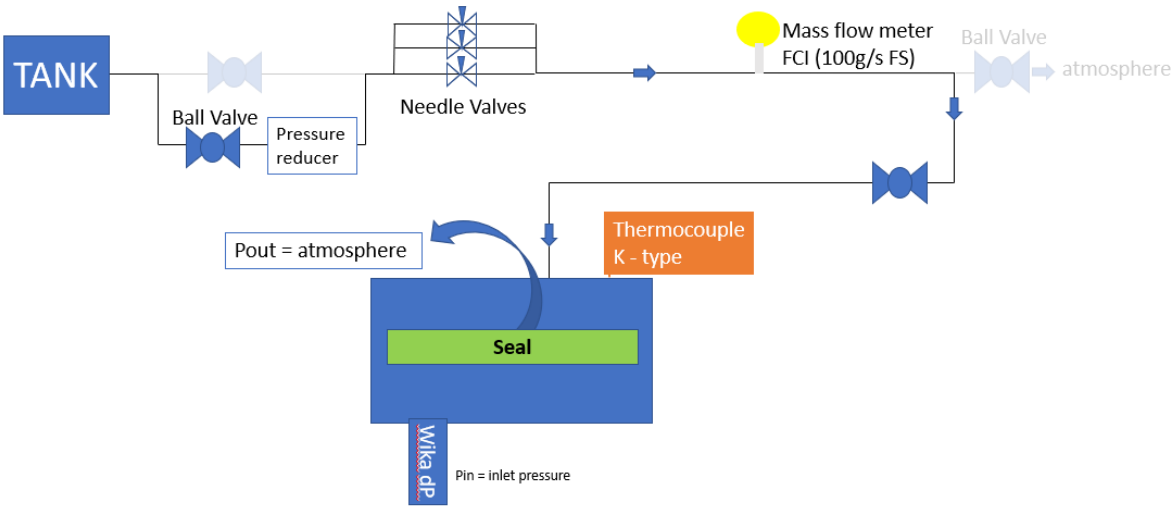

Figure 3.2 - Test rig - Air line scheme – Layout 2

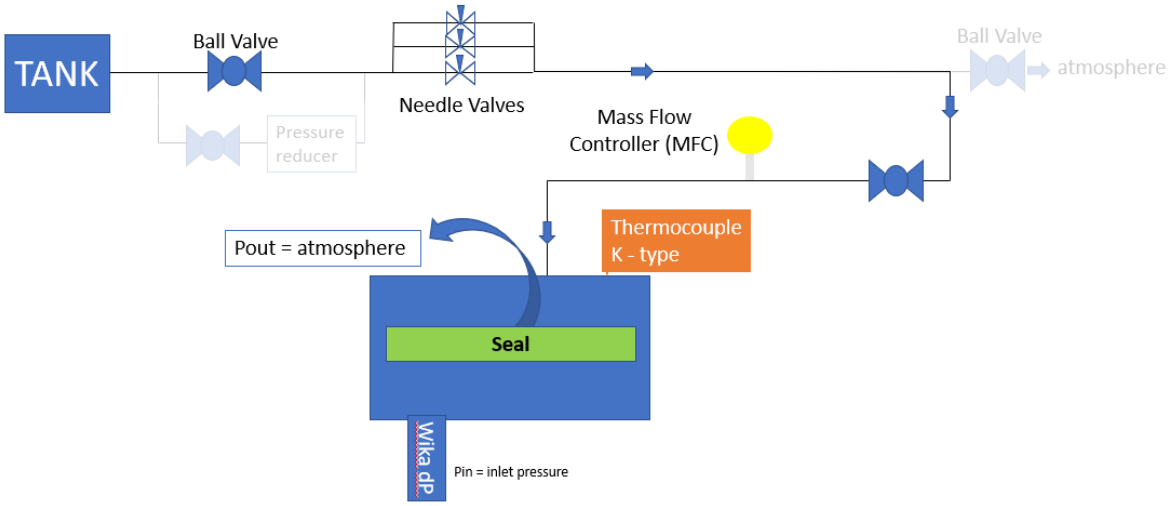

Figure 3.3 - Test rig - Air line scheme – Layout 3

The test rig is fed with compressed and dry air coming from a pressurized tank mounted downstream two compressors. The compressors are switched on when the gauge pressure in the tank is below 8.5 [barG] and switched off when it reaches 10 [barG]. A dryer is employed to remove the water content. DN50 piping feeds the compressed and dry air to the line; after that it passes through the Intelliflow (Figure 3.4), an Ingersoll Rand component that has the aim of controlling the system air pressure and guaranteeing its stability.

Figure 3.4 - View of the Intelliflow

Then it is split in two possible ways both endowed with a ball valve: one goes straight to the rig (Figure 3.1 and Figure 3.3) and a second one has a pressure reducer set to 3 [barG] (Figure 3.2). Downstream this part, three parallel-mounted needle valves (1", 1 ½" and 2") allow for a fine inlet mass flow rate and pressure regulation in layouts shown in Figure 3.1 and Figure 3.2. For what concerns the set-up reported in Figure 3.3, they were fully open.

As function of the adopted layout, the thermal mass flow meter is installed on a straight pipe after the regulation stage (Figure 3.1 and Figure 3.2) or the mass flow controller is adopted (Figure 3.3) but in a different line's location. The last instrument mentioned allows to measure and control the mass flow across itself (so the test article) with an internal valve.

After the mass flow meter there is a separation of the line in two parts. Each one can be sealed with an on/off ball valve; the first one is a leakage which discharge to the atmosphere, the second one leads to the test rig. The first mentioned was closed during all the tests reported in the present document.

The test line proceeds with a DN20 (3/4") pipe that feeds a plenum by a threaded hole positioned at the bottom. Finally, compressed air flows into the rig plenum placed below the strip seal where both air temperature and pressure are measured. Compressed air then flows across the seal and to the atmosphere, so the outlet pressure is the ambient one that it is acquired by a barometer and recorded.

3.2 Assembly

3.2.1 Test rig

In the following picture the air plenum that stands below the strip to be tested can be recognized. In that plenum pressure and temperature are measured.

Figure 3.5 – rig plenum

Innercover and innerframe components are manufactured different shape in order to create an aligned and misaligned groove hosting the strip seal. For what concerns the aligned configuration, the innerframe (Figure 3.6) has a flat surface with an opening slit in the center onto which it is placed the strip seal.

Figure 3.6 – aligned rig – innerframe

The innercover (Figure 3.7) is mounted on top of the innerframe and together they form the housing for the strip to be tested.

Figure 3.7 – aligned rig – innercover

The innerframe-innercover assembly creates a confined volume with the seal to be tested inside. This volume is sealed by a rubber O-ring.

Compressed air from the plenum will flow through the inner frame slit and will push the seal lifting it against the innercover surface. The innercover itself presents an opening slit to let the air flow out to the atmosphere. The two fundamental component's dimensions are shown in the table below:

Table 3.1 – aligned rig's dimensions

$\frac{\text{Groove depth}}{h_0}$	1.13 [adim]
Slit opening's length	305 [mm]

The quantity "h_0" is the *current-thick* strip seal's thickness. Noticing the groove depth ratio to h_0, it is clear that *current-thick* strip seal has a small space to move inside the rig.

Misaligned rig (Figure 3.8) allows to simulate the most typical engine's groove configuration. Due to geometrical tolerances and thermomechanical displacement, two seat sides may be not at the same radial coordinate thus the groove can be characterized by a misalignment. This particular condition is replicated by the presence of a constant height step in misaligned test rig (Figure 3.8).

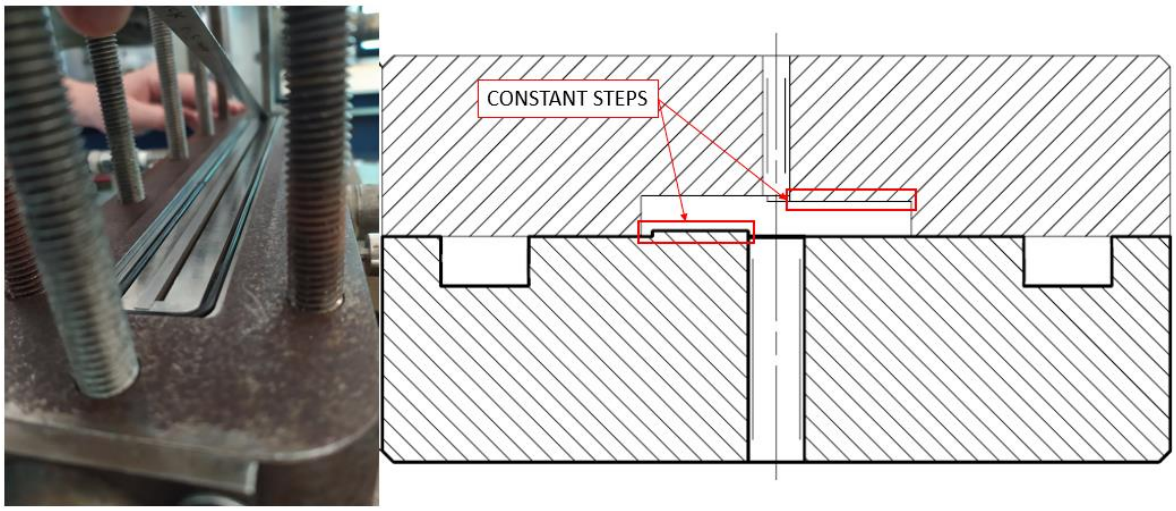

Figure 3.8 - rig in misaligned case - Innerframe and Innercover

Misaligned configuration (Figure 3.8) is characterized by a constant step in opposite side for the inner frame and the inner cover. Main dimensions are reported in the following table.

Table 3.2 – misaligned rig's dimensions

$\frac{\text{Groove depth}}{h_0}$	1.07 [adim]
Slit opening's length	305 [mm]
$\frac{\text{Step height}}{h_0}$	0.17 [adim]

In misaligned configuration, the manufactured rig is characterized by a smaller groove depth than the aligned one, due to the manufacturing tolerances.

In the engine, two groove sides are manufactured in the vane platform, this means that the groove is facing the other in the azimuthal direction. In experimental ambient, because of constructive necessities, innerframe and innercover simulate respectively the entire lower and upper groove surfaces. As consequence of the rig manufacturing, it is assembled "vertically".

3.2.2 Test articles

The different strip seals' characteristics are reported in the table below; worn seals' thickness distribution is also represented in Figure 3.9 in order to be as accurate as possible.

Table 3.3 - Seals' characteristics

Seal	Condition	Measured surface roughness Ra [μm]	Thickness [mm]		
			Trailing Edge	Center	Leading Edge
Current-thick	new	0.2	h_0	h_0	h_0
Thicker	new	0.6	h_1	h_1	h_1
Upgrade-thin	new	0.2	h_2	h_2	h_2
Current-thick - S3	worn	2.5	$\frac{h_0}{n} = h_3$	$\frac{h_0}{n} = h_3$	$\frac{h_0}{m} = h_4$
Current-thick - S2	worn	0.8	h_0	h_0	$\frac{h_0}{n} = h_3$
Current-thick - S1	worn	3.3	h_0	h_0	$\frac{h_0}{n} = h_3$
Upgrade-thin - worn	worn	0.2	h_2	h_2	h_2

In the columns related to seals' thickness, the values are expressed as parameters. Quantities h_0, h_1, h_2 represent the new seal thickness respectively for *current-thick*, *thicker* and *upgrade-thin*. It is verified the following condition: $h_1 > h_0 > h_2$

Regarding worn strip seals, instead, thickness is quantified with two non-dimensional coefficients: *m* and *n*. they comply with the following relations: $n, m > 1$ and $m > n$. Thus, the following relation is verified: $h_1 > h_0 > h_2 > h_3 > h_4$.

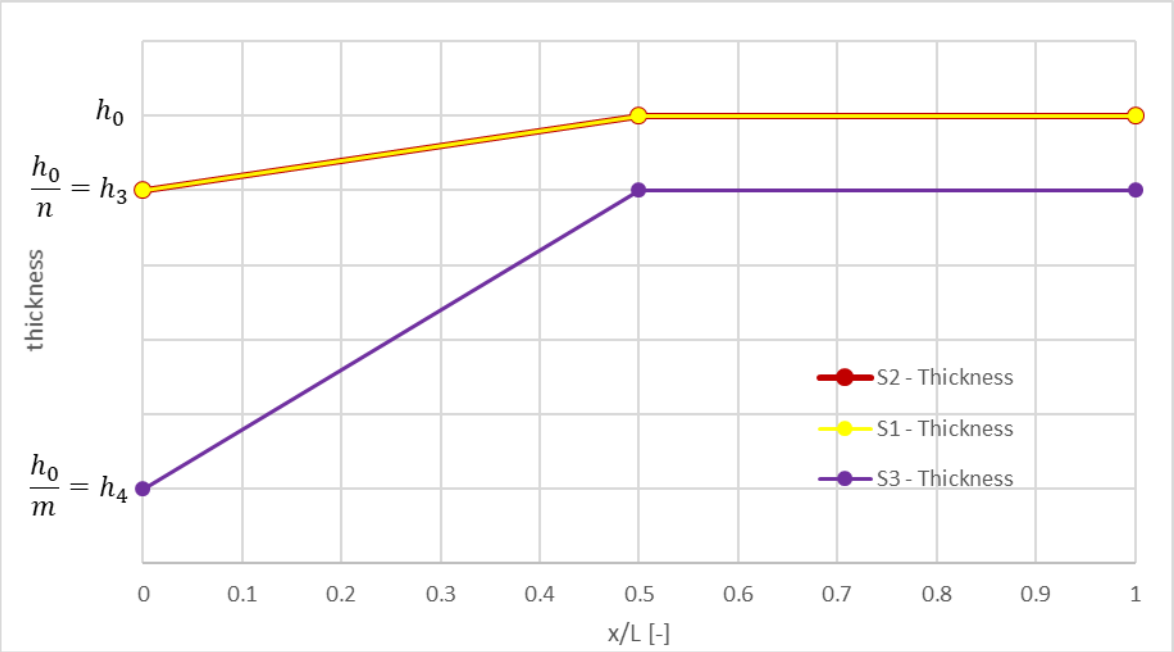

Figure 3.9 – worn thick seal's thickness distribution along its axis (0: LE; 1: TE)

All tested strip seals were cut to share the same length of about 305 [mm]. *Current-thick*, as already specified, is the seal geometry at the moment adopted in AE engines, *upgrade-thin* is the upgraded seal geometry and *thicker* strip seal has the aim to reproduce a particular scenario of the construction tolerances: it simulates the condition in which the seal has almost the same groove depth in the aligned configuration which is the most typical in AE gas turbines because of the nominal play(see the sketch in Figure 3.10).

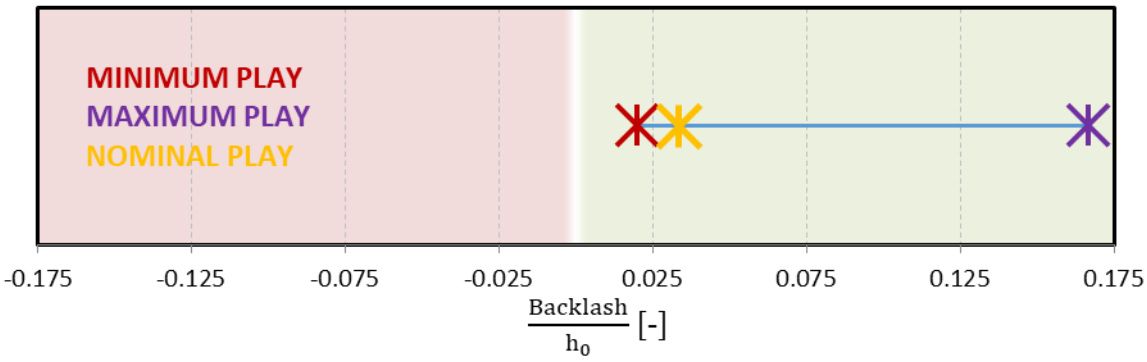

Figure 3.10 - nominal backlash range of engine seal-groove assembly

The AE94.3A seal has a nominal thickness of h_0. Figure 3.10 shows the constructive backlashes related to the grooves. Its nominal backlash is > 0 (Figure 3.10, orange star symbol), i.e., nominal groove depth is greater than h_0, but with order of magnitude of tens of [μm].

Whenever the rig groove is thicker than h_0 summed to nominal play, as it happens in the aligned rig (Table 3.1), *current-thick* seal can move quite freely inside the groove. Instead misaligned one, Table 3.2, is closer to the nominal condition.

If the groove depth is the same as the seal thickness (h_0) or really close (as it happens for nominal backlash) the seal cannot move. In order to evaluate this particular condition, *thicker* strip seal (thickness: h_1) was tested in the aligned assembly.

As it can be seen in Table 3.3, three worn *current-thick* seals were tested together with only one worn *upgrade-thin*. Worn *current-thick* seals present an inhomogeneous thickness along their length and it has been measured in three positions to account for this effect (see Table 3.3 and Figure 3.10).

New strip seals are shown in the following pictures.

Figure 3.11 –example of current-thick strip seal

Figure 3.12 – example of upgrade-thin strip seal

3.2.2.1 Worn strip seals

Different worn thick seals are reported in the following pictures.

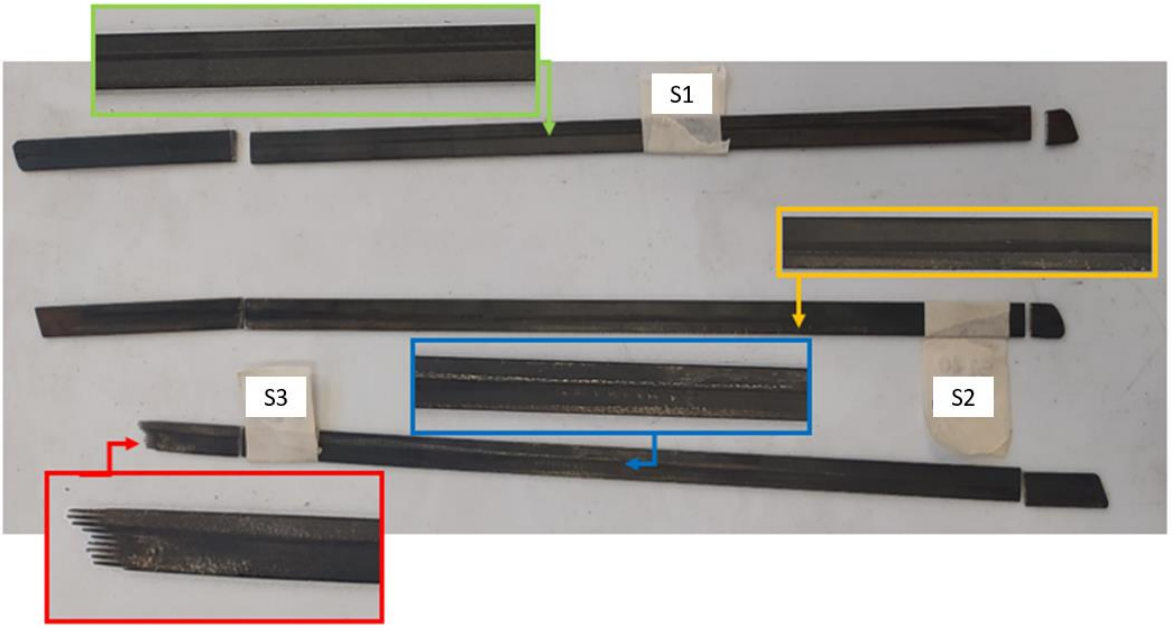

Figure 3.13 – example of current-thick strip seal – worn

Figure 3.14 – example of upgrade-thin strip seal – worn

It is evident from Figure 3.13 that the worst case is represented by the seal "S3" as its thickness is extremely eroded on one side (red box). Moreover, contact side shows a marked line on the center, where the seal is facing the hot gases (blue box); this particular mark is also found in the other two worn strip seals ("S2" in the orange box and "S1" in the green box) but in a lighter way than the worst one. This side of the seal displays the highest roughness. The other side instead does not show any particular sign.

Worn *upgrade-thin* strip seal tested was operated only few equivalent operative hours in Birr test center facility. The chosen seal was too large (transversally) to fit into the innercover so it was cut (Figure 3.14) by EDM to the right dimension. The cut was realized to preserve the central longitudinal region where the seal is facing the hot gases.

3.3 Test matrix

In the following table the tests that were performed in this campaign are reported.

Table 3.4 – test matrix

Test id	Configuration	Groove depth / h_0	Step height / h_0	Test article	Seal thickness (avg.)
1	aligned	1.13	-	Current-thick - new	h_0
2	aligned	1.13	-	Upgrade-thin – new	h_2
3	aligned	1.13	-	thicker	h_1
4	misaligned	1.07	0.17	Current-thick – new	h_0
5	misaligned	1.07	0.17	Upgrade-thin – new	h_2
6	misaligned	1.07	0.17	Current-thick – S3	$\frac{2 \cdot h_3 + h_4}{3}$
7	misaligned	1.07	0.17	Current-thick – S2	$\frac{2 \cdot h_0 + h_3}{3}$
8	aligned	1.13	-	Current-thick – S3	$\frac{2 \cdot h_3 + h_4}{3}$
9	aligned	1.13	-	Current-thick – S2	$\frac{2 \cdot h_0 + h_3}{3}$

10	misaligned	1.07	0.17	Current-thick – S1	$\frac{2 \cdot h_0 + h_3}{3}$
11	misaligned	1.07	0.17	Upgrade-thin - worn	h_2
12	aligned	1.13	-	Current-thick – S1	$\frac{2 \cdot h_0 + h_3}{3}$
13	aligned	1.13	-	Upgrade-thin - worn	h_2

Table 3.4 reports the non-dimensional groove depth and the average thickness for each test performed; moreover, non-dimensional step height is shown when the misaligned configuration is analyzed. Some tests were repeated multiple times to check for repeatability: different repetitions are identified by a letter which follows the test number (such as “1a”, “1b”, or “2c”).

3.3.1 Mounting procedure

The assembly procedure of the rig parts is an essential part: it needs to be done carefully to avoid any problem that can influence the tests results. First of all, inner frame is positioned into the rig’s plenum (Figure 3.5); “o-ring” has to be well positioned in its seat on the innerframe. After this, strip seal is placed on the center of the inner frame (Figure 3.15 - a, b), then it is covered with the innercover (Figure 3.15 - c, d). To lock up all the components, on the top of this, entire assembly was covered with the lid (Figure 3.15 - g). To perform a leakage test of the assembly, a blind flange provided with o-rings is placed on top of the slit lid (Figure 3.15- h). The procedure is reported below in Figure 3.15.

Figure 3.15 - assembly procedure for the assembly

3.3.2 Instrumentation

The instrumentation adopted during the test campaign and the inherent characteristics are reported in the table below. Notably, three different mass flow meters were used to cover different ranges of mass flow rate.

Table 3.5 - Instruments table

Sensor name	Sensor type	Quantity	Full scale (FS)	Error
Model ST75V Standard	Mass flow meter	Mass flow rate	100 [g/s]	1% of the measure + 0.5% of the FS
Brook instruments - Model SLA5853	Mass flow controller	Mass flow rate	3 [g/s]	0.9% of the measure if measure > 20 % FS; 0.18% of the FS if measure > 20 % FS

Brook instruments - Model SLA5853	Mass flow controller	Mass flow rate	20 [g/s]	0.9% of the measure if measure > 20 % FS; 0.18% of the FS if measure > 20 % FS
Thermocouple	Thermocouple k-type	temperature	1200 [°C]	0.75% of the measure
Trafag type 8253,79,24	Gauge pressure sensor	Gauge pressure	16 [bar]	0.1% of the measure

The characteristic of the instruments are used to report also the error bands in the charts that describe the seals behavior. In addition, since different mass flow meters were used in different repetitions of the tests, the correlation between the meter, the test numbers and the layout adopted (shown in paragraph 3.1) is reported in the table below.

Table 3.6 – mass flow meters adopted

Instrument	Experimental apparatus layout	Test-repetition
Mass flow controller - 3 [g/s]	Layout 3	2-c, 11-b, 13-b
Mass flow controller - 20 [g/s]	Layout 3	1-e, 12-b
Mass flow meter	Layout 2	1-d
Mass flow meter	Layout 1	All the other tests

3.4 Rig inherent leakage assessment

A blank test was performed prior to each test with the purpose of evaluating the leakages of the test rig. The rig is pressurized at 9 [barG] after being sealed with a blind flange closing the opening slit of the innercover (Figure 3.15 - h). A ball valve is closed upstream the rig to isolate it from the rest of the piping. The pressure decay into the rig is measured versus time (see Figure 3.16).

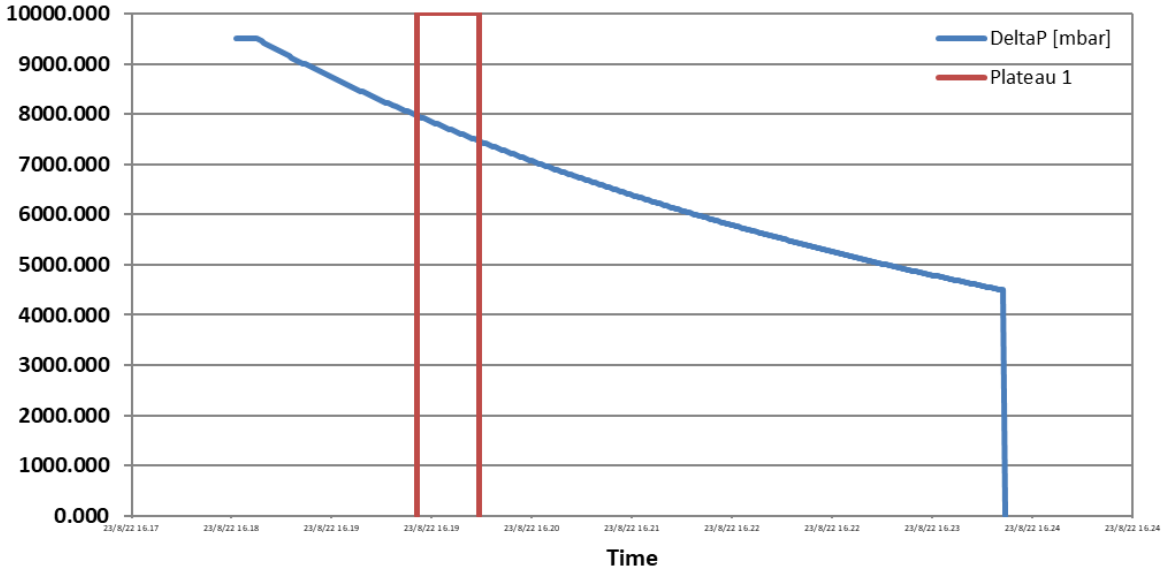

Figure 3.16 - leakage test - related to test 1

In order to evaluate the mass flow of air leaving the rig, the pressure decay function has been analyzed in the interval 7.5 [barG] < p < 8 [barG] (see the red box "Plateau 1" in the plot above). In the presented pressure range the experimental data are fitted with a straight line and the slope dp/dt is computed. According to the ideal gas law, it is possible to calculate the mass flow rate starting from the time variation of the pressure (dp/dt) as shown below:

$$p \cdot V = n \cdot R_0 \cdot T \tag{3.1}$$

$$\frac{dp}{dt} \cdot V = \frac{dn}{dt} \cdot R_0 \cdot T$$

$$\frac{dp}{dt} \cdot V = \frac{d}{dt}(n \cdot P_m) \cdot \frac{R_0}{P_m} \cdot T$$

$$\frac{d}{dt}(n \cdot P_m) = \dot{m}$$

$$\frac{R_0}{P_m} = R = 287\ [\frac{J}{kg \cdot K}] \tag{3.2}$$

$$\frac{dp}{dt} \cdot V = \dot{m} \cdot R \cdot T \tag{3.3}$$

Where:

p is the pressure;

V is the isolated volume;

n is the mole number;

R_0 is the universal gas constant;

T is the temperature;

t is the time;

P_m is the molecular weight;

$\dot{m}$ is the mass flow rate which exits from the rig;

R is the characteristic air constant.

Once the mass flow rate is evaluated, it is possible to estimate the equivalent area and the equivalent gap as follow.

$$A_{eq} = \frac{\dot{m}}{\sqrt{2 \cdot \rho \cdot \bar{p}}} \tag{3.4}$$

$$J_{eq} = \frac{A_{eq}}{L} \tag{3.5}$$

Where:

A_{eq} is the equivalent gap area un-directly measured;

ρ is the air density;

$\bar{p}$ is the average pressure in the range analyzed;

L is the length of the open gap;

J_{eq} is the equivalent gap.

The equivalent gap J_{eq} is computed using the length of the strip seal in order to compare the rig inherent leakage to the leakage of the seal measured during the tests.

The results of the blank tests are reported below, where in the column "TEST" the number identifies the test number (from 1 to 13) and the letter identify the repetition of the same test.

Table 3.7 - equivalent gap of the rig with the closing flange

TEST	$J_{eq}/J_{eq_{ref}}$	**TEST**	$J_{eq}/J_{eq_{ref}}$	**TEST**	$J_{eq}/J_{eq_{ref}}$
1a	8.55E-03	3b	6.26E-03	9a	6.52E-03
1b	8.19E-03	4a	4.67E-03	10a	6.58E-03
1c	5.92E-03	4b	8.56E-03	11a	8.12E-03
1d	6.83E-03	5a	6.37E-03	11b	5.02E-03
1e	6.49E-03	5b	8.46E-03	12a	7.13E-03
2a	9.38E-03	6a	7.19E-03	12b	3.89E-03
2b	7.47E-03	7a	7.26E-03	13a	5.43E-03
2c	2.59E-03	8a	6.77E-03	13b	4.80E-03
3a	6.97E-03				

As seen in Table 3.7, the equivalent gap values (scaled with a reference value which is the same that will be adopted in Chapter 4 referred to *current-thick* strip seal in aligned configuration) obtained with the sealed rig are neglectable compared to results that will be discussed in next chapter.

4 Test outcomes

In this chapter experimental tests results are discussed. The aim is to better understand the strip seal technology behavior and gain insight into the seal behavior once mounted in the real gas turbine.

The test campaign is aimed to quantify the characteristic leakage of the *strip seals* used to separate the stator-stator parts in gas turbines. A comparison of the sealing capability of *current-thick* strip seals (adopted at the moment) and *upgrade-thin* ones (upgraded version) is reported in this section. Moreover, in order to have more representative data, brand-new and worn strip seals have been tested in different geometries, namely hosted inside both aligned and misaligned groove sides.

All the tests have been conducted in the same way, that is by increasing the pressure drop across the seal in discrete steps of dp = 0.5 [barG] till reaching the maximum pressure of 10 [barG] and then going back to dp = 0 [barG] in an analogous manner. At each step, a stabilization time of about 60 seconds was waited to ensure a good quality of the data. The pressure was ramped up and down to check for hysteresis cycles. For same tests the rig was disassembled and re-assembled in order to have independent measurements on the same test object.

All the shown experimental results display the mass flow rate and equivalent gap scaled with reference values, as related to *current-thick* strip seal. Mass flow ratio and equivalent gap ratio will be reported in the following plots with reference values as denominator; this caution is due to privacy restrictions about sensitive data. The mentioned quantities are defined as $\dot{m}_{ref}$ and $J_{eq_{ref}}$ (which is the same value adopted in paragraph 3.4) and they are contained in the range from 1 [g/s] to 10 [g/s], for what concerns $\dot{m}_{ref}$, and from 0.001 [mm] to 0.100 [mm].

4.1 Activation phenomenon and hysteresis cycle

Whenever the seal can move inside the groove, it is subjected to “activation phenomenon”.

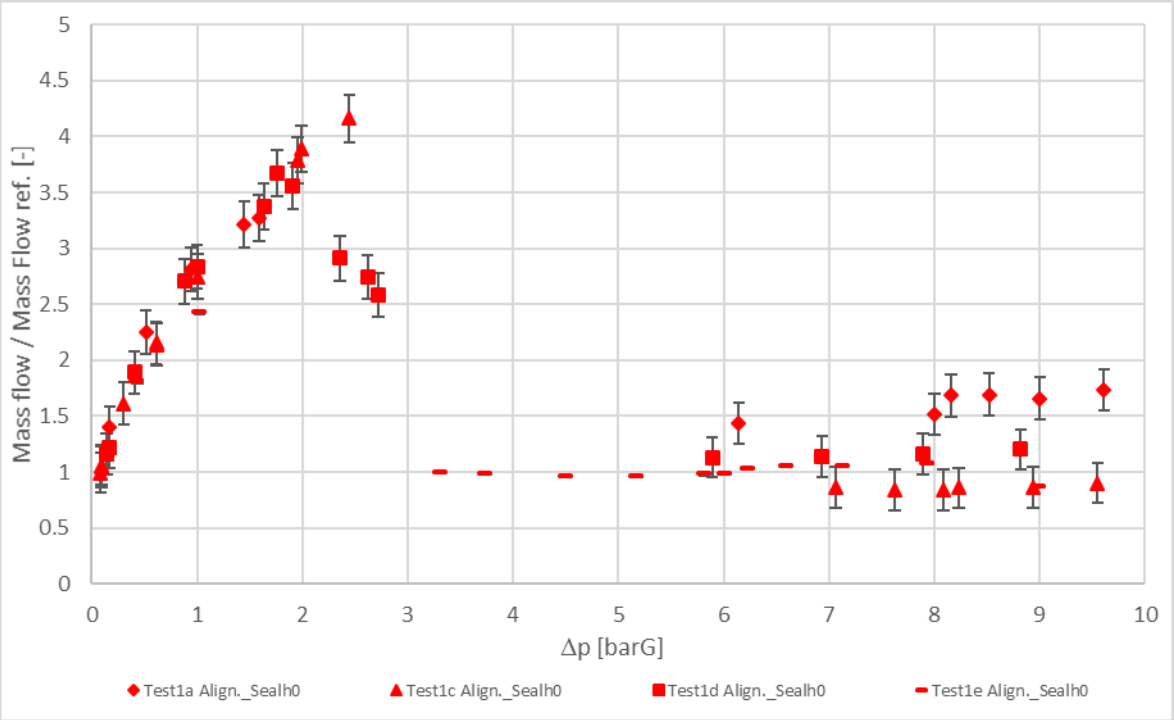

Figure 4.1 - activation phenomenon (TEST 1)

Figure 4.1 describes the non-dimensional mass flow rate versus the pressure drop across the seal (dp); the chart shows a mass flow increase until almost dp = 2 [barG], while at larger pressure gradient values the mass flow quickly decays.

The intermediate pressure range where the mass flow rate drops is the "*activation region*": this region is unstable, pressure drop cannot be controlled since a slight variation of the pressure regulation valve brings to a strong, uncontrolled, variation of dp. Pressure drop can jump from 2 [barG] to 6 [barG] in few seconds and dimension-less mass-flow ratio abruptly drops down from 4 to 1 at the same time. In this dynamic condition, a stable regime cannot be reached, and no reliable experimental points can be taken. This particular behavior is due to the strip seal activation, a mechanism which could be explained as follow: as hypothesis, the seal is lifted up from the air flow and pressed against the exit slit of the innercover; once the pressure force is enough to increase the seal-innercover contact force, the sealing effect improves, hindering the air flow. In this condition we assist to a pressure build-up upstream of the seal which in turn improves the sealing ability of the strip seal itself thus realizing a positive feedback effect.

Moreover, typically, the seal behavior is described by a hysteresis cycle. Below the strip's behavior (related to test 1) with a distinction between the ramp-up and down is reported.

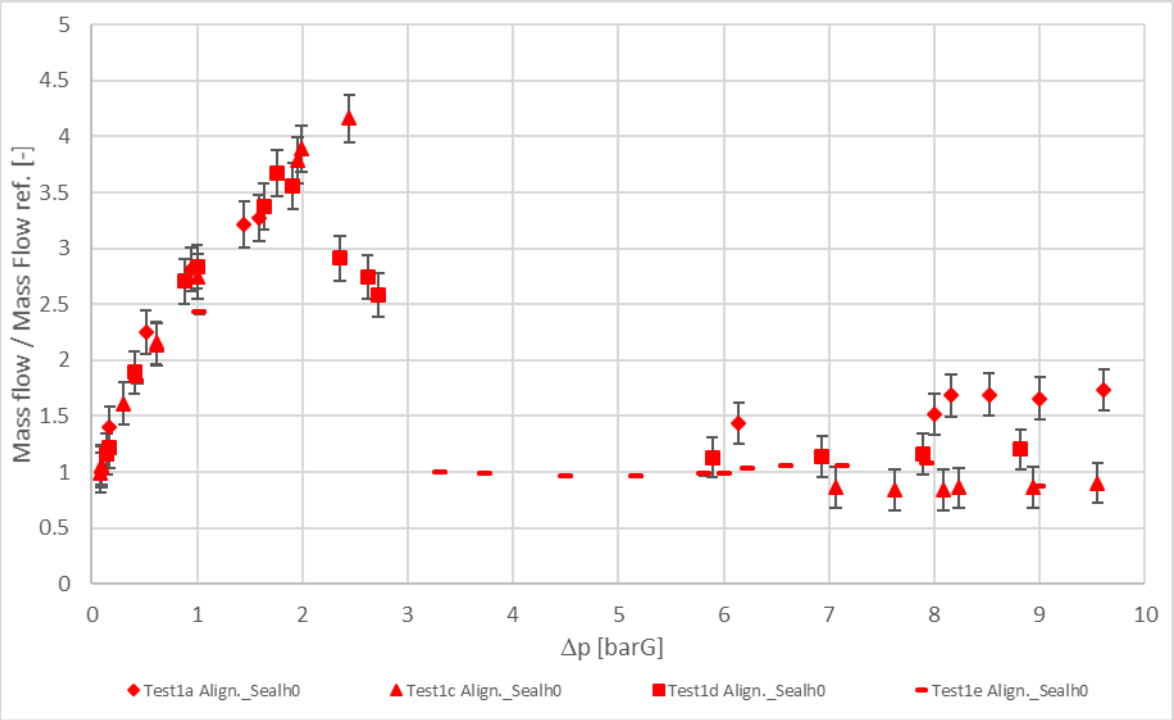

Figure 4.2 - hysteresis cycle (TEST 1); ramp-up and ramp-down

Figure 4.2 shows the test 1 results with a distinction between the pressure ramp-up (blue symbols) and down (orange symbols). Different repetitions are identified by different symbols. If the ramp-up symbols are considered (blue ones), it can be concluded that the activation pressure is between 1.5 [barG] and 2.5 [barG]. Instead, when the ramp-down is observed different values are found, with a de-activation pressure gradient between 3 [barG] and 6 [barG].

4.2 Outcomes analysis

4.2.1 Test comparison: new seals, 2019 vs 2022

The presented activity originally started in 2019, with some differences on the misaligned test rig. Instead, the same aligned test rig of previous internal studies is adopted. As a first step in the test campaign, some tests already performed in the previous 2019 test campaign were repeated to check for repeatability. All the following charts comply with the legend reported in Appendix A: charts legend.

A comparison between old and new experimental data will be presented here; this is possible only in the aligned configuration for *current-thick* and *upgrade-thin* strip seal as it was explained few lines above. The two following graphs show the non-dimensional air mass flow ratio across the strip seal versus the pressure drop across it.

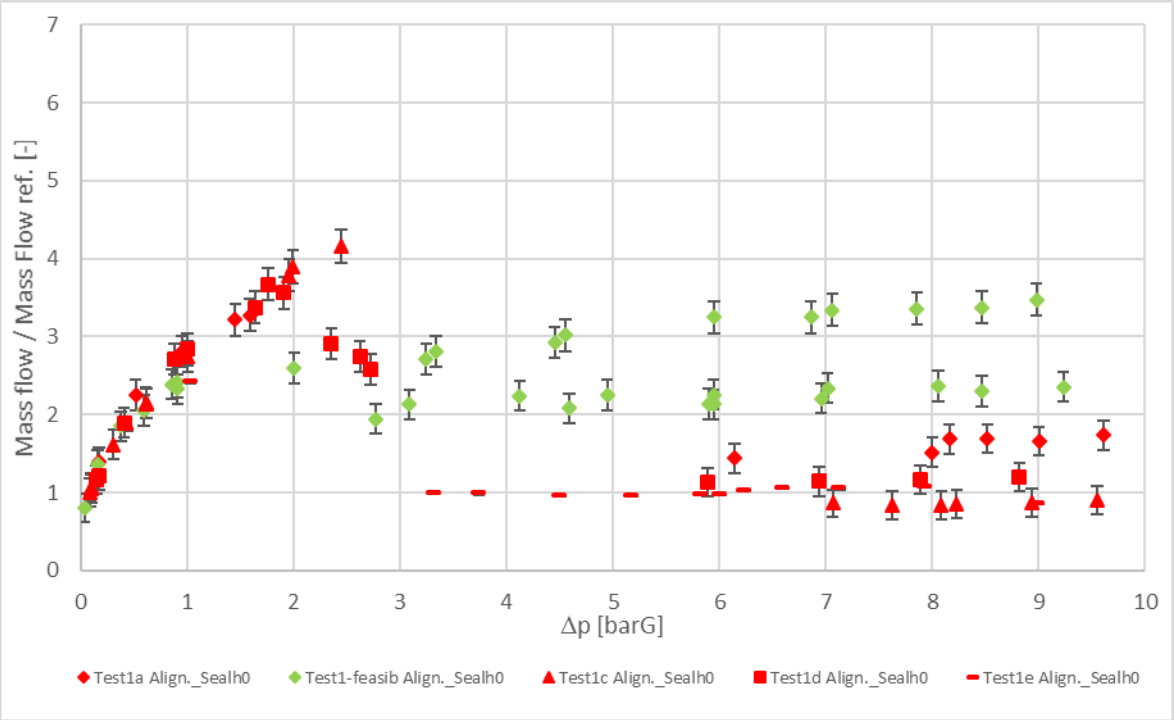

Figure 4.3- mfr -Test 1 - aligned – current-thick - 2019 vs 2022

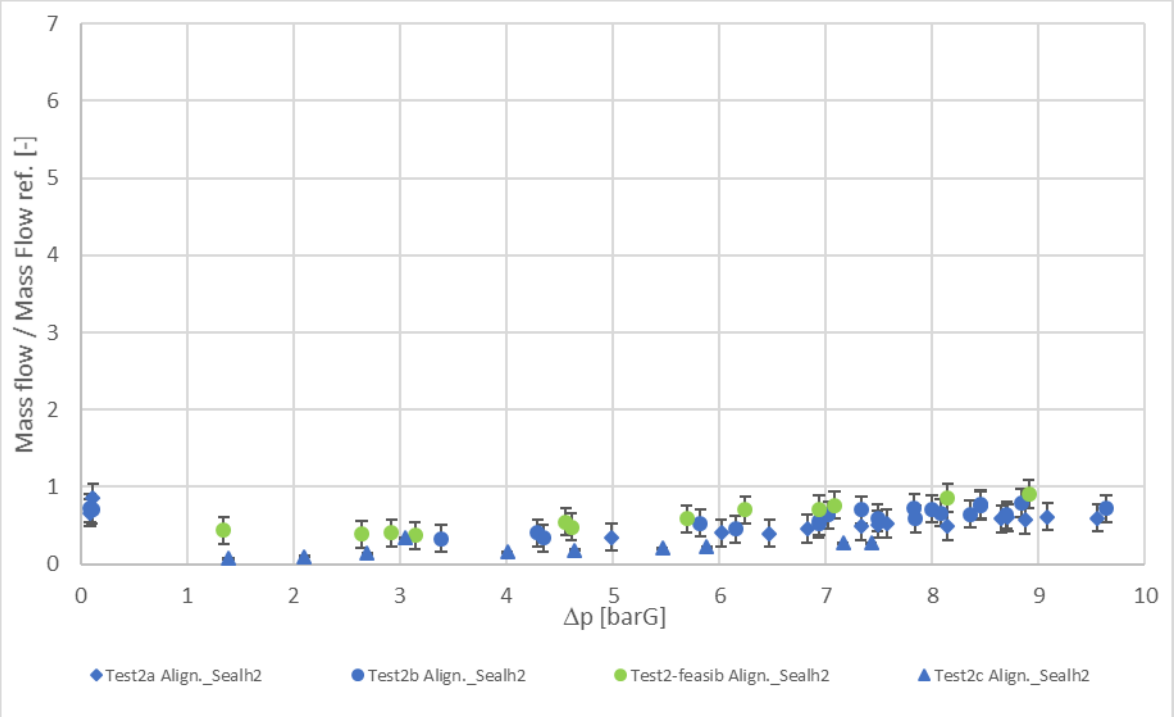

Figure 4.4 - mfr – Test 2 - aligned – upgrade-thin - 2019 vs 2022

The behavior of *current-thick* and *upgrade-thin* strip seals measured in 2022 (blue and red symbols) is compared to the same sealing measured in 2019 (green symbol) in the graphs above. Data are presented with error bars (black bars) estimated from the instrumentation nominal precision.

Some differences between old and new results (see Figure 4.3) are present especially in high pressure regime while in low pressure regime there is a good overlap of the data. Test 1 has been repeated four times (test 1 - a, c, d, e) showing a good repeatability of the test with the hardware currently used. Care was taken in cleaning the rig from dust and grease and during mounting of the seal in order to leave it free to move and not clamped in between the innercover and innerframe. Despite all these precautions, the data measured in 2019 results to be about a factor of 2 higher than the one measured in 2022 for *current-thick* strip seal in high pressure regime.

The scatter between the 2022 repetitions is likely due to the various positions that the seal can assume in the groove because its activation movement has a sort of randomic behavior.

For what concerns the *upgrade-thin* strip seal (test 2), it can be said that no significant differences between the old and new data (see Figure 4.4) are present.

Below, the two analogues plots are shown but, in this case, it is analyzed the equivalent gap ratio instead of the mass flow rate.

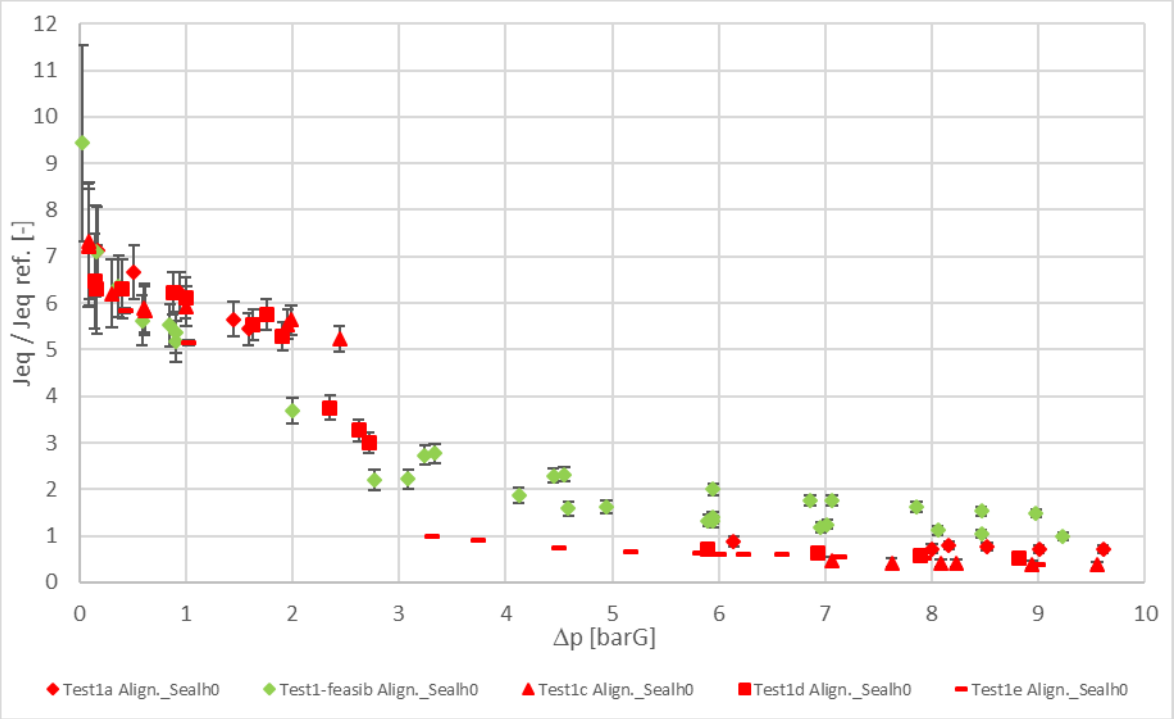

Figure 4.5 – J_{eq} – Test 1 - aligned – current-thick - 2019 vs 2022

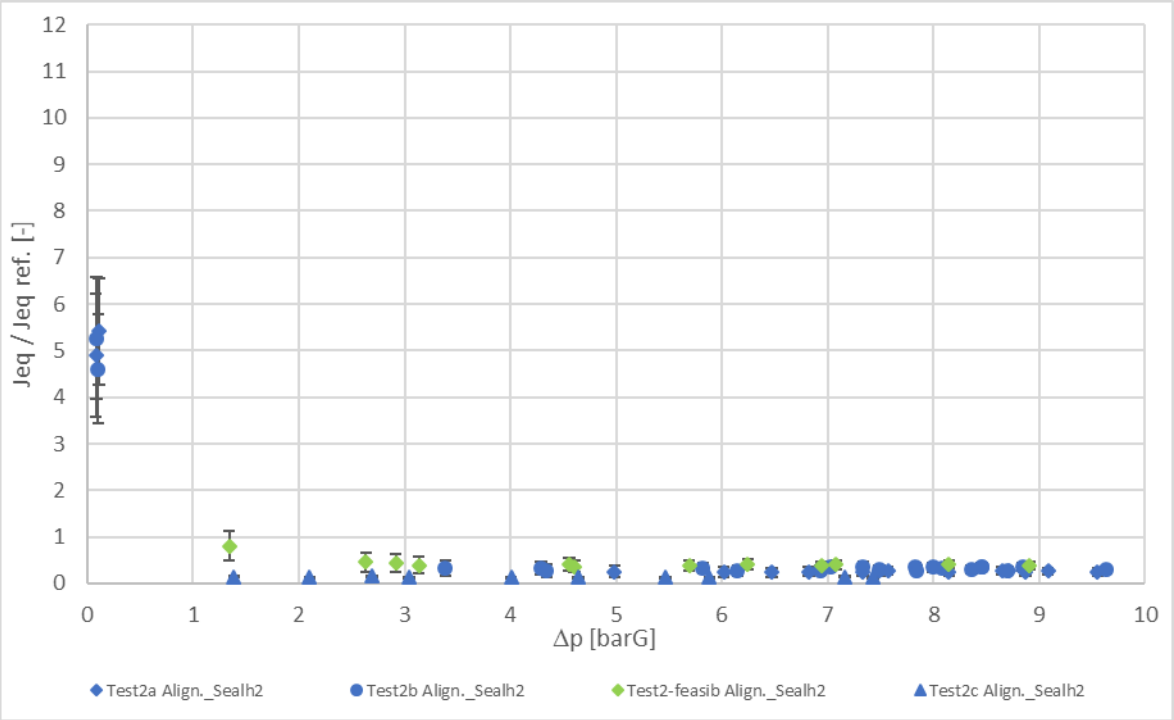

Figure 4.6 – J_{eq} – Test 2 - aligned – upgrade-thin - 2019 vs 2022

When the equivalent gap J_{eq} versus dp is considered, it can be noticed that 2019 and 2022 data is qualitatively the same for what concerns *upgrade-thin*. However, it is now shown that the largest difference between 2019 and 2022 data related to *current-thick* seal (dp > 3 [barG]) happens at rather low J_{eq} ratio values (< 2) so, since the reference value is in order of [µm], it is of minor importance.

4.2.2 Comparison: new seals aligned; *current-thick* vs *upgrade-thin* (test 1 vs test 2)

In this section the differences between new *current-thick* and *upgrade-thin* strip seals will be analyzed, in terms of mass flow and equivalent gap ratios.

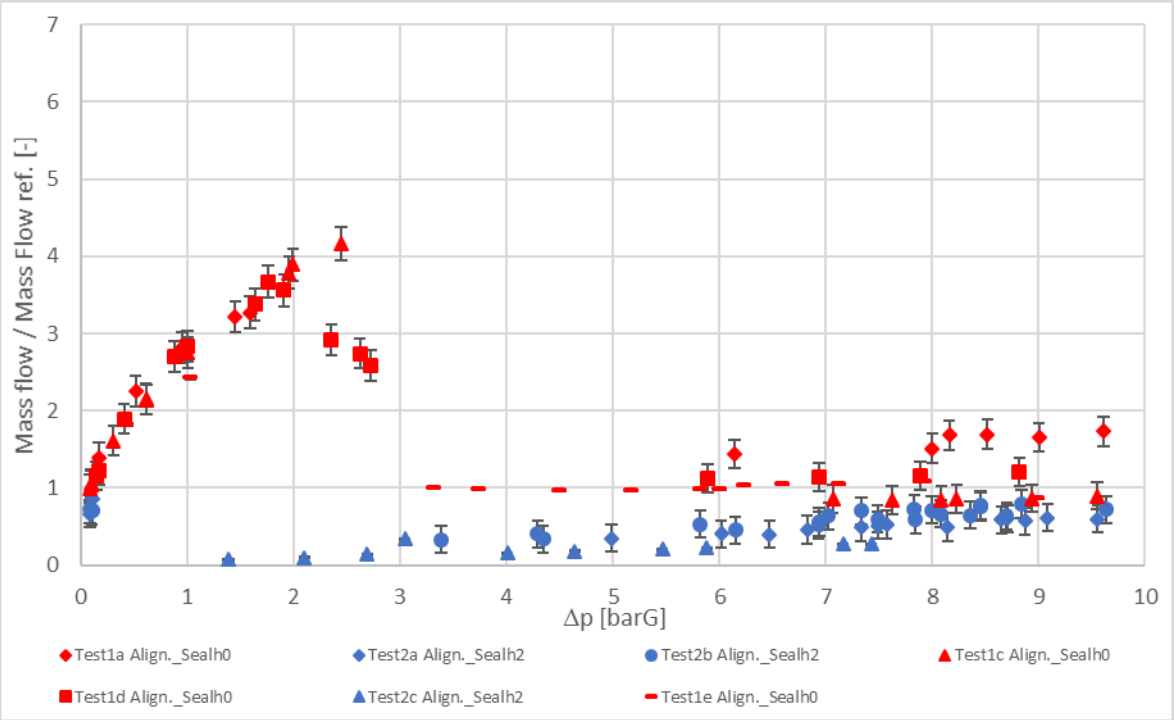

Figure 4.7 - mfr - Test 1 vs 2 - aligned – current-thick vs upgrade-thin

In Figure 4.7 it can be seen that in test 1 the mass flow rate increases almost linearly until about $dp \sim 2.3$ [barG] and then it decreases rapidly and remains almost constant in the high pressure regime (after the activation, paragraph 4.1).

Something different happens for *upgrade-thin* strip seal, in fact the activation phenomenon is at lower pressure because of the lower seal's weight; after the activation the mass flow rate slightly increases with the pressure but remaining always below what measured with the *current-thick* seal.

Similar considerations hold true for the equivalent gap which is reported below for the same tests.

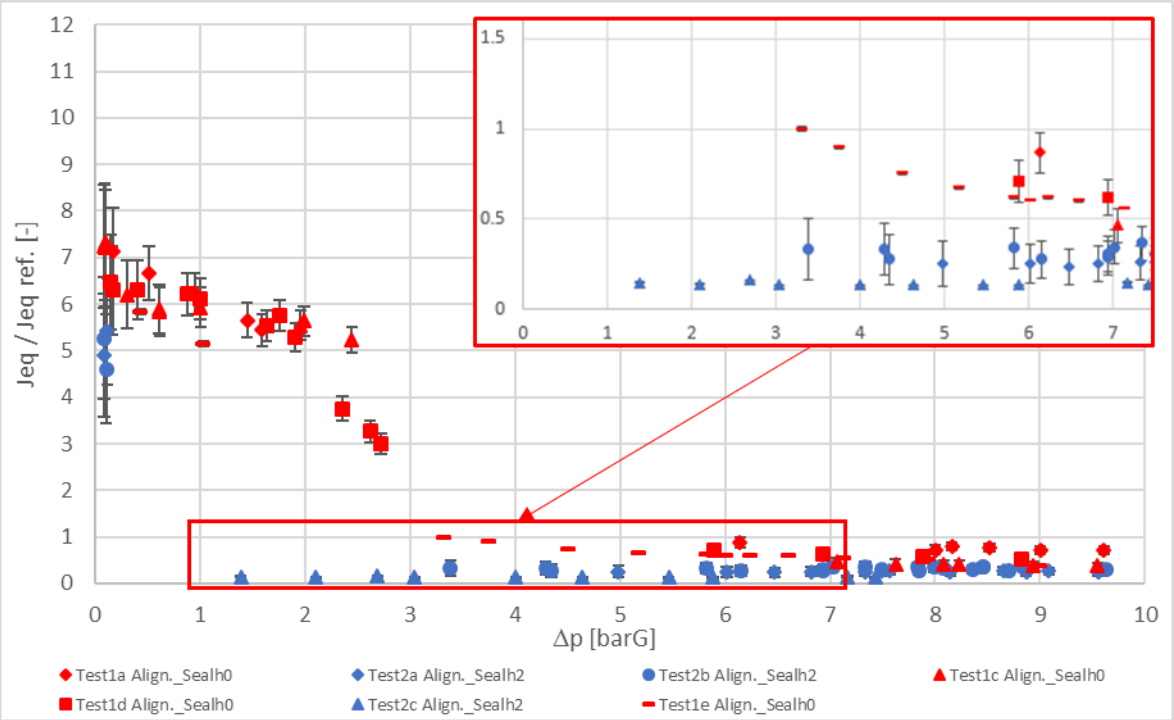

Figure 4.8 - J_{eq} - Test 1 vs 2 - aligned - current-thick vs upgrade-thin

Figure 4.8 shows a higher equivalent gap for *current-thick* strip seal compared to thinner one. Differences at high pressure are not significant while in the engine pressure range (up to 5 [barG], Figure 2.16), *upgrade-thin* seal performs better than *current-thick* one. Elastic deformation capability that characterizes *upgrade-thin* strip seal could be at the origin of its better performances in high pressure range (dp > 3 [barG]), seal's weight, so the activation pressure, ensures lower J_{eq} values in low pressure range (dp < 3 [barG]).

4.2.3 *Thicker* strip seal

As it was mentioned about Figure 3.10 discussion, also *thicker* strip seal was tested. In this particular case there is not the activation phenomenon because the strip seal cannot move into the groove, as it was specified in paragraph 3.2.2. The mass flow ratio chart is reported below.

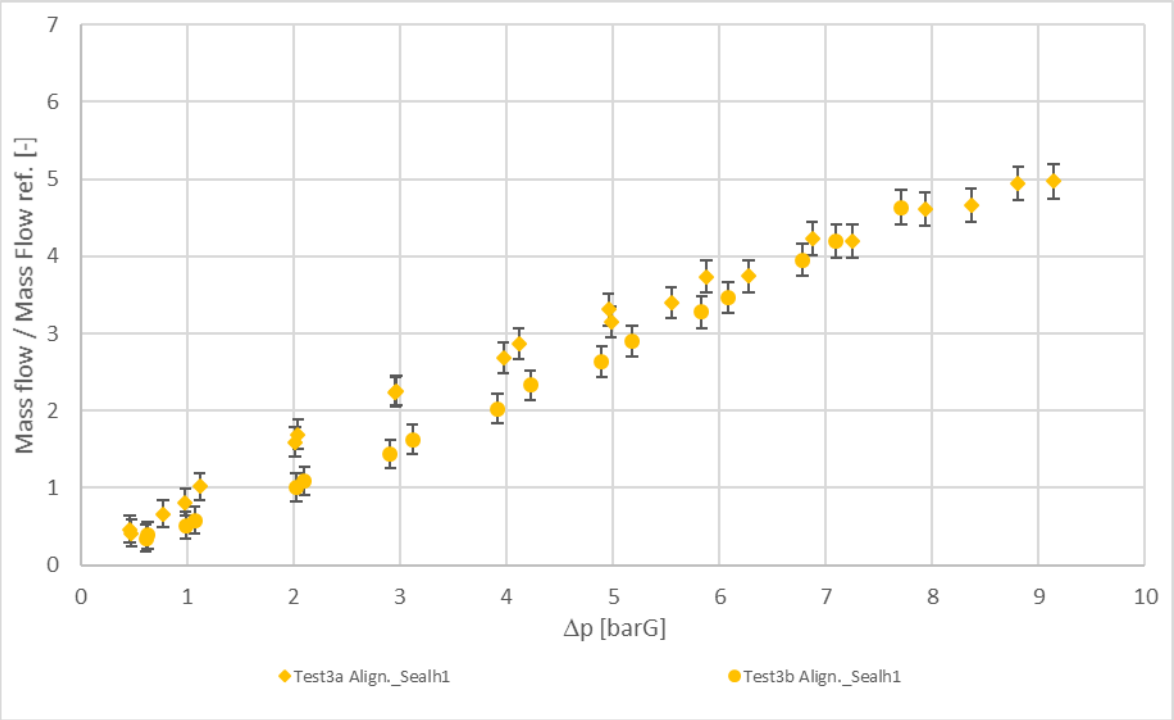

Figure 4.9 – mfr - Test 3 - aligned - thicker

The mass flow rate increases linearly with the pressure and no activation of the seal is observed (Figure 4.9). A slight difference, out of the error measurement bars, between the two repetitions of the test, especially in the pressure range between 2 [barG] up to 5 [barG], is reported. It can probably be ascribed to a different positioning of the seal into the groove. Following the equivalent gap is reported.

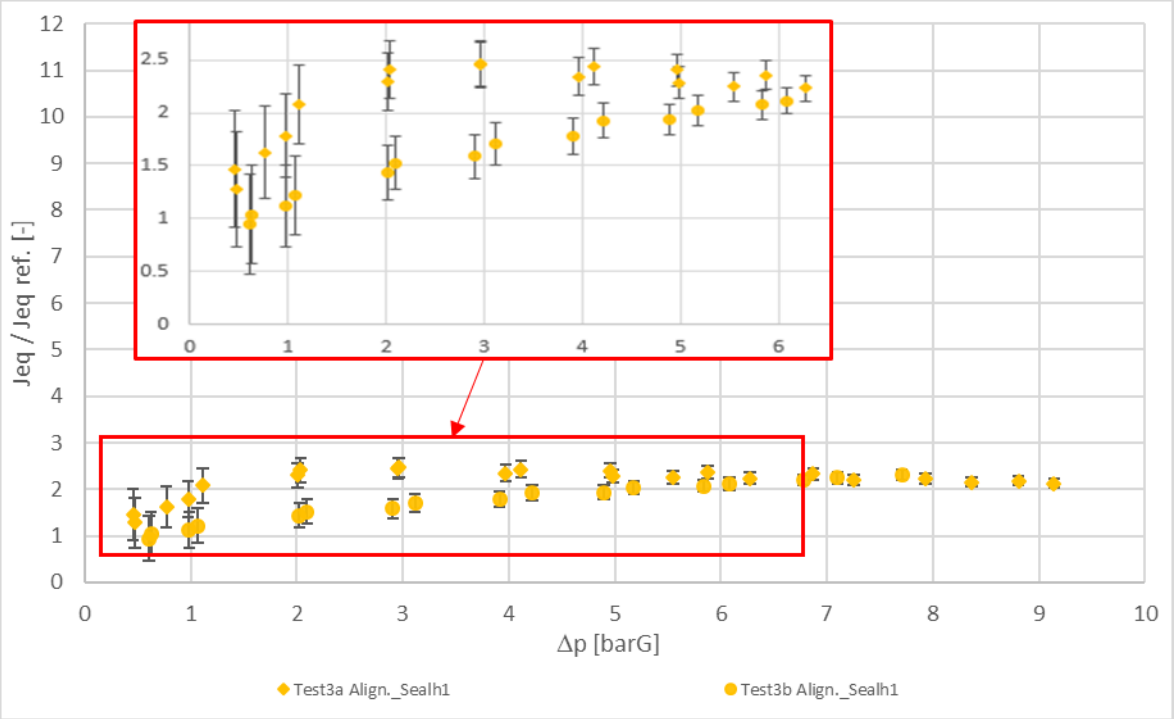

Figure 4.10 – J_{eq} - Test 3 - aligned - thicker

In the plot above, the differences between the two repetitions are still detectable (Figure 4.10, red box). Moreover, both the repetitions are characterized by a smooth increase of J_{eq} until a "saturation" level at about $\frac{J_{eq}}{J_{eq_{ref}}} = 2$ that is reached at almost dp = 3 or 4 [barG].

4.2.4 Comparison: new *upgrade-thin* strip seal, misaligned vs aligned (test 2 vs test 5)

In the real engine it often happens that two stator vanes presents a little radial displacement which results into a misalignment of the groove where the strip seal is lodged. This condition is simulated in the laboratory by employing a new innercover and innerframe (already described in paragraph 3.2.1, Figure 3.8) which replicates a particular misaligned condition. Experimental results, related to *upgrade-thin* strip seal, obtained with this particular rig are presented in this paragraph and compared to the aligned configuration. The mass flow chart is reported as follow.

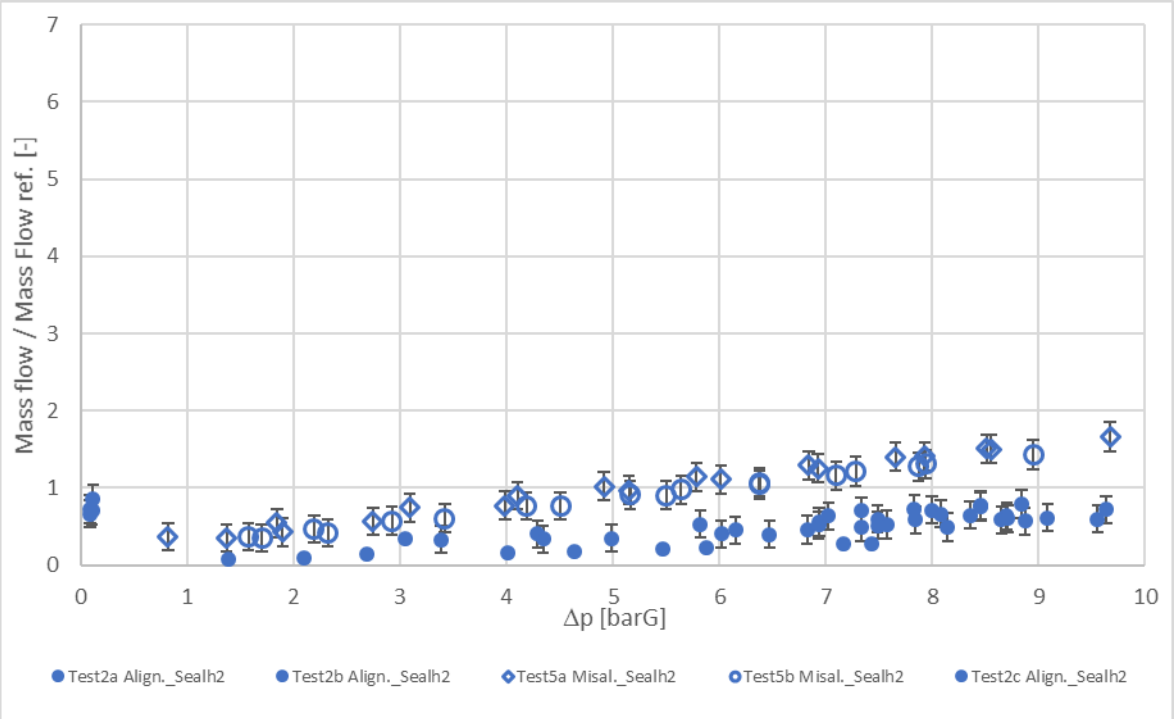

Figure 4.11 - mfr - Test 2 vs 5 - upgrade-thin – aligned vs misaligned; solid symbols: aligned; open symbols: misaligned

The mass flow increases in the misaligned case compared to the aligned one and the activation process happens at lower pressure in the misaligned rig. The mass flow ratio increase in the misaligned case can be partially attributed to a spurious contribution due to a triangular shaped hole (A_{hole}) which is formed by the tilted seal into the misaligned geometry (Figure 4.12).

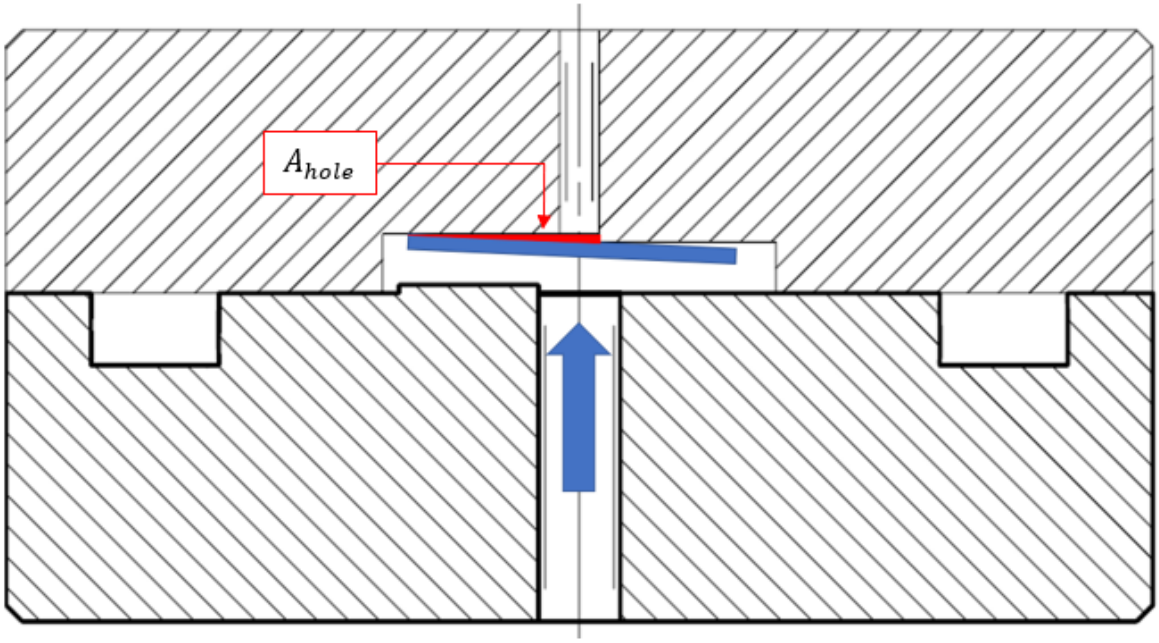

Figure 4.12 - misaligned geometry – upgrade-thin - The blue arrow represents the direction of the air flow impinging on the seal

The rig's geometry changes, thus the contact type will be different compared to the aligned configuration; as it was said above, because of the step presence, the seal is slightly tilted and a triangular area A_{hole} is formed at both the extreme sides of the seal. The pressurized air can potentially flow and exit the rig from these two open triangular gaps. With reference to the misaligned rig's geometry, it is admissible to estimate A_{hole} with the hypothesis of un-deformable strip seal. As result of the present consideration the triangular area is shown in Figure 4.12.

However, during the tests it was observed that the air flowed out from only one side of the rig, the opposite one seemed to be completely close. Probably the seal positioned itself in a particular configuration in which it is pressed to one side of the rig and thus one of these triangular gaps is closed. As conclusion of the present remark, A_{hole} can be considered only once. In order to better compare the J_{eq} values obtained in aligned and misaligned configurations, it is possible to remove the area A_{hole} from the measured equivalent area as explained in the equation below:

$$J_{eq} = \frac{A_{eq-measured} - A_{hole}}{L} \tag{4.1}$$

Where:

$A_{eq-measured}$ is the equivalent gap area measured during the acquisition;

A_{hole} is the lateral triangular shaped open gap;

L is the strip seal length;

J_{eq} is the equivalent gap related to the seal-rig contact.

As result of the presented considerations, the equivalent gap chart is shown below.

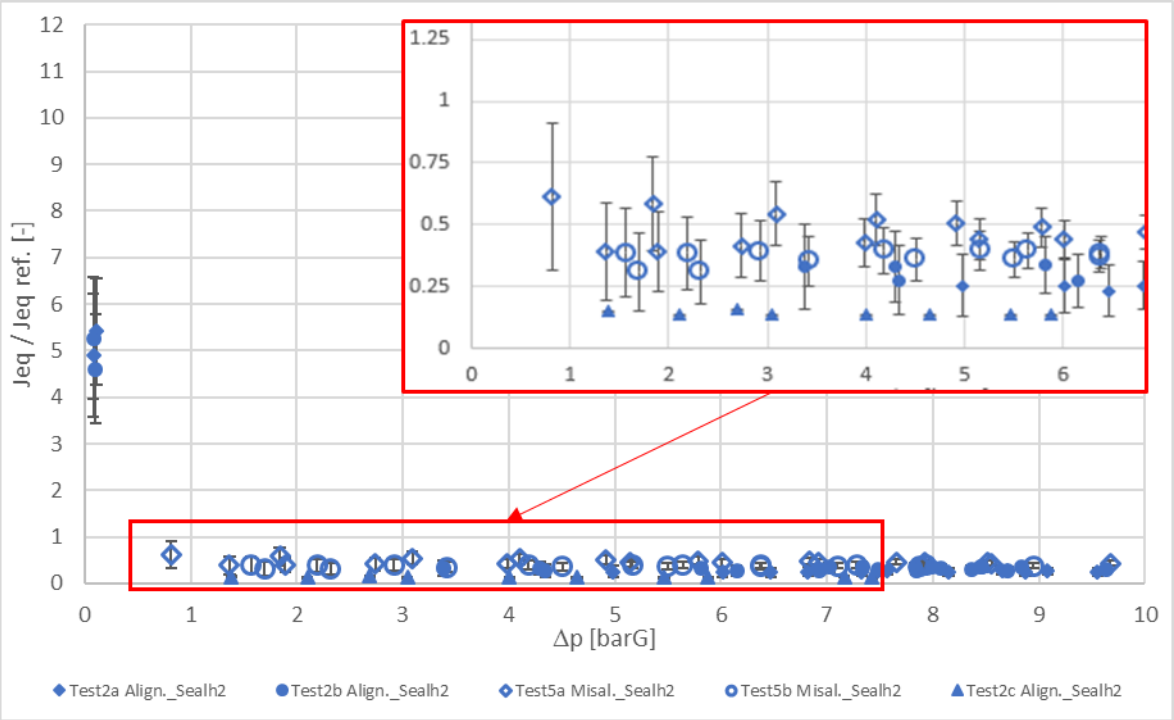

Figure 4.13 - J_{eq} - Test 2 vs 5 - upgrade-thin – aligned vs misaligned; solid symbols: aligned; open symbols: misaligned

It can be noticed that the J_{eq} is almost the same for the configurations tested even if the contact type is not planar. The present consideration can be validated if Figure 4.13 – red box – is considered. The results can be ascribed to linear contact which, because of the high local stress, generates local deformations that increase the sealing capability (as described by Bricaud et al. [16] and already introduced in paragraph 2.1).

4.2.5 Comparison: new *current-thick* strip seal, aligned vs misaligned (test 1 vs test 4)

The discussion related to the *current-thick* strip seal in misaligned rig will follow the same steps of *upgrade-thin* one. Following the mass flow ratio chart vs. *dp* is reported.

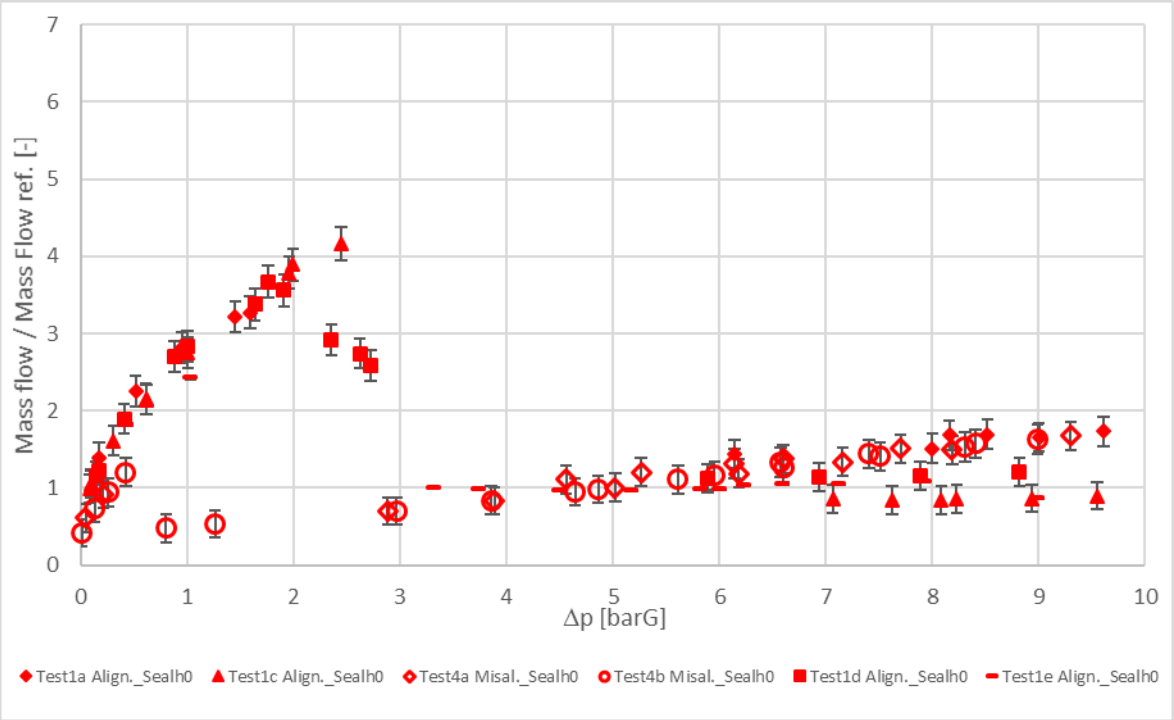

Figure 4.14 - mfr - Test 1 vs 4 - current-thick – aligned vs misaligned; solid symbols: aligned; open symbols: misaligned

In Figure 4.14 it is possible to see that, in the same way as the previous paragraph, the sealing activation happens at lower pressure ($dp \sim 0.5$ [barG]) than the aligned case. Because of the present consideration, the mass flow rate is lower in low pressure regime. Once the activation pressure in the aligned configuration is reached, about $dp = 3$ [barG], the difference between the two configuration disappears. Before to quantify the equivalent gap reduction, the seal's position into the groove is analyzed.

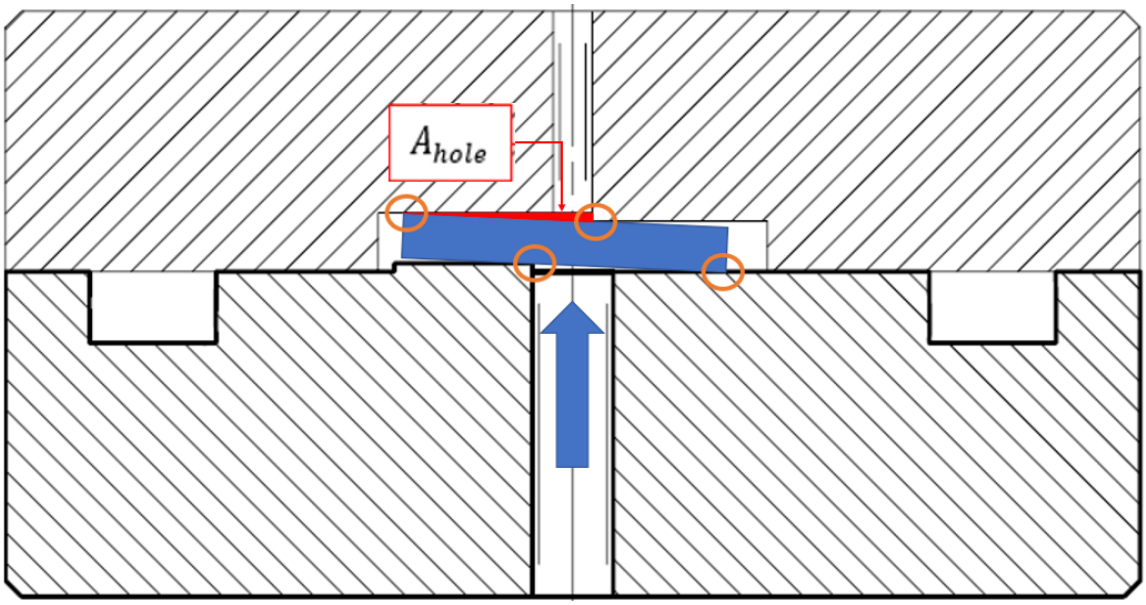

Figure 4.15 - misaligned geometry – current-thick - The blue arrow represents the direction of the air flow impinging on the seal

The groove's depth and the seal's thickness combined with the misaligned geometry induce a seal clamping in four points (because of the seal positioning) evidenced with orange circles in the cross-section of the assembly shown in Figure 4.15. Moreover, the sketch reported shows an overlap between the seal and the rig, due to the mentioned interference when the two rig's components are closed with bolts. The closing force should generate high stresses in contact points. The lateral gap area A_{hole} is remarked in red color in the sketch and substituted in equation (4.1).

The equivalent gap chart is reported as follow.

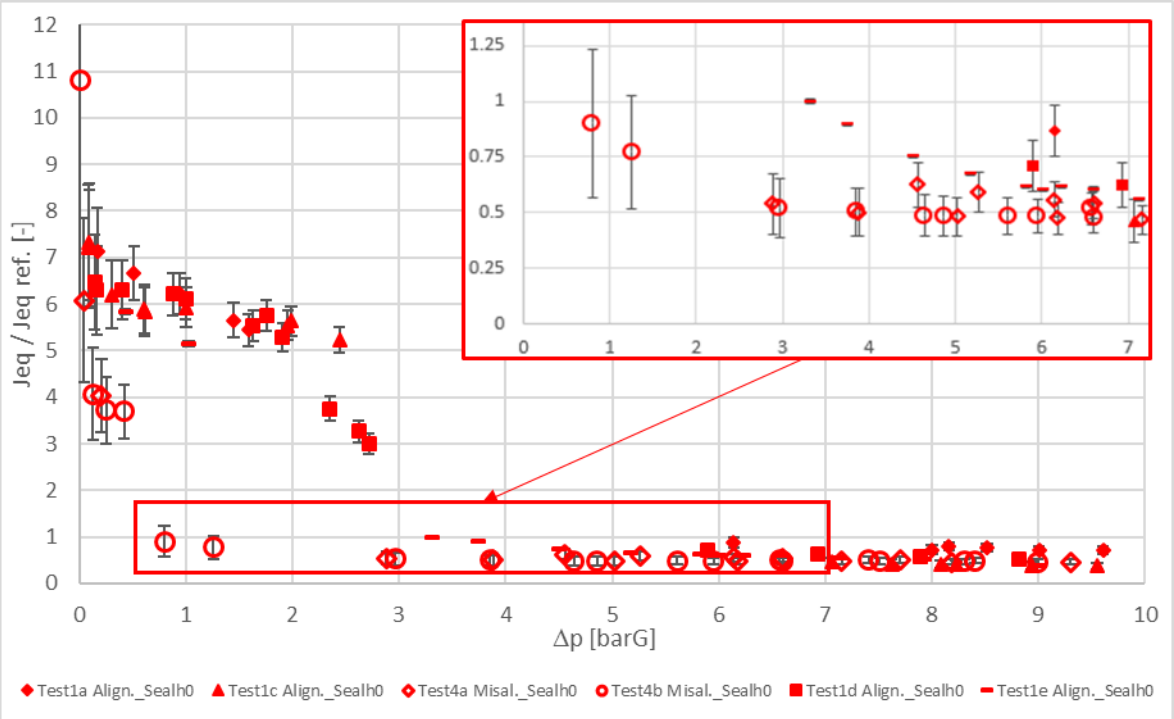

Figure 4.16 - J_{eq} - Test 1 vs 4 - current-thick – aligned vs misaligned; solid symbols: aligned; open symbols: misaligned

As it is possible to see in Figure 4.16, all the points referred to the misaligned configuration are positioned almost at the same equivalent gap that describe the aligned one after the activation process with the distinction that, in the misaligned geometry, it is anticipated. The very good sealing performance shown in the chart can be attributed to the linear contact remarked in Figure 4.15, as it is explained by Bricaud et al. [16] and paragraph 2.1.

4.2.6 Comparison: misaligned new seals, *current-thick* vs *upgrade-thin* (test 4 vs test 5)

In this section the differences between *upgrade-thin* and *current-thick* strip seals in misaligned configuration will be analyzed. As usual, the mass flow chart is the first plot reported.

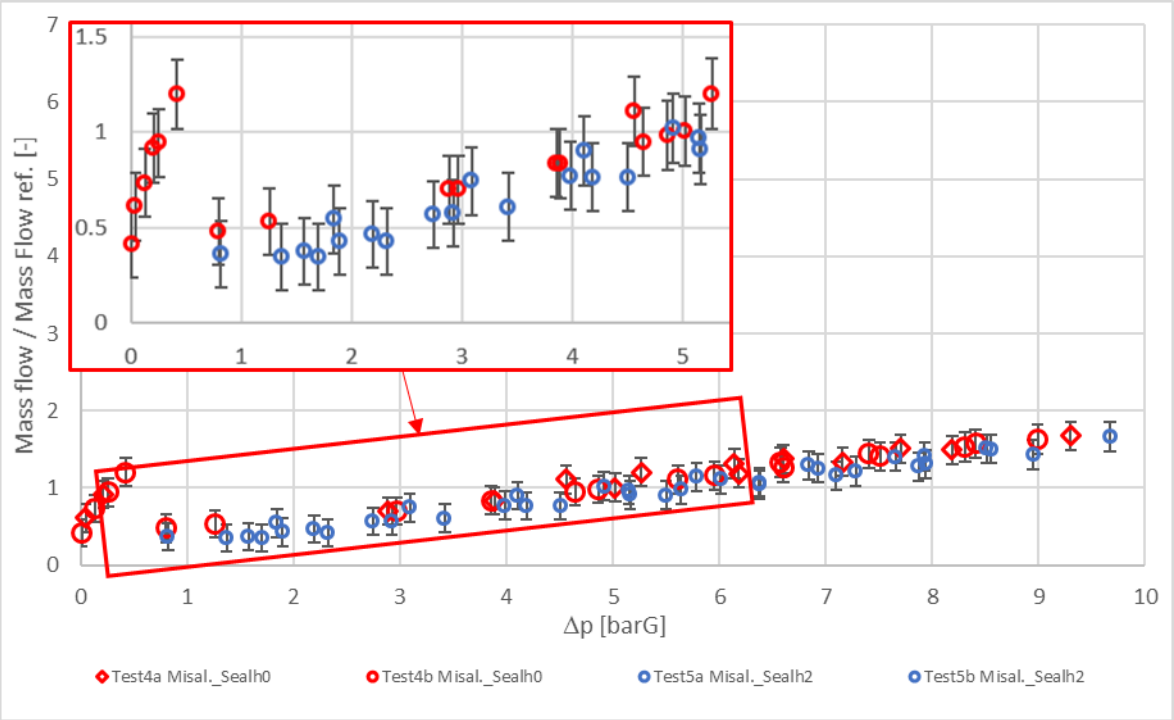

Figure 4.17 - mfr - Test 4 vs 5 - misaligned – current-thick vs upgrade-thin

Figure 4.17 shows that the mass flow is almost the same for both the seals in this particular configuration. The behaviors reported can probably be ascribed to local stress combined with the seal's deformability.

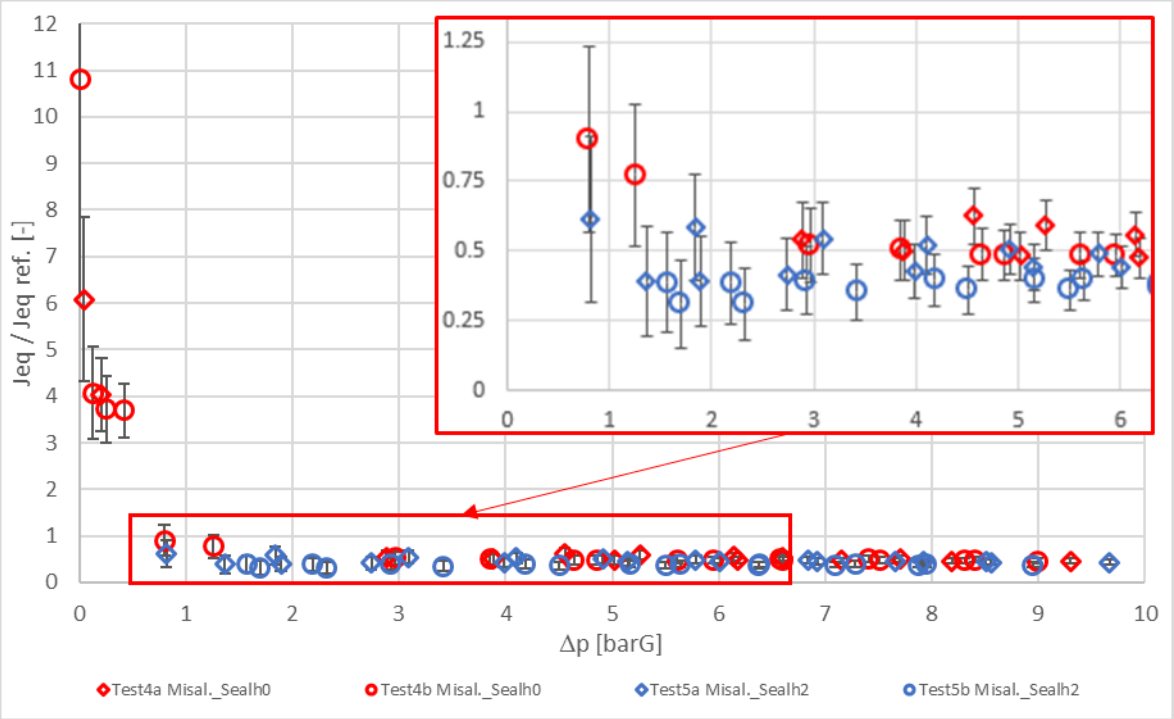

Figure 4.18 - J_{eq} - Test 4 vs 5 - misaligned - current-thick vs upgrade-thin

By analyzing Figure 4.18, it can be noticed that the two seals are characterized almost by the same sealing capability. More tests are needed to understand the step's height influence.

4.2.7 Comparison: new seals, all cases, aligned vs misaligned

To summarize the new seal's behavior, all the cases previously discussed are reported in the present paragraph.

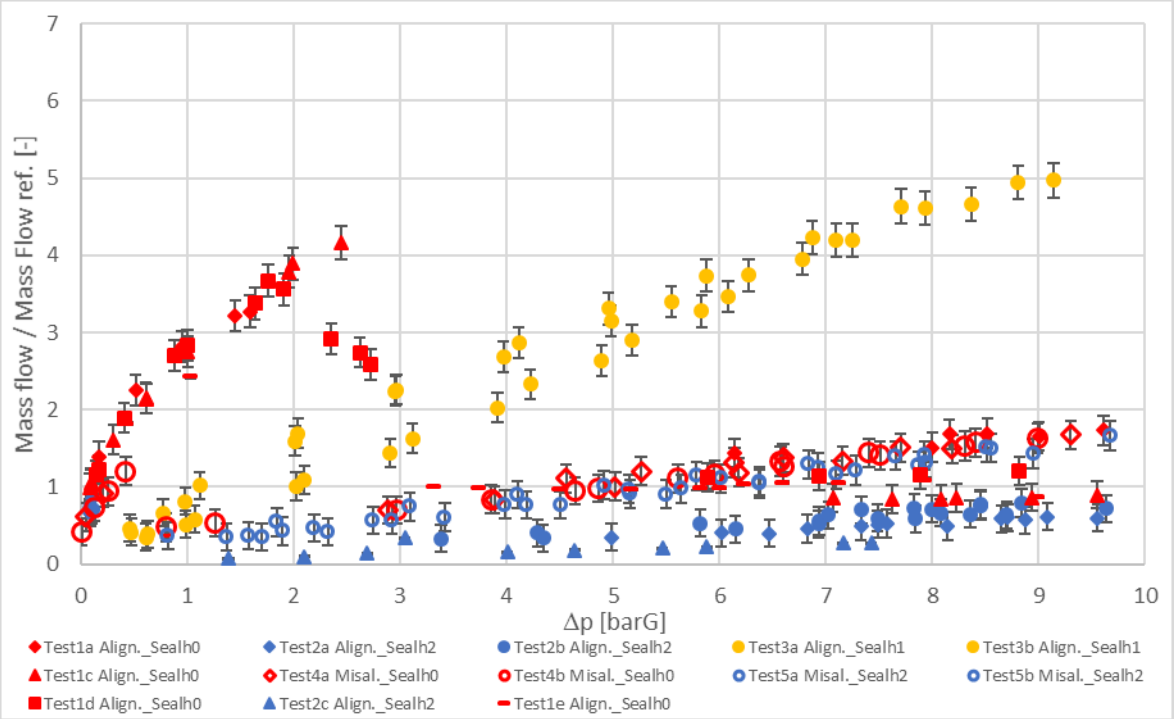

Figure 4.19 - mfr - upgrade-thin, current-thick, thicker – aligned & misaligned

Figure 4.19 shows that *upgrade-thin* strip seal (blue symbols) performs better than the others reported in the aligned configuration. For the same rig's geometry, until a gauge pressure of almost 3 [barG] *thicker* strip seal (orange symbols) grants a lower mass flow than *current-thick* one (red symbols). Instead high pressure range (dp > 3 [barG]) *ticker* strip seal is showing higher leakage than *current-tick* one.

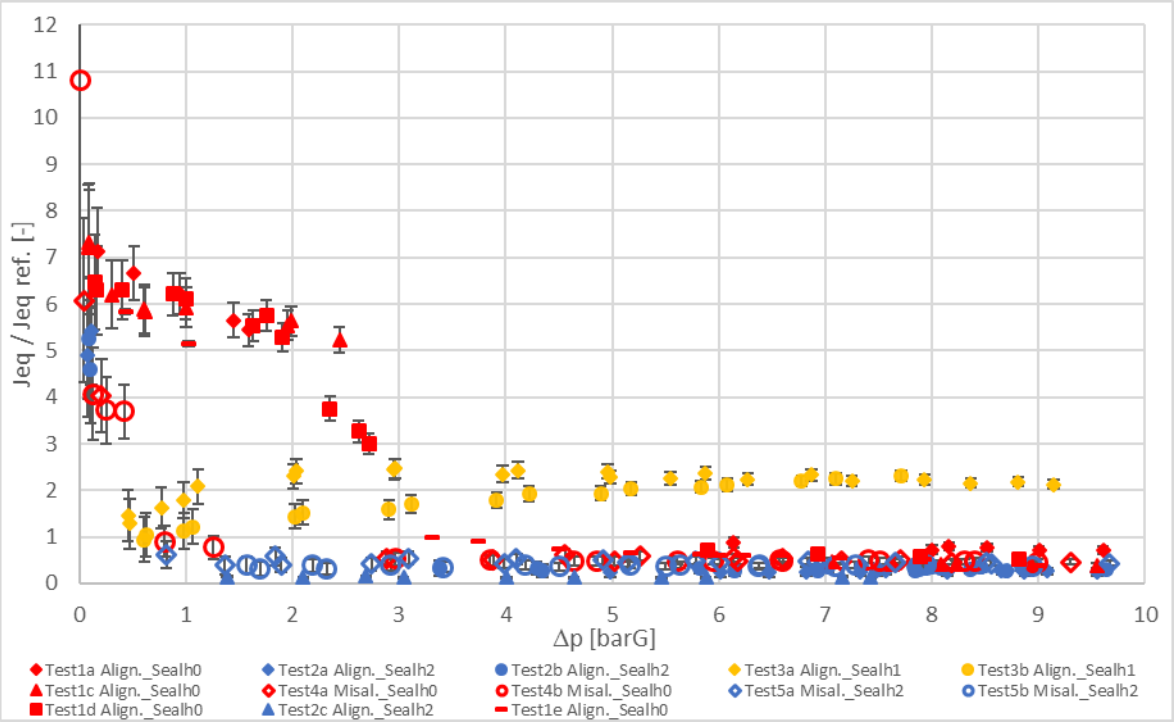

Figure 4.20 - J_{eq} - upgrade-thin, current-thick, thicker – aligned & misaligned

Figure 4.20 shows the equivalent gap ratio for all the new seals analyzed. The differences are less appreciable for $dp > 3$ [barG] due to the scale. *Thicker* strip seal grants better sealing performance in aligned configuration for $dp < 3$ [barG] compared to *current-thick* one, at $dp > 3$ [barG], *current-thick* strip seal ensures a lower J_{eq} comparted to *thicker*. Regarding *current-thick* and *upgrade-thin* strip seals, J_{eq} values are small and the differences can be neglected.

The analysis carried out so far is referred only to new seals, on the contrary in the next section an analysis about the worn seals behavior will be presented.

4.2.8 Comparison: aligned *upgrade-thin* seals, new vs worn (test 2 vs test 13)

Worn *upgrade-thin* strip seal comes from one Ansaldo Energia's test facility center, and the equivalent operative hours (about 100 [eoh]) are less than the worn *current-thick* strip seals, which come from site engines. It is for this reason that no big differences are expected between new and worn *upgrade-thin* strip seal. Below, the chart which describes the mass flow ratio versus the pressure drop across the seal is reported.

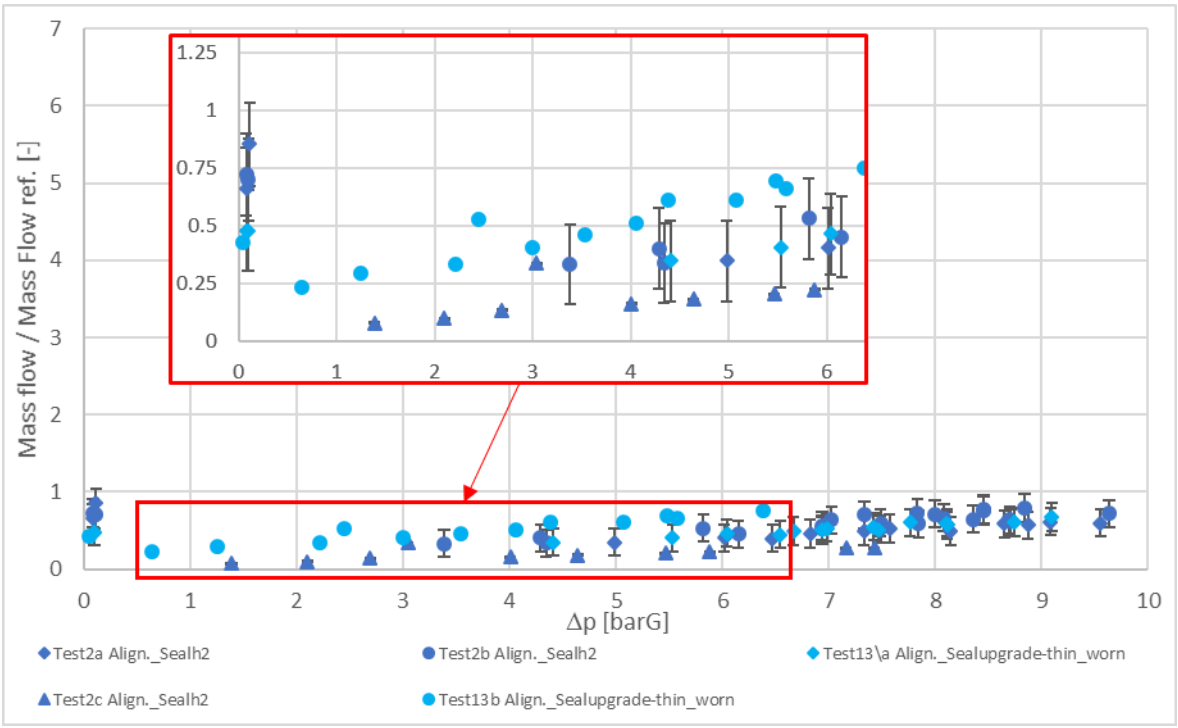

Figure 4.21 - mfr - Test 2 vs 13 - aligned – upgrade-thin - new vs worn

Figure 4.21 does not show big differences between new and worn seal, as expected. At high pressure the difference is not appreciable, but it is for $dp < 5$ [barG]. In particular, a slightly greater mass flow can be observed in the red box. To check the differences between the two cases the J_{eq} chart is considered.

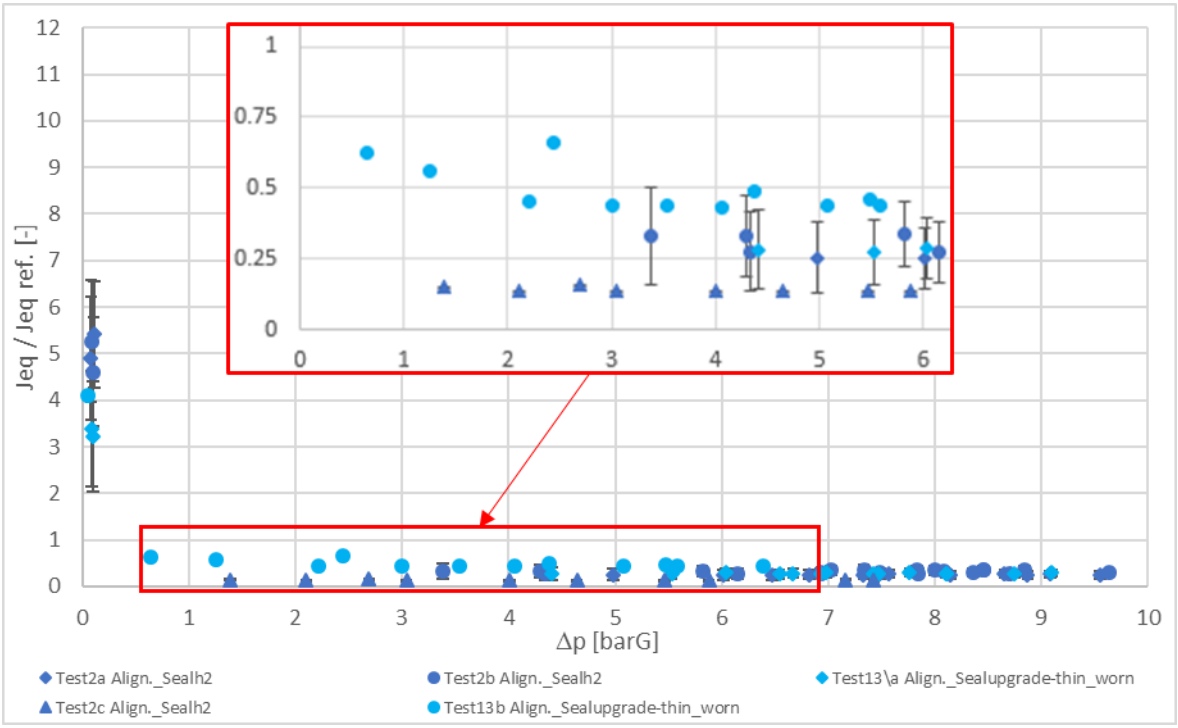

Figure 4.22 - J_{eq} - Test 2 vs 13 - aligned – upgrade-thin - new vs worn

Figure 4.22 confirms what just said above. No big differences are noticed at high pressure, but something different happens at low pressure in the strip seal operative range (reported in Figure 2.16). The differences shown in the plots above are remarked because they are due to the low wear of the seal. More tests are needed to estimate what happens after 25000 or 33000 [eoh].

4.2.9 Comparison: misaligned upgrade-thin strip seal; new vs worn (test 5 vs test 11)

In the present section the performance of the worn *upgrade-thin* strip seal in misaligned configuration will compared to the new one. The mass flow plot is reported below.

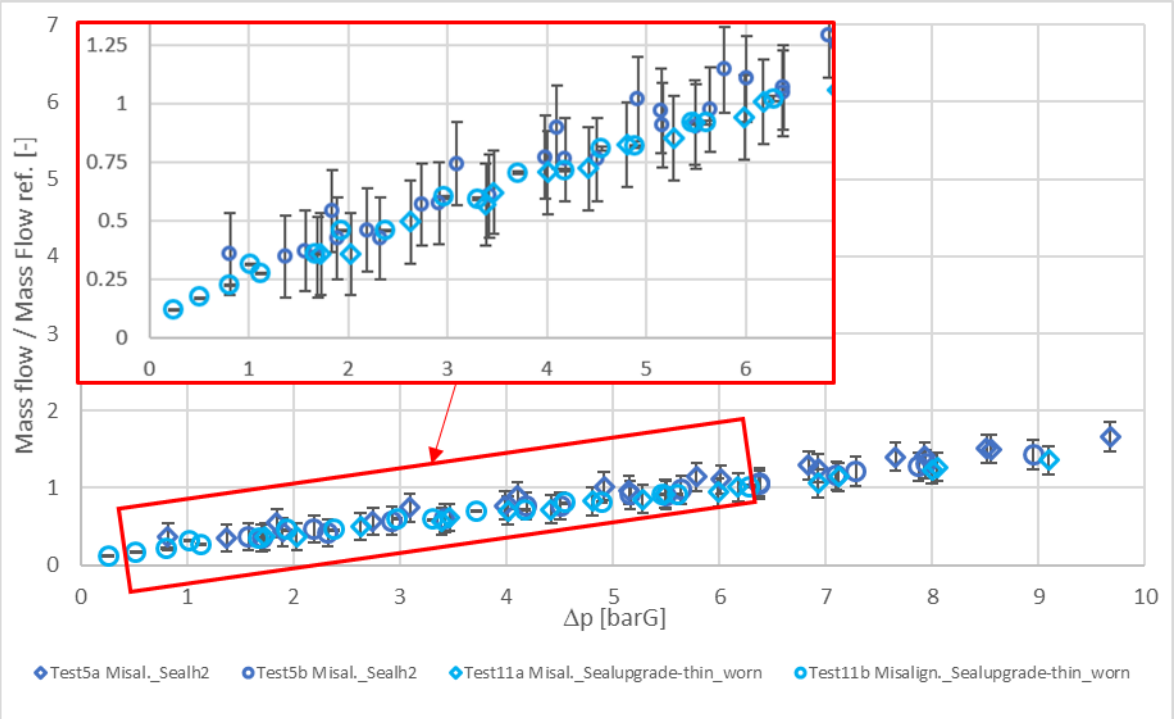

Figure 4.23 - mfr - Test 5 vs 11 - upgrade-thin - misaligned - new vs worn

Figure 4.23 shows almost the same mass flow for both the seals reported, in fact all the points related to worn seal overlap new seal results (shown in detail in the red box).

The equivalent gap plot is below reported.

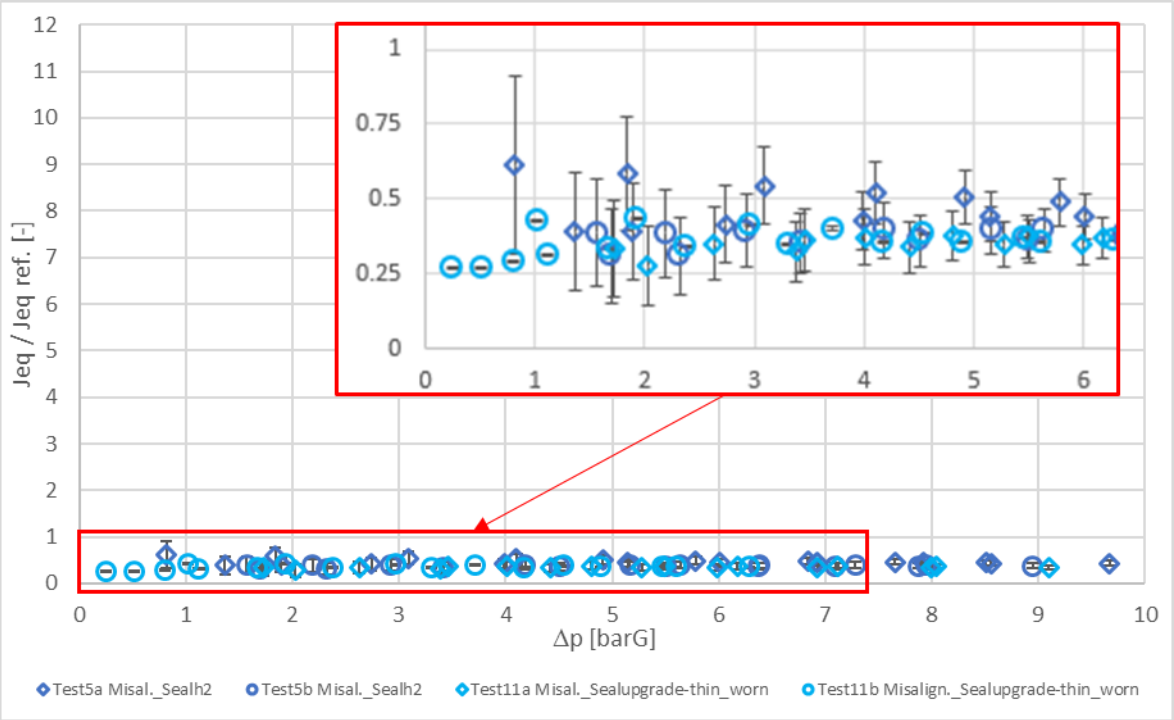

Figure 4.24 - J_{eq} - Test 5 vs 11 - upgrade-thin - misaligned - new vs worn

The same thing happened for Figure 4.23 is detected in Figure 4.24 too. Worn *upgrade-thin* strip seal has comparable performances to the new one, it is probably due to its little amount of equivalent operating hours and hence the little amount of wear.

4.2.10 Comparison: aligned *current-thick* seals, new vs worn (test 1 vs test 8 vs test 9 vs test 12)

In the following discussion, worn *current-thick* strip seals will be analyzed. The thickness measurements (Figure 3.9 and Table 3.3) were taken in order to evaluate which is the degree of wear of the worn strips. S3 present an inhomogeneous thickness (smaller than S2 and S1) along its length and hence represents the worst case; the other two are similar from the thickness measurement point of view. The differences between these last two strips can be attributed to the roughness (which is also reported in Table 3.3): S2 has a lower roughness with respect to S1. Following the mass flow plot is reported.

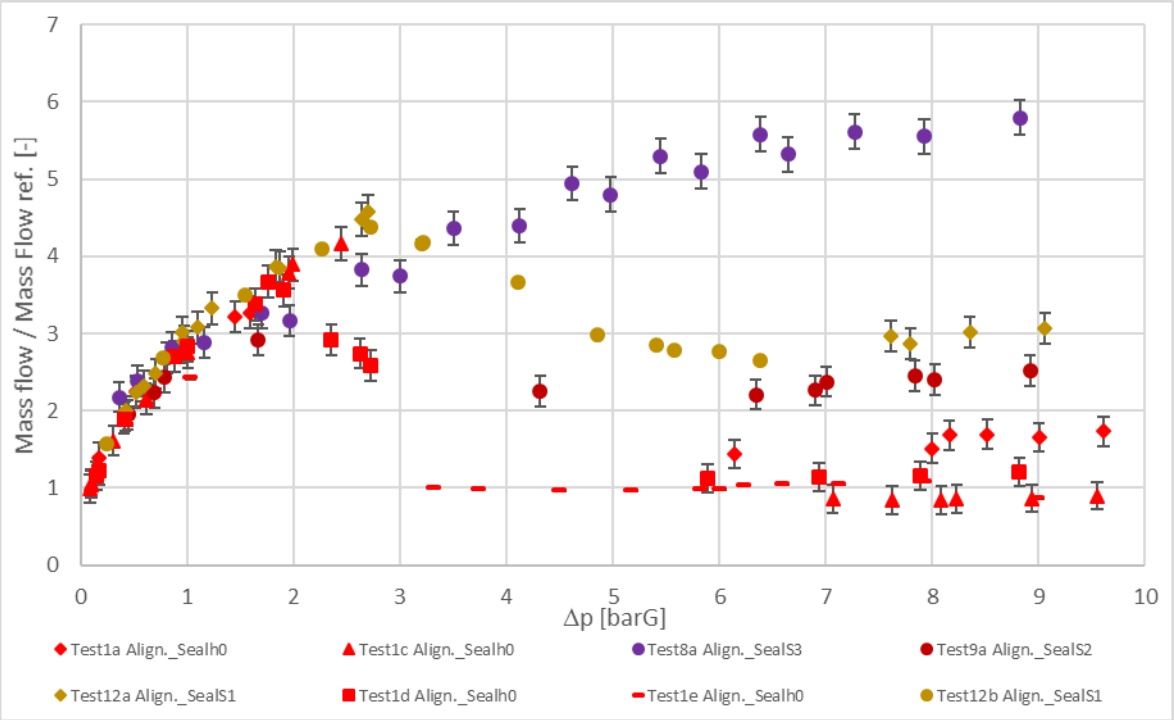

Figure 4.25 - mfr - Test 1 vs 8 vs 9 vs 12 - aligned – current-thick - new vs worn (S3, S2, S1)

Figure 4.25 reports the mass flow rate for each *current-thick* strip seal tested in the aligned configuration. In the present rig's configuration, the worst case is represented by S3 and the best one by S2 (if new seal is not considered); it seems that S2 is the less ruined since its roughness and thickness parameters are closer to new seal and it is confirmed if the chart above is observed. If the "activation region" is looked into, it can be noticed that it is shifted at higher pressure when worn strip seals are observed; the analyzed phenomenon disappears when the wear level is higher as it happens for S3. Before the activation the seals perform in the same way. To expand the discussion the equivalent gap chart is now considered.

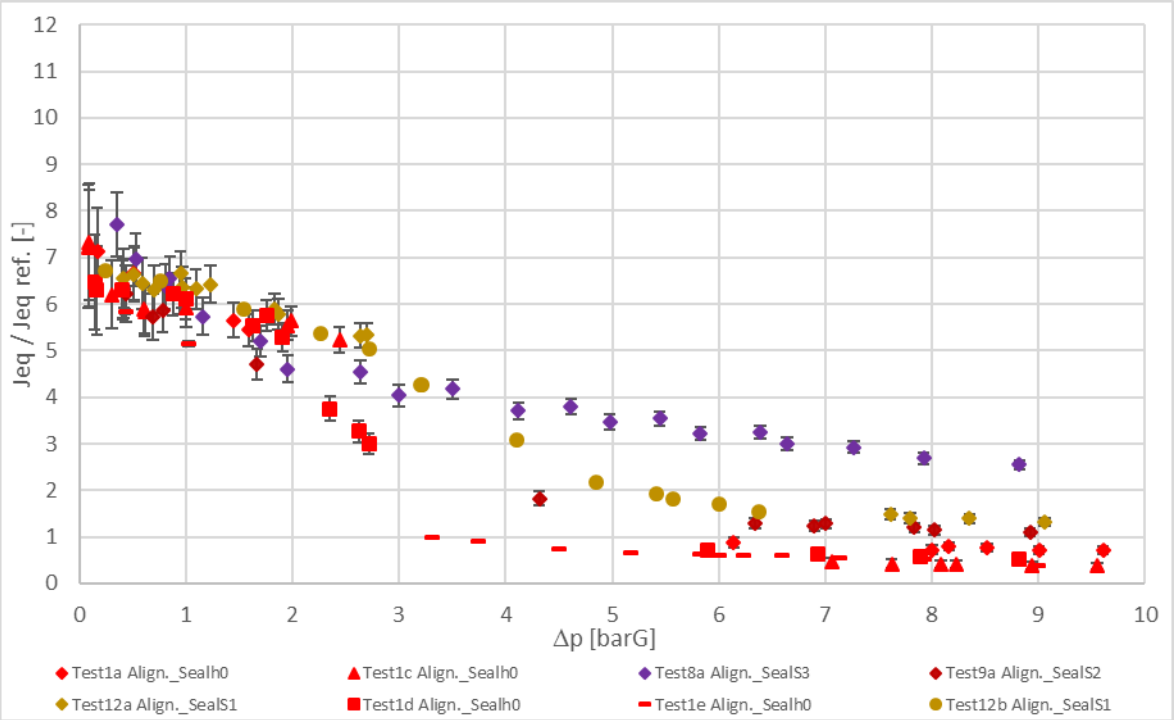

Figure 4.26 - Test 1 vs 8 vs 9 vs 12 - J_{eq} - aligned – current-thick - new vs worn (S3, S2, S1)

Figure 4.26 confirms that at low pressure all the seals perform in the same way. On the contrary, at higher pressure, worn seals show a delayed activation with respect to new one. S3 displays a larger J_{eq} with respect to the other new and worn seals. S2 and S1 perform similarly to the new seal at high pressure. After the new seal activation, from the best case (new) to the worst one (S3) the equivalent gap ratio difference is greater than 3 (ex. at *dp* about 4.5 [barG], new seal: $\frac{J_{eq}}{J_{eq_{ref}}} = 0.75$; S3: $\frac{J_{eq}}{J_{eq_{ref}}} = 3.79$), so a big performance loss is detected.

4.2.11 Comparison: aligned worn seals, *upgrade-thin* vs *current-thick* (test 8 vs test 9 vs test 12 vs test 13)

In order to understand which worn seal ensures the best performance, a comparison between worn *upgrade-thin* and *current-thick* strips is needed, even if it is difficult to be evaluated, because of low operative hours worked by the first seal mentioned compared to the second ones. Because of this difference, it is important to consider the following results carefully and make at least another one test for the worn thin strip seal. Below the mass flow chart is reported.

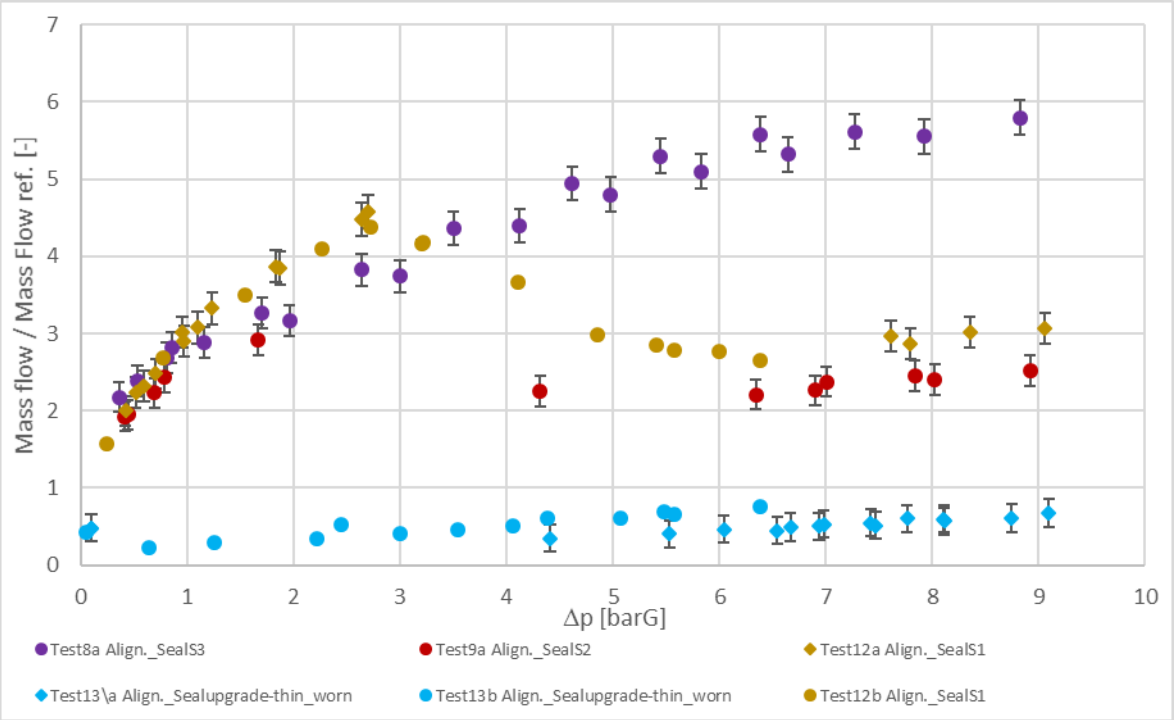

Figure 4.27 - mfr - Test 8 vs 9 vs 12 vs 13- aligned - worn – upgrade-thin vs current-thick (S3, S2, S1)

Upgrade-thin strip seal overperform the others across all the tested pressure range, with an almost constant mass flow ratio lower than 1. This difference is even bigger for $dp < 4$ [barG] where *current-thick* strip seals are not activated. These observations are even more validated when the J_{eq} ratio is considered as in the picture below.

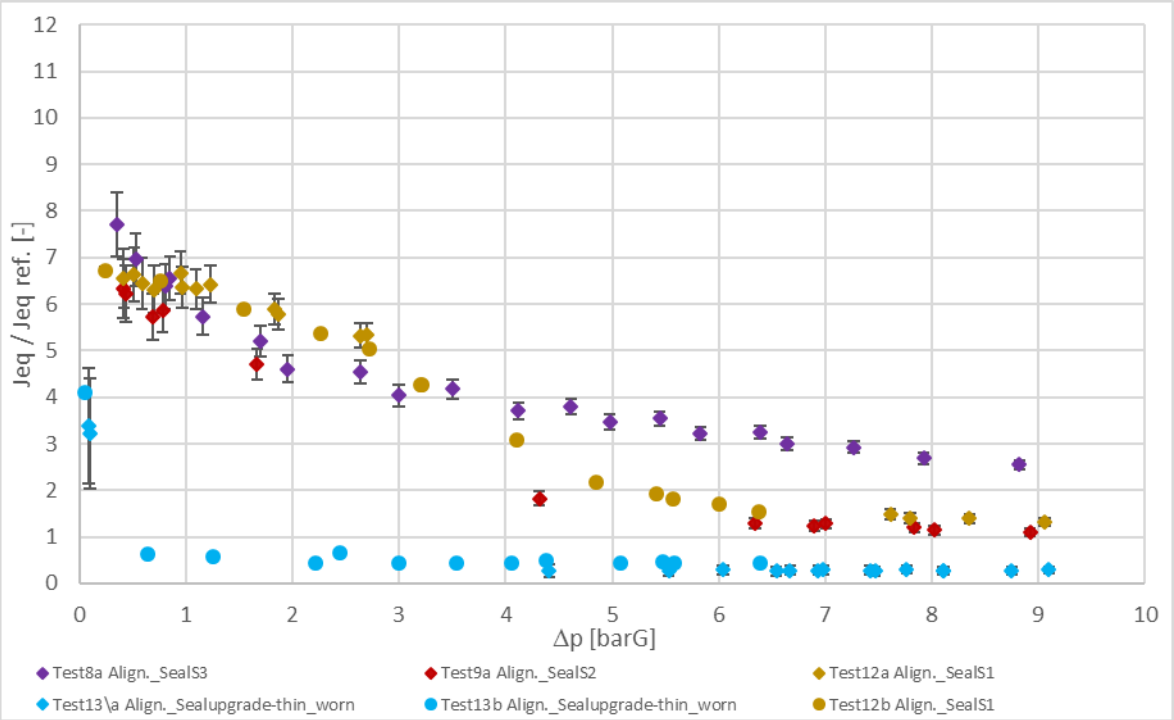

Figure 4.28 - J_{eq} - Test 8 vs 9 vs 12 vs 13- aligned - aligned - worn - upgrade-thin vs current-thick (S3, S2, S1)

As it was expected, the equivalent gap measured with worn *upgrade-thin* seal is the lower one and there is a huge difference between the mentioned geometry and the others represented in the entire pressure range measured. The presented difference, as already said in the present chapter, could be ascribed to low cumulated [eoh] by the analyzed strip seal. A more reliable comparison would need an *upgrade-thin* seal with a similar amount of equivalent operating hours of the *current-thick* strips: a new experimental test campaign is needed to clarify this aspect.

4.2.12 Comparison: worn *upgrade-thin* strip seal, aligned vs misaligned (test 11 vs test 13)

In the following analysis, the differences between the aligned and misaligned configuration for the worn *upgrade-thin* strip seal will be analyzed. The mass flow plot is here reported.

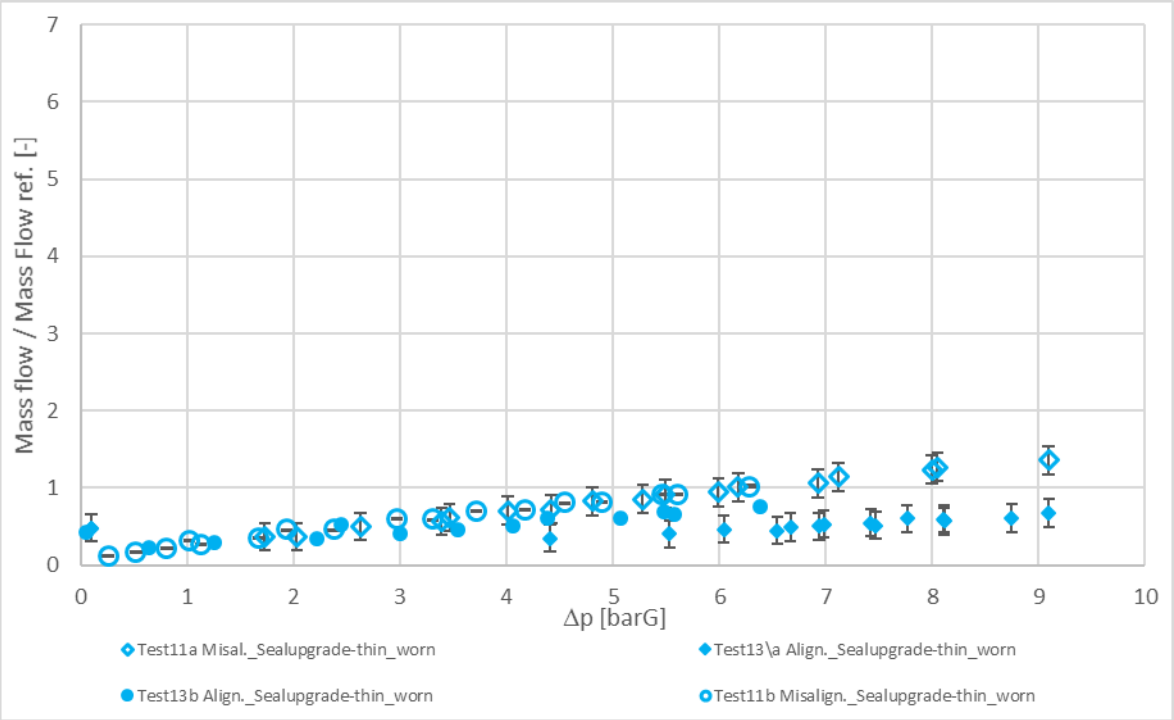

Figure 4.29 - mfr - Test 11 vs 13 - upgrade-thin - worn - aligned vs misaligned; solid symbols: aligned; open symbols: misaligned

In high pressure range (*dp* > 6 [barG]) and misaligned case (open symbols), the analyzed strip presents a slightly higher mass flow rate with respect to the same seal tested in aligned condition (full symbols). On the contrary, the mismatch is neglectable at low pressure.

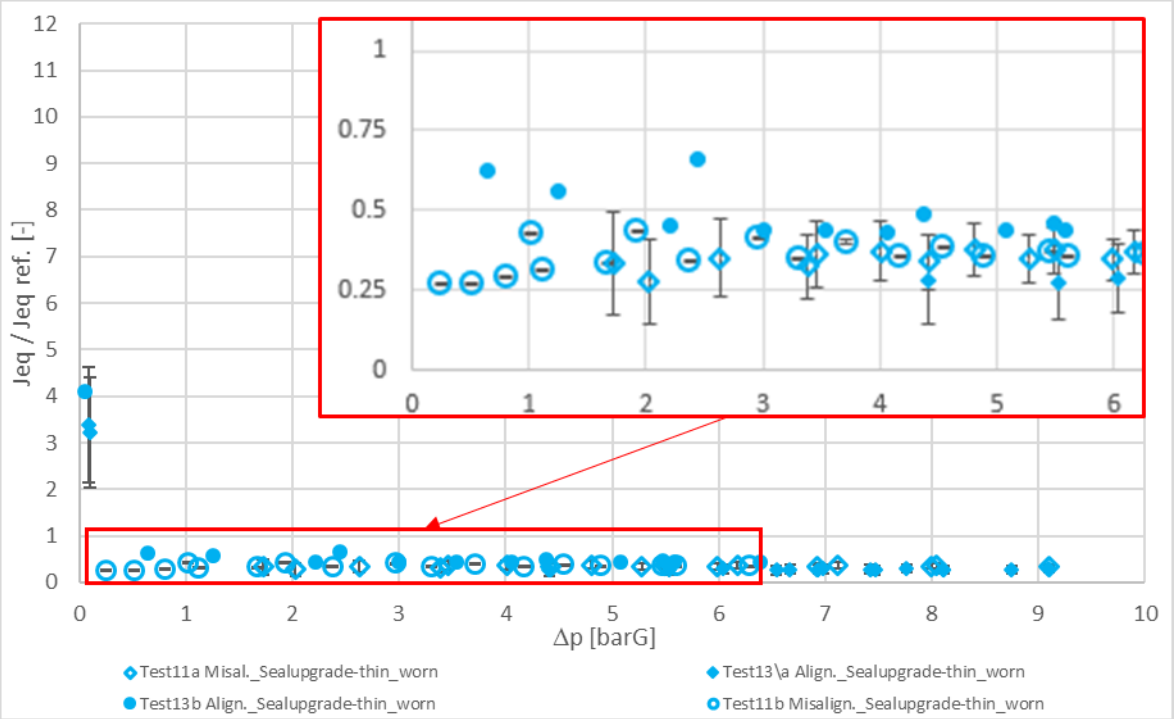

Figure 4.30 - J_{eq} - Test 11 vs 13 - upgrade-thin – worn - aligned vs misaligned; solid symbols: aligned; open symbols: misaligned

In the chart above the same comparison is reported in terms of J_{eq} ratio. It can be observed in Figure 4.30's red box that misaligned configuration present a slightly lower equivalent gap compared to aligned one at low pressure. At dp > 2 [barG] the data lay into the error bars. New tests with more worn *upgrade-thin* strip seal are needed to better characterize it.

4.2.13 Comparison: worn *current-thick* strip seal, aligned vs misaligned (test 6 vs test 7 vs test 8 vs test 9 vs test 10 vs test 12)

In the following analysis the differences between aligned and misaligned geometry for the worn thick seal cases will be discussed. In the present analysis, the linear contact is related to the seal's local thickness (Figure 3.9). Following the mass flow chart is reported.

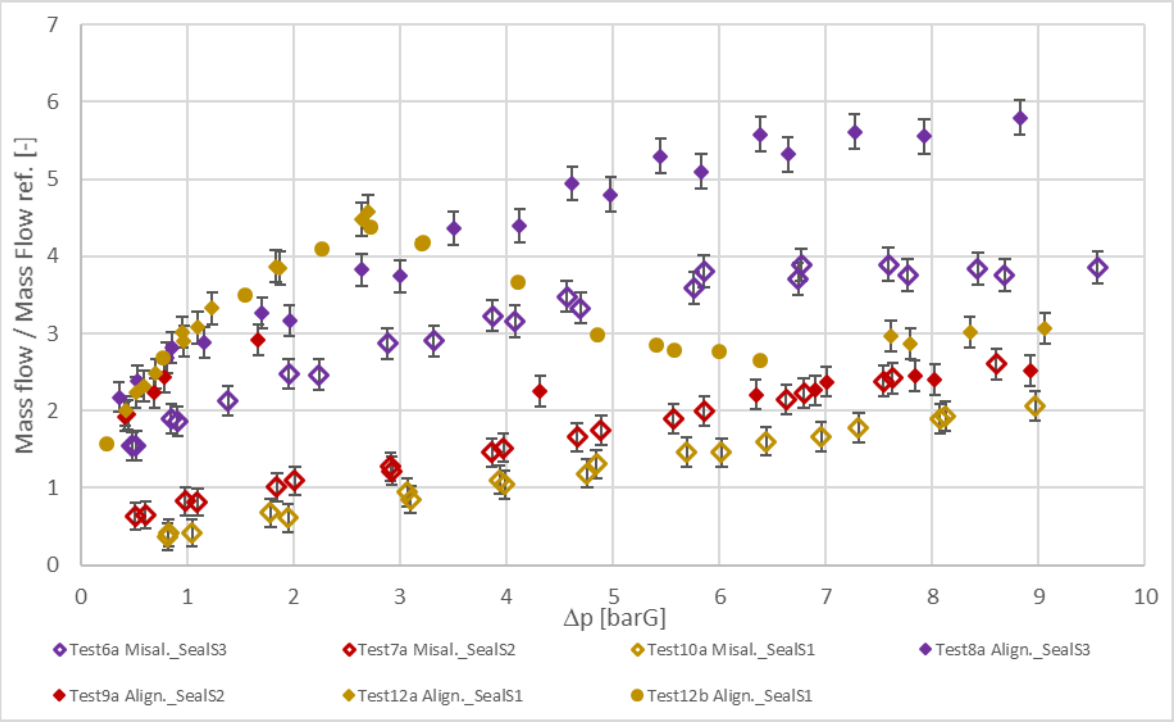

Figure 4.31 - mfr - Test 6 vs 7 vs 8 vs 9 vs 10 vs 12 - current-thick - worn - aligned vs misaligned; solid symbols: aligned; open symbols: misaligned (S3, S2, S1)

Figure 4.31 shows the differences between the aligned and misaligned case; thanks to the already discussed linear contacts, all the seals in misaligned configuration let less mass flow pass than in the aligned rig. For what concerns S1 and S2, their activation pressure happens at lower values in the misaligned rig's geometry. Moreover, S2 (roughness = 0.8 [µm]) performs better than S1 (roughness = 3.3 [µm]) in the aligned configuration, but the opposite happens in misaligned case: the different roughness of the two seals could play a role in the effectiveness of the linear contact. It can be speculated that because of the high stress generated by the linear contact, the roughness micro-asperities deform themselves thus a better sealing is obtained. Finally, the "activation process" is not detected in misaligned configuration if it is not admissible in the aligned case (see S3). J_{eq} chart is reported below.

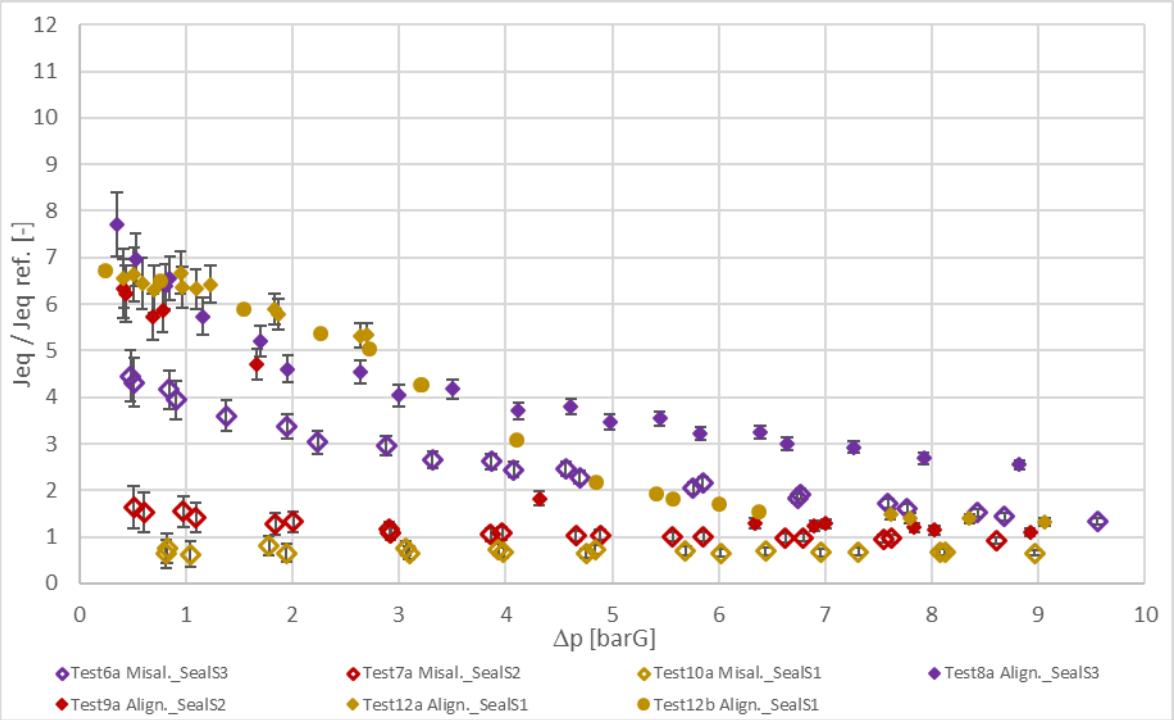

Figure 4.32 - J_{eq} - Test 6 vs 7 vs 8 vs 9 vs 10 vs 12 - current-thick - worn - aligned vs misaligned; solid symbols: aligned; open symbols: misaligned (S3, S2, S1)

Figure 4.32 shows that the biggest differences between the different seals can be found at low pressure before the activation phenomenon in the aligned configuration. If the sealing performance are considered after the activation in the aligned configuration, it can be noticed that their decay is not so relevant; the biggest difference between the two configurations is related to the activation pressure, which is much lower in aligned configuration.

4.2.14 Comparison: misaligned *current-thick* strip seal; new vs worn (test 4 vs test 6 vs test 7 vs test 10)

In the present section the evaluation of the performance decay in misaligned configuration due to seals worsening will be discussed. The mass flow chart is below reported.

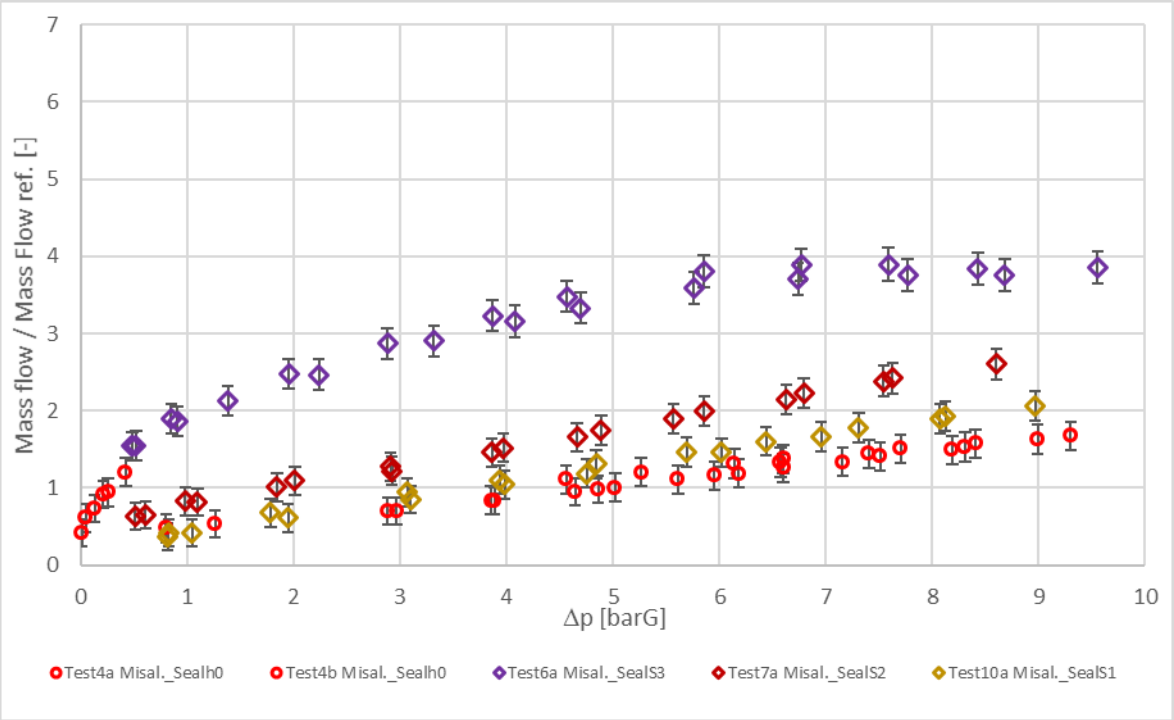

Figure 4.33 - mfr - Test 4 vs 6 vs 7 vs 10 - current-thick - misaligned - new vs worn (S3, S2, S1)

Figure 4.33 shows that less worn seals (S1 and S2) and new one (red symbols) share a similar behavior. Larger differences are detected if S3 is considered, for which the activation is not happening (as explained in paragraph 4.2.13). The J_{eq} chart is shown as follow.

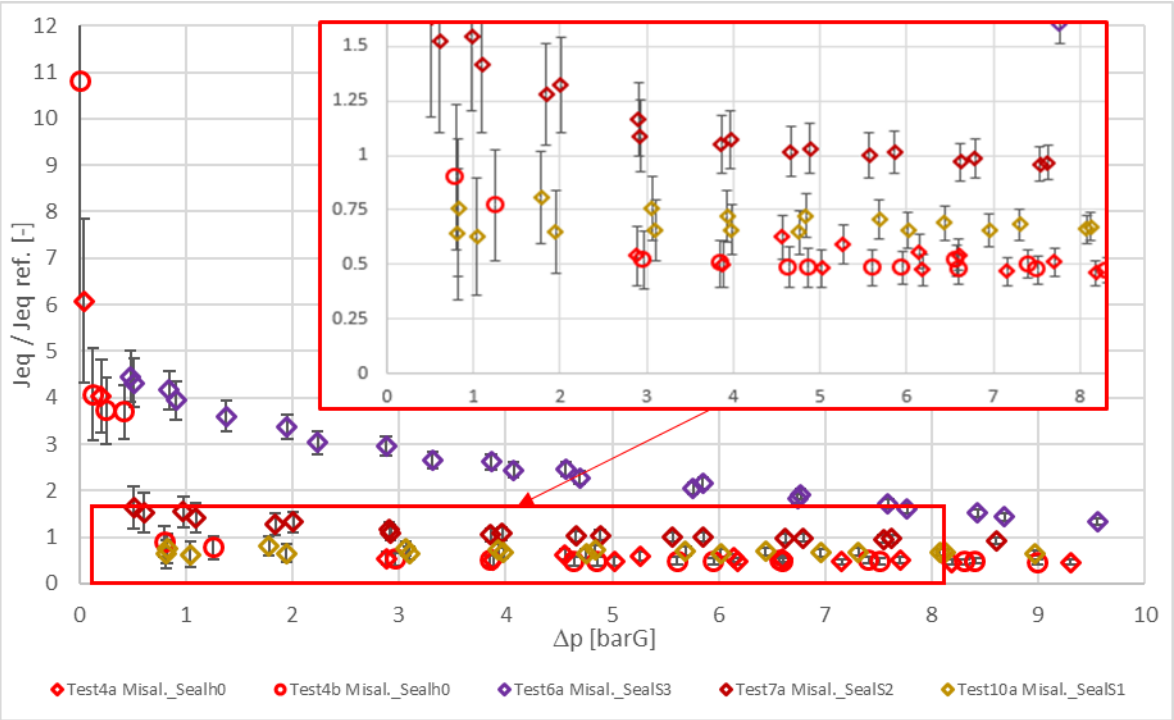

Figure 4.34 - J_{eq} - Test 4 vs 6 vs 7 vs 10 - current-thick - misaligned - new vs worn (S3, S2, S1)

The chart above confirms that the differences between the new seal and S1 and S2 in the misaligned configuration are not as marked as in the aligned one (Figure 4.34 – red box) since in the present case the activation happens at lower pressure. Bigger differences are detected in the worst case (S3) especially at low pressure, because of the absence of activation. Anyway, even S3 reduces the J_{eq} with the pressure rising.

4.2.15 Comparison: worn seals, all cases, aligned vs misaligned

As it was done in paragraph 4.2.7, in the present section all the worn seals analyzed are compared to each other. The chart which follows shows the mass flow ratio vs *dp*.

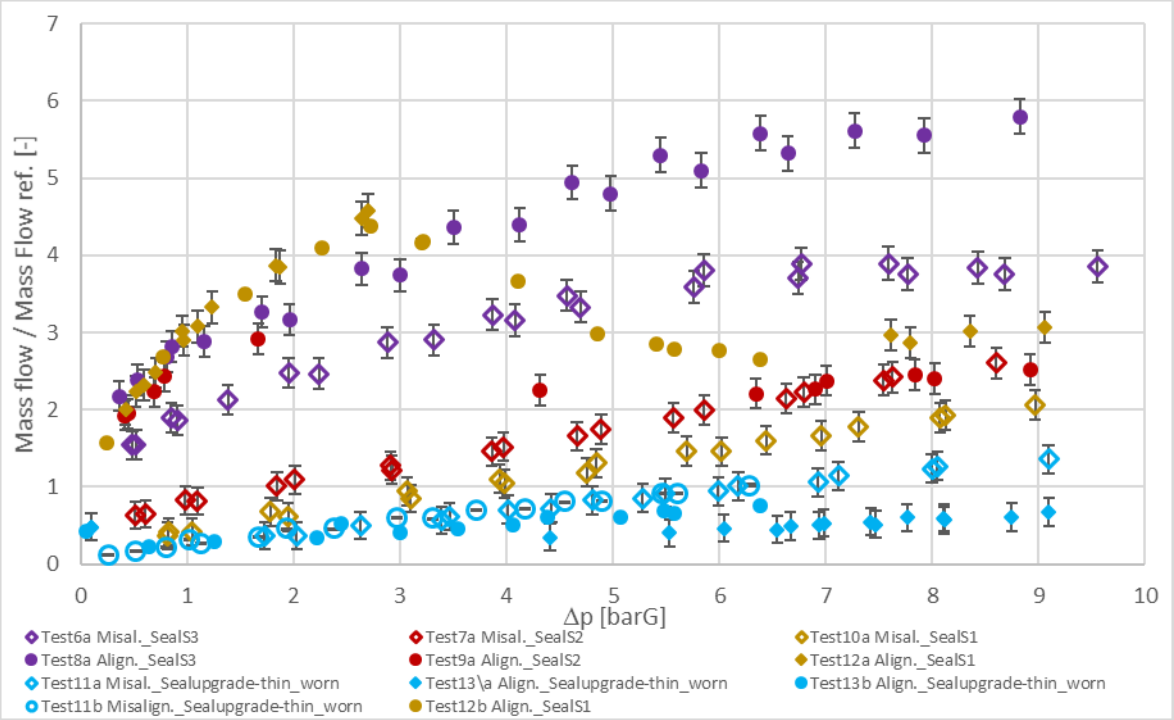

Figure 4.35 - mfr – upgrade-thin & current-thick - worn - aligned & misaligned

In the chart shown above, the best worn case seems to be *upgrade-thin* strip seal in aligned configuration, but, as already discussed, it is characterized by a low amount of operating hours. For this reason is fundamental to perform additional tests on a more ruined *upgrade-thin* strip seal. The equivalent gap ratio chart is reported as follow.

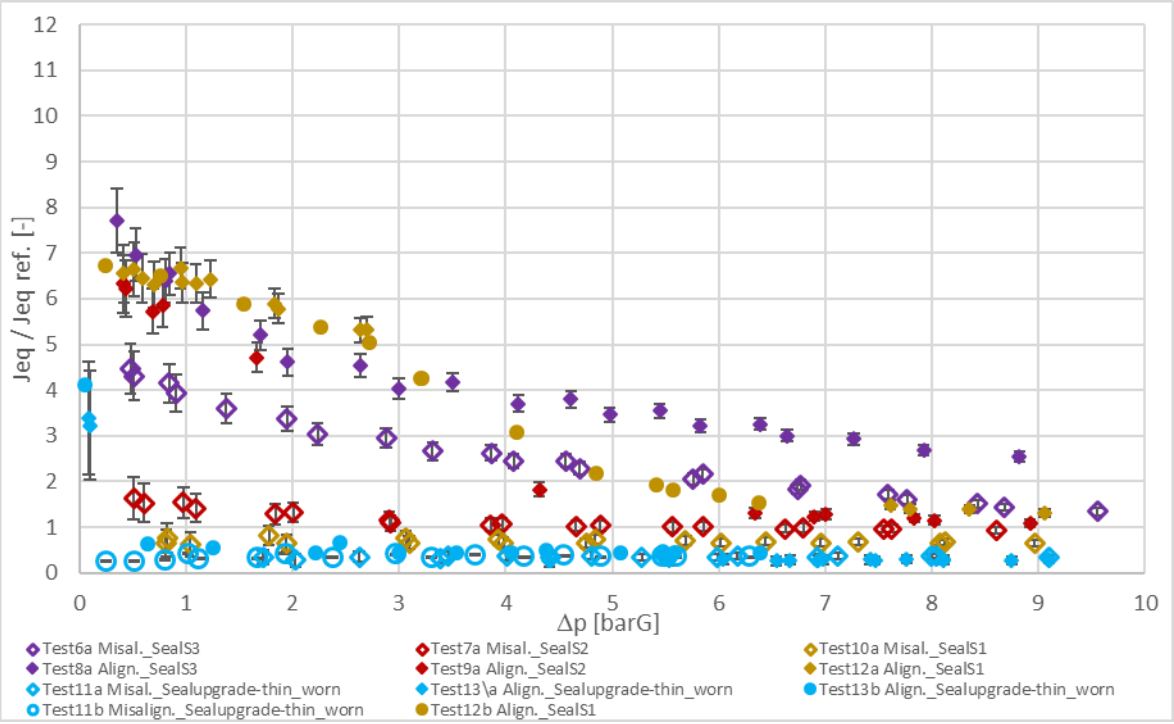

Figure 4.36 - J_{eq} – upgrade-thin & current-thick - worn - aligned & misaligned

If Figure 4.36 is considered, the same thing observed for Figure 4.35 can be concluded. Misaligned results related to worn *upgrade-thin* ensure slightly greatest performance than S1 and S2, but it is important to understand the performance decay due to the seal worsening. Bigger differences are detected if the aligned rig geometry is analyzed.

4.3 Characteristic curves

In the present section the results shown in the previous one will be elaborated in order to obtain the characteristic functions for each seal tested. An interpolation was carried out with the aim to fit the experimental data. In order to do this all the repetitions for each test were considered.

Before the definition of the characteristics curves it is fundamental to remember that the seal's behavior changes before and after activation. Moreover, activation region, which is unstable, has one another behavior and not in all the tests it was characterized. It is for this reason that typically the seal has three different characteristic functions[1], each one is strictly related to a specific pressure range. The characteristics curves reported in this paragraph are only related to the equivalent gap.

4.3.1 *Current-thick* strip seal, aligned and misaligned

In the following discussion the characteristic curves related to *current-thick* strip seal will be analyzed.

[1] The characteristic functions will be distinguished by their pressure range: low pressure if before the activation, transition or high pressure if after the activation.

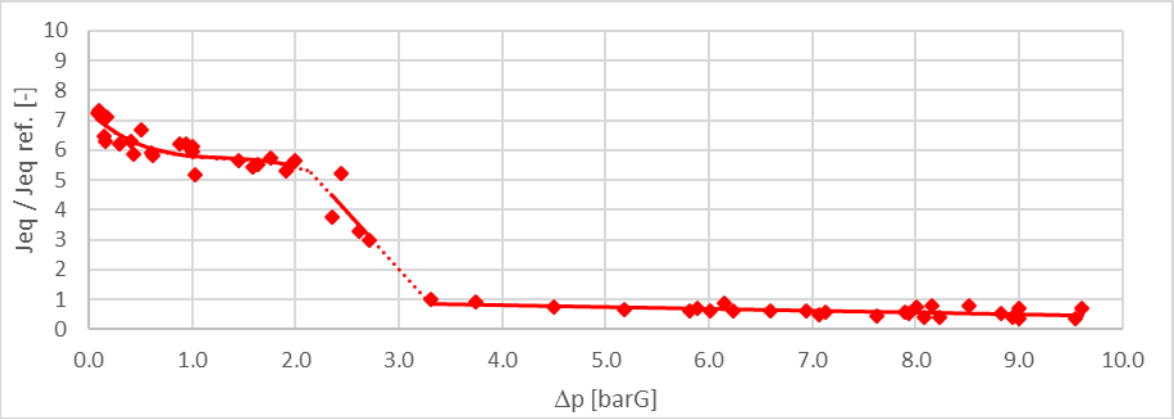

Figure 4.37 - Test 1 - Current-thick – aligned - Characteristics curves

In the plot above all the test 1 points are shown together with three characteristics curves. The first one is related to low pressure behavior, the second one related to the transition region and the last one fits high pressure points (after the activation process).

For what concerns the misaligned geometry, fit results are shown in the chart as follow.

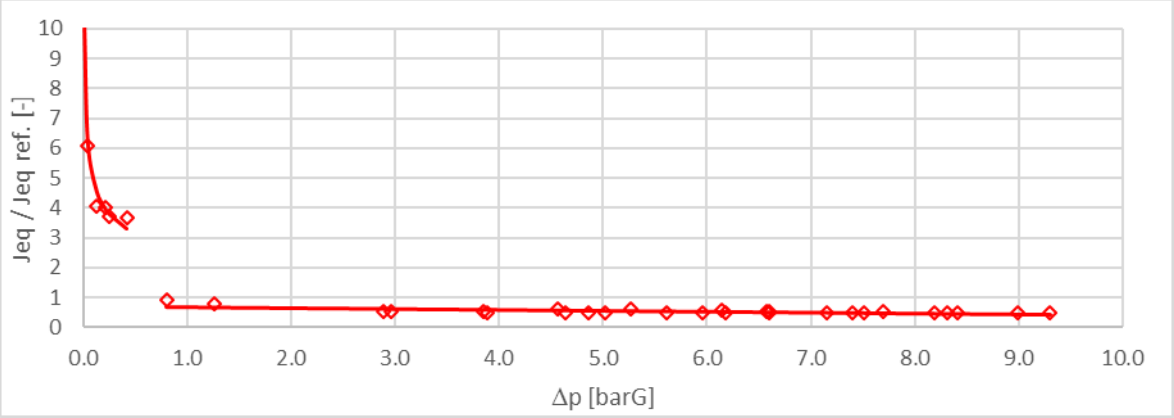

Figure 4.38 - Test 4 - Current-thick - misaligned - Characteristic curves

The characteristic function shown in Figure 4.38 is reliable only for the specific misalignment tested. In the present test two different behaviors were observed, instead, the "*activation region*" was not characterized (0.4 [barG]<dp<0.8 [barG]).

In the following table the different functions shown in the charts above are reported with the correlation factor R^2.

Table 4.1 – current-thick – aligned configuration – fitting functions

Seal	**Range**	**Fitting function**	$\boldsymbol{R^2}$
Current-thick	Low pressure (dp<2 [barG])	$\frac{J_{eq}}{J_{eq_{ref}}} = -6.03 \cdot 10^{-1} \cdot dp^3 + 2.37 \cdot dp^2 - 3.27 \cdot dp + 7.28 \cdot 10^{-1}$	0.743

Current-thick	Transition ($dp \in [2, 3.5]$ [barG])	$\frac{J_{eq}}{J_{eq_{ref}}} = -3.81 \cdot dp + 13.4$	0.406
Current-thick	High pressure (dp>3.5 [barG])	$\frac{J_{eq}}{J_{eq_{ref}}} = -6.07 \cdot 10^{-2} \cdot dp + 1.05$	0.369

Table 4.2 - current-thick – misaligned configuration – fitting functions

Seal	Range	Fitting function	R^2
Current-thick	Low pressure (dp<0.4 [barG])	$\frac{J_{eq}}{J_{eq_{ref}}} = 2.41 \cdot dp^{-2.68 \cdot 10^{-1}}$	0.970
Current-thick	High pressure (dp>0.8 [barG])	$\frac{J_{eq}}{J_{eq_{ref}}} = -3.16 \cdot 10^{-2} \cdot dp + 7.10 \cdot 10^{-1}$	0.498

4.3.2 *Upgrade-thin* strip seal, aligned and misaligned

In this section the characteristic curves related to the *upgrade-thin* strip seal in both aligned and misaligned configuration will be described.

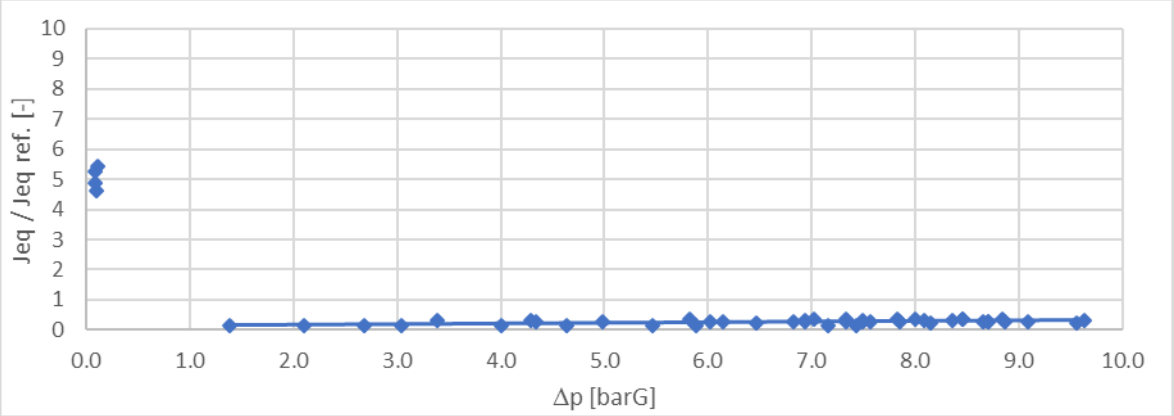

Figure 4.39 - Test 2 - Upgrade-thin - aligned - Characteristic curves

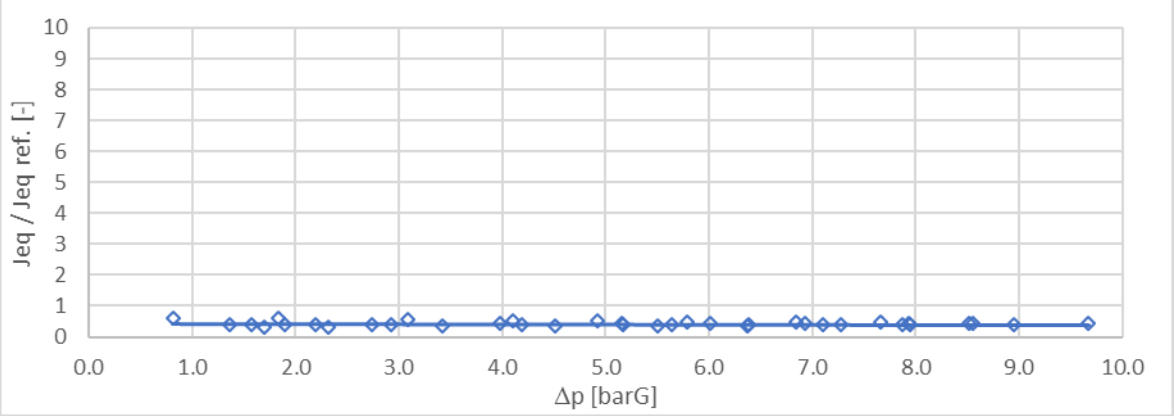

Figure 4.40 - Test 5 - Upgrade-thin - misaligned - Characteristic curves

Figure 4.39 and Figure 4.40 describe the *upgrade-thin* strip seal behavior respectively related to the aligned and misaligned configuration. Meanwhile in paragraph 4.3.1 more than one function for each rig geometry is shown in order to describe different regions, in the present section only one for each case is reported. This happens because low pressure points are not spaced enough to determine the low pressure and transition regions behavior in the aligned configuration; in misaligned one, instead, any point was not taken.

As follow the fitting functions are reported with the correlation factor.

Table 4.3 – upgrade-thin – aligned configuration – fitting functions

Seal	Range	Fitting function	R^2
Upgrade-thin	High pressure (dp>1.5 [barG])	$\frac{J_{eq}}{J_{eq_{ref}}} = 1.83 \cdot 10^{-2} \cdot dp + 1.36 \cdot 10^{-2}$	0.267

Table 4.4 – upgrade-thin – misaligned configuration – fitting functions

Seal	Range	Fitting function	R^2
Upgrade-thin	High pressure (dp>0.8 [barG])	$\frac{J_{eq}}{J_{eq_{ref}}} = -2.02 \cdot 10^{-3} \cdot dp + 4.33 \cdot 10^{-1}$	0.00571

4.3.3 *Thicker* strip seal, aligned

The characteristic curve related to the *thicker* strip seal is not described with three distinct functions but only one, as it was discussed in the paragraph 4.2.3, in fact it is not characterized by the activation phenomenon. Below the seal's behavior is reported with the fitting curve and the experimental points.

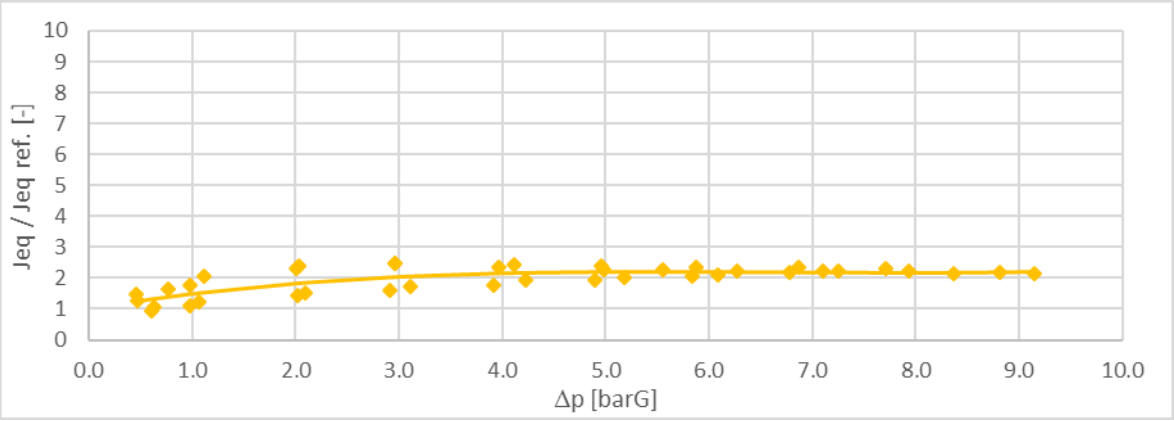

Figure 4.41 - Test 3 - Thicker - aligned - Characteristic curves

The characteristic function shown above ensures a good fit with the experimental data across all the investigated pressure range. Below the characteristic function and the correlation factor is reported.

Table 4.5 – thicker – aligned configuration – fitting function

Seal	Range	Fitting function	R^2
Thicker	All domain	$\frac{J_{eq}}{J_{eq_{ref}}} = 4.42 \cdot 10^{-3} \cdot dp^3 - 8.85 \cdot 10^{-2} \cdot dp^2 + 5.72 \cdot 10^{-1} \cdot dp + 1.01$	0.586

4.3.4 Worn *current-thick* strip seal, aligned and misaligned

In the present section worn *current-thick* strip seals are described with their fitting functions. Below, all the charts related to the aligned configuration are reported.

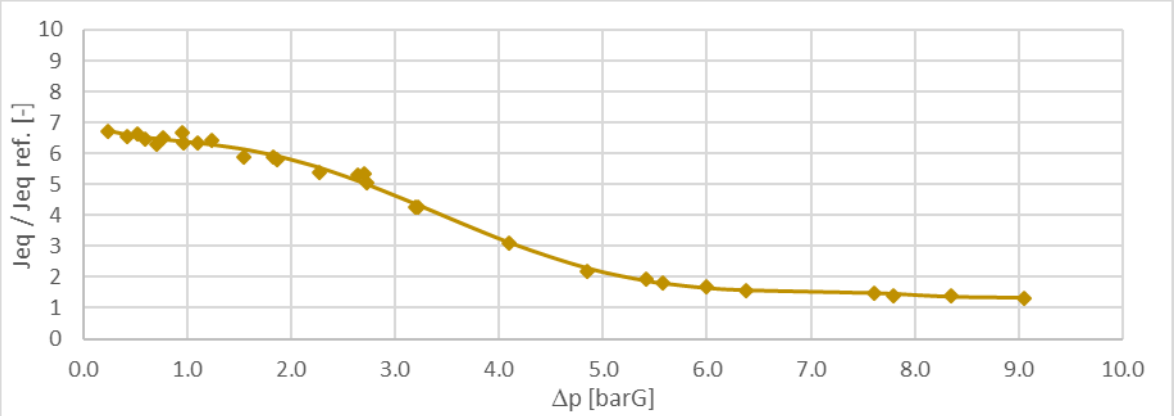

Figure 4.42 – Test 12 – Current-thick S1 - aligned - Characteristic curves

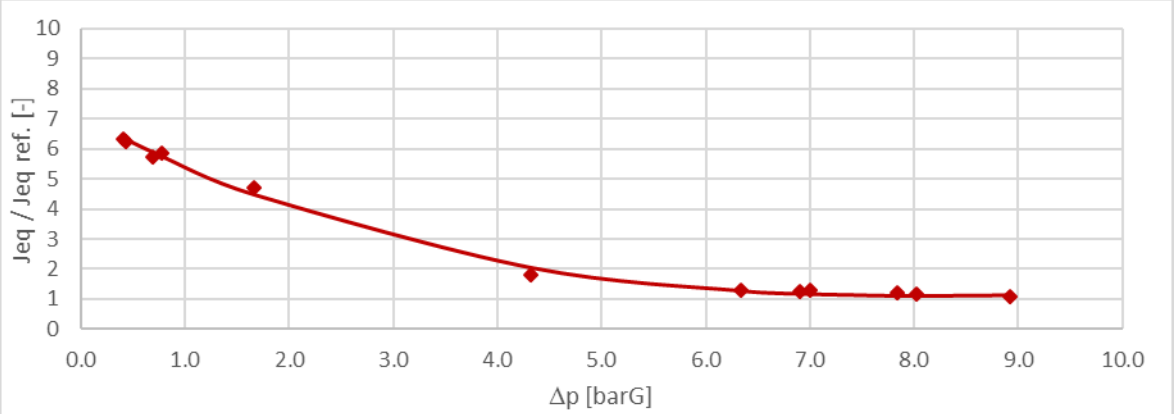

Figure 4.43 – Test 9 - Current-thick S2 - aligned - Characteristic curves

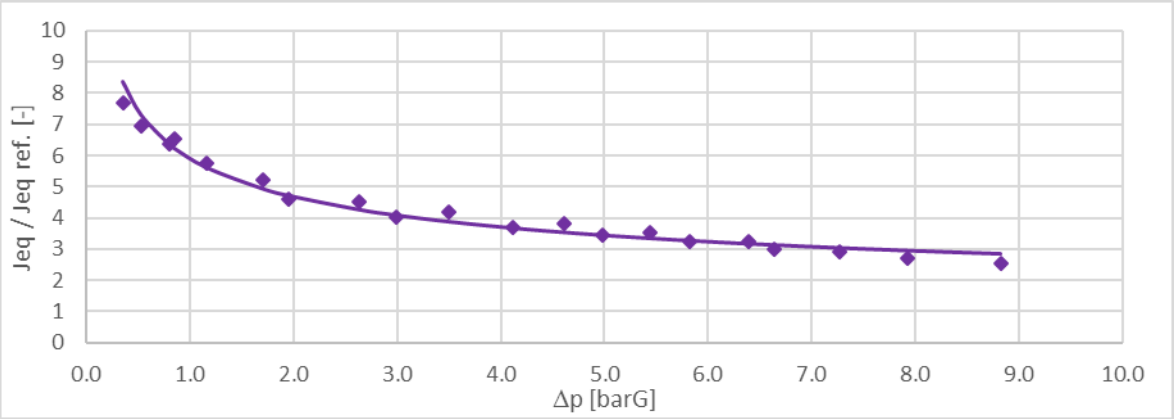

Figure 4.44 – Test 8 - Current-thick S3 - aligned - Characteristic curves

The images shown above describe the worn *current-thick* strip seals behavior. It can be noticed that all the seals are fitted with only one curve. For what concerns Figure 4.44, it is due to the fact that the presented seal isn't subjected to the activation process as discussed in paragraph 4.2.10. If Figure 4.42 and Figure 4.43 are considered, it can be observed that the activation phenomenon is more gradual than new *current-thick* strip seal (as explained in paragraph 4.2.10); it is for this reason that the behaviors which describe S1 and S3 can be fitted with only a characteristic function.

The graphs related to the misaligned configuration are shown as follow.

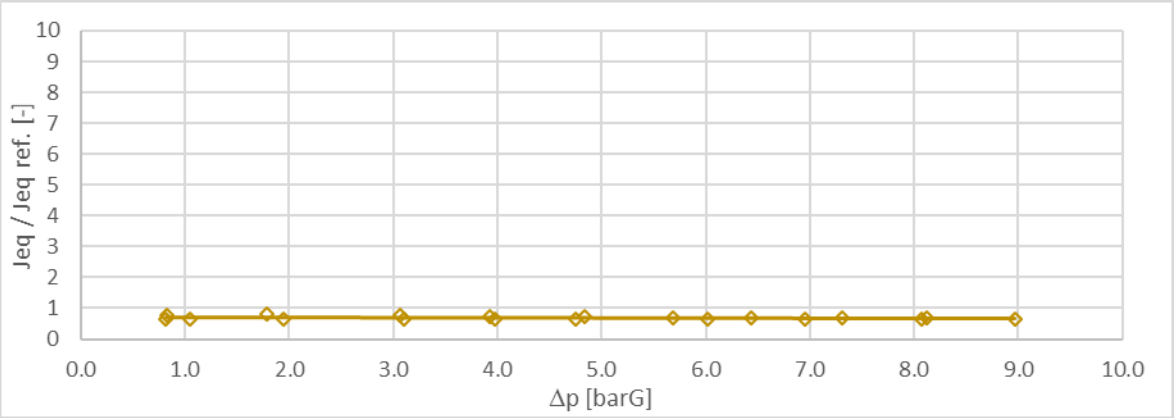

Figure 4.45 – Test 10 - Current-thick S1 - misaligned - Characteristic curves

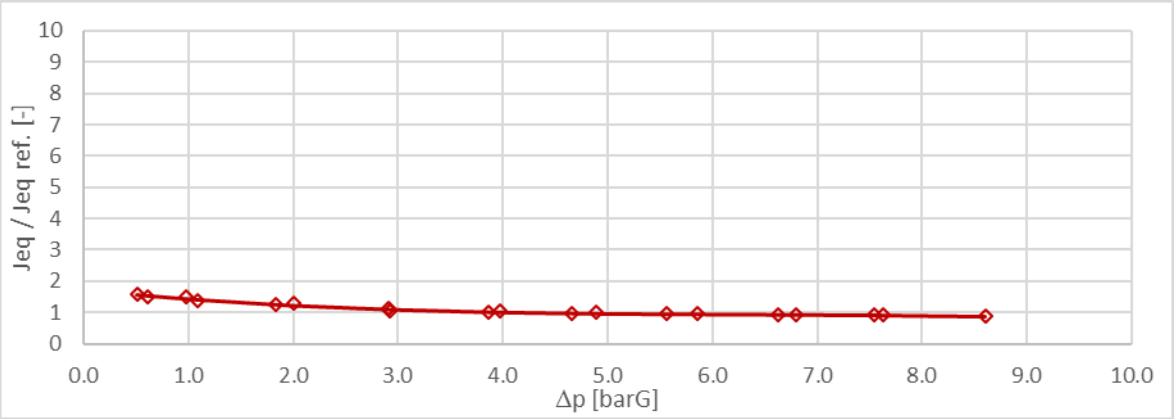

Figure 4.46 – Test 7 - Current-thick S2 - misaligned - Characteristic curves

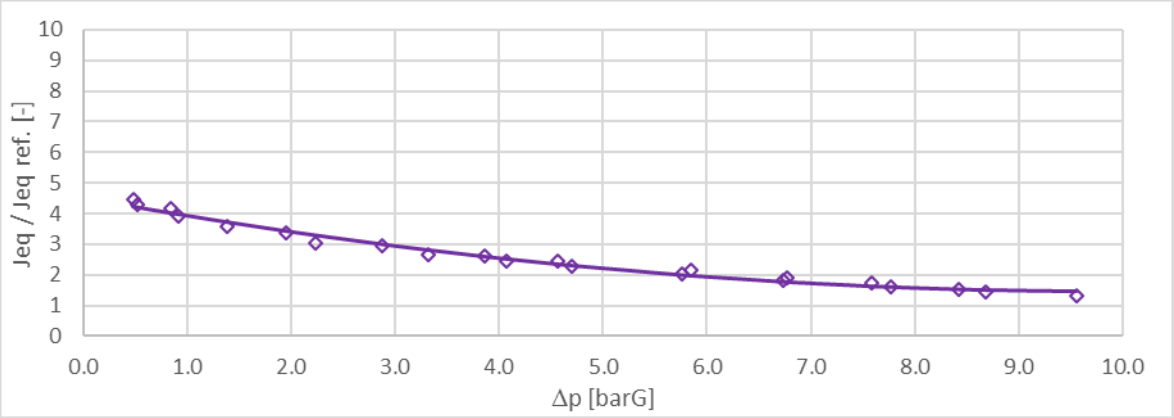

Figure 4.47 – Test 6 - Current-thick S3 - misaligned - Characteristic curves

The plots above reported show a characteristic function each one. The curves related to S2 and S3 are verified in the whole pressure range; the reason of that is the same exposed for the aligned rig configuration. S1's fitting function (Figure 4.45) is determined after the activation process, so it is reliable only in high pressure regime.

Table 4.6 – current-thick - worn - aligned configuration – fitting function

Seal	Range	Fitting function	R^2
S1	High pressure (dp>0.8 [barG])	$\frac{J_{eq}}{J_{eq_{ref}}} = 4.79 \cdot 10^{-4} \cdot dp^6 - 1.40 \cdot 10^{-2} \cdot dp^5 + 1.51 \cdot 10^{-1} \cdot dp^4 - 7.02 \cdot 10^{-1} \cdot dp^3 + 1.26 \cdot dp^2 - 1.31 \cdot dp + 6.98$	0.997
S2	All domain	$\frac{J_{eq}}{J_{eq_{ref}}} = -5.84 \cdot 10^{-3} \cdot dp^3 + 1.86 \cdot 10^{-1} \cdot dp^2 - 1.86 \cdot dp + 7.07$	0.997
S3	All domain	$\frac{J_{eq}}{J_{eq_{ref}}} = 5.90 \cdot dp^{-3.38 \cdot 10^{-1}}$	0.972

Table 4.7 – current-thick - worn - misaligned configuration – fitting function

Seal	Range	Fitting function	R^2
S1	High pressure (dp>0.8 [barG])	$\frac{J_{eq}}{J_{eq_{ref}}} = -4.64 \cdot 10^{-3} \cdot dp + 7.07 \cdot 10^{-1}$	0.0655
S2	All domain	$\frac{J_{eq}}{J_{eq_{ref}}} = -2.69 \cdot 10^{-3} \cdot dp^3 + 5.12 \cdot 10^{-2} \cdot dp^2 - 3.39 \cdot 10^{-1} \cdot dp + 1.72$	0.982
S3	All domain	$\frac{J_{eq}}{J_{eq_{ref}}} = 3.12 \cdot 10^{-2} \cdot dp^2 - 6.19 \cdot 10^{-1} \cdot dp + 4.53$	0.985

4.3.5 Worn *upgrade-thin* strip seal, aligned and misaligned

The fitting results related to worn *upgrade-thin* strip seal are shown in the present section for both the aligned and misaligned configuration.

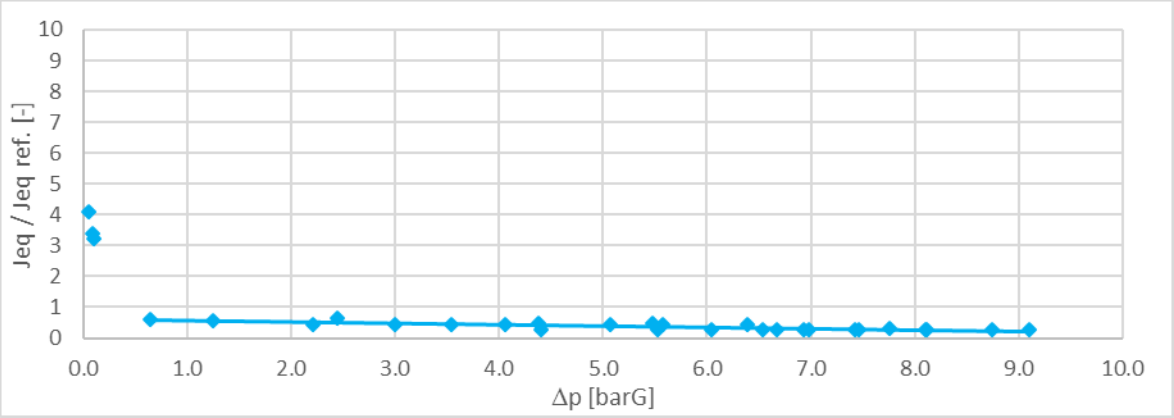

Figure 4.48 – Test 13 – Upgrade-thin worn - aligned - Characteristic curves

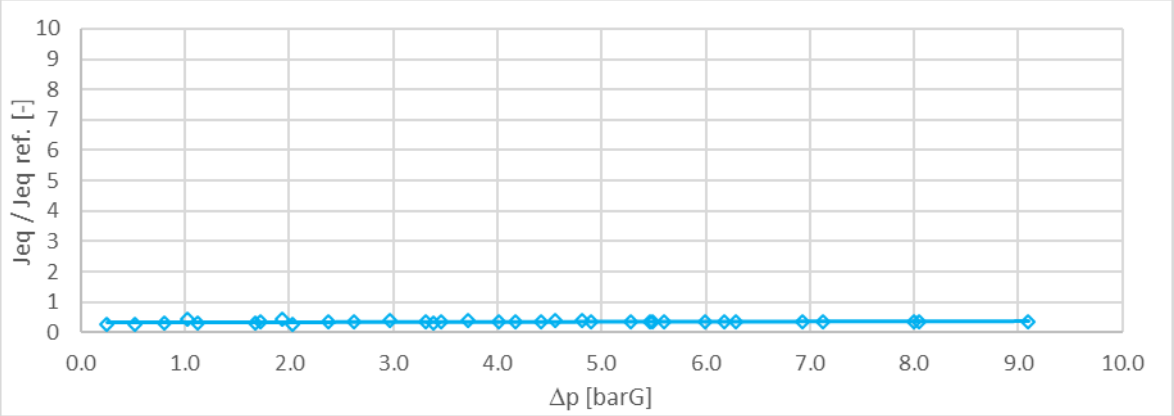

Figure 4.49 – Test 11 - Upgrade-thin worn - misaligned - Characteristic curves

Both the plots reported above represent the characteristic curve of worn *upgrade-thin* strip seal as a straight line. In Figure 4.48, low pressure behavior is not fitted since low pressure

points are not enough, in the misaligned case (Figure 4.49) any low pressure point was not obtained. In the table below the fitting function are reported.

Table 4.8 – upgrade-thin - worn – aligned & misaligned configuration – fitting function

Seal	Range	Config.	Fitting function	R^2
Upgrade-thin - worn	High pressure (dp>0.5 [barG])	Aligned	$\frac{J_{eq}}{J_{eq_{ref}}} = -4.29 \cdot 10^{-2} \cdot dp + 6.13 \cdot 10^{-1}$	0.688
Upgrade-thin - worn	High pressure (dp>0.2 [barG])	Misalign.	$\frac{J_{eq}}{J_{eq_{ref}}} = 4.91 \cdot 10^{-3} \cdot dp + 3.32 \cdot 10^{-1}$	0.0870

4.4 Measurement repeatability assessment

To be confident that test results reported in this document can be trusted, standard deviation was calculated between the different repetition of each test. In order to calculate it, it is fundamental that more than one repetition was performed for a particular condition to calculate the mass flow and equivalent gap at different pressure levels; not every test was made more times, it is for this reason only some tests are reported in the table below.

Table 4.9 - test number and repetition

Test n°	Numbers of repetition
1	4
2	3
3	2
4	2
5	2
11	2
12	2
13	2

The standard deviation is more reliable if the test is repeated multiple times. However, due to time constraints, the tests were repeated only if some issue was present. In order to compute the standard deviation, the set of data J_{eq} vs. dp related to each repetition was subjected to a resampling procedure.

4.4.1 Resample process

To do this task, first of all an interpolation for the points related to the same repetition (ex. test “1a”, “4b”, …) was made; the method adopted is the least square methods. The criteria utilized to make the best choice of the fitting function consists in using the lowest possible order of the polynomial fitting function and maximizing the R^2 parameter. Each repetition was fitted with only one function and each repetition of the same test was fitted with the same polynomial function, despite to what was done in paragraph 4.3. On the contrary,

different tests were fitted with slightly different functions in order to try to reproduce the experimental data with the lowest possible error.

After that, from dp = 1 [barG] to 7 [barG] with 1 [barG] step the resample was made for each test repetition. The resample was not made for pressure higher than 7 [barG] because not every test reaches 8 or 9 [barG] and it is out of the operative engine's pressure range (Figure 2.16). With the results for the same test and pressure, but different repetition the standard deviation was calculated.

4.4.2 Standard deviation

In this paragraph the standard deviation's behavior will be discussed for each test in which it is admissible to calculate (these tests are listed in Table 4.9). The charts are reported below, and they comply with the legend reported in Appendix A: charts legend.

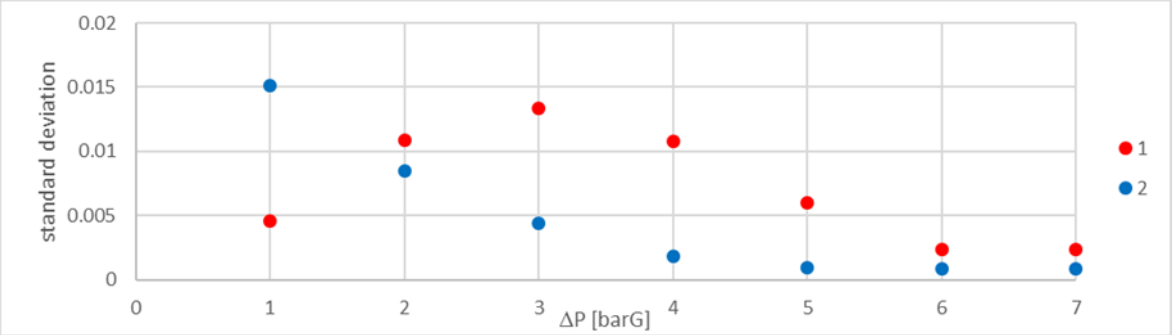

Figure 4.50 - test 1 & 2 - standard deviation

The chart above shows that the test 2 is more reliable than the test 1. To confirm that, it can be noticed the standard deviation increases for the test 1 until 3 [barG] and then it decreases again. Test 2 has a different behavior: it starts from high values but it decreases in a fast way and remains under the values calculated for the test 1 for the all pressure values greater than 2 [barG].

The values related to the tests 3 and 4 are even lower than those just discussed, and they are shown in the following plot.

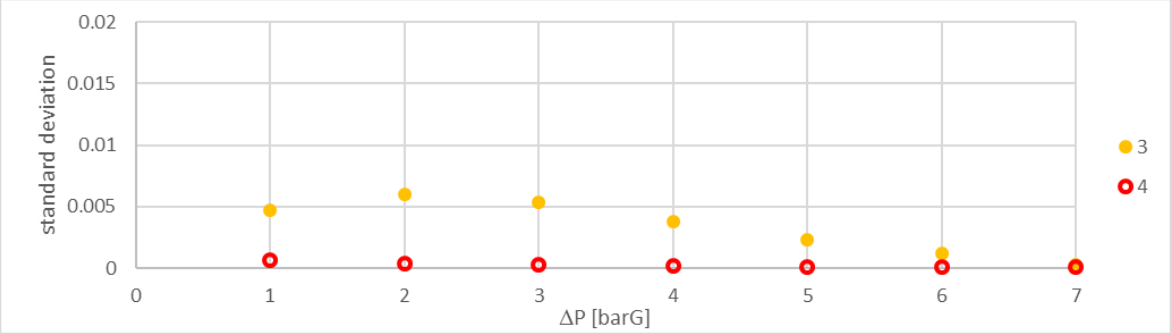

Figure 4.51 - test 3 & 4 - standard deviation

Figure 4.51 shows that the values obtained for tests 3 and 4 are more consistent than tests 1 and 2, in fact the results shown in Figure 4.50 are higher than the data reported in the chart above.

Below the other four standard deviation plots are represented.

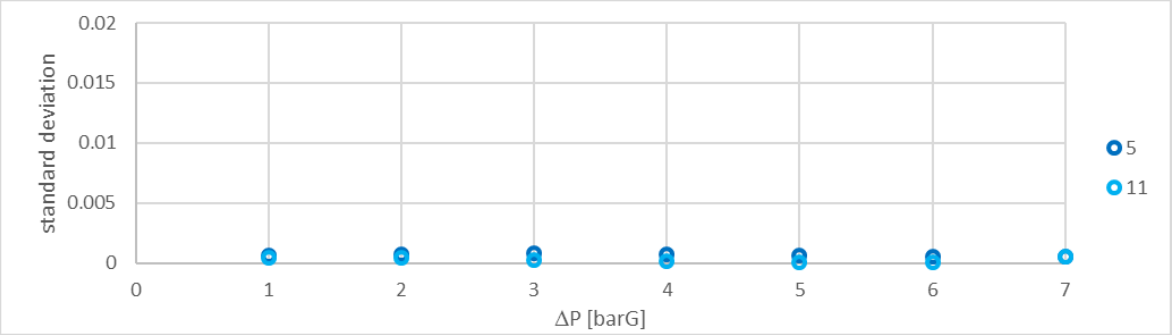

Figure 4.52 - test 5 & 11 - standard deviation

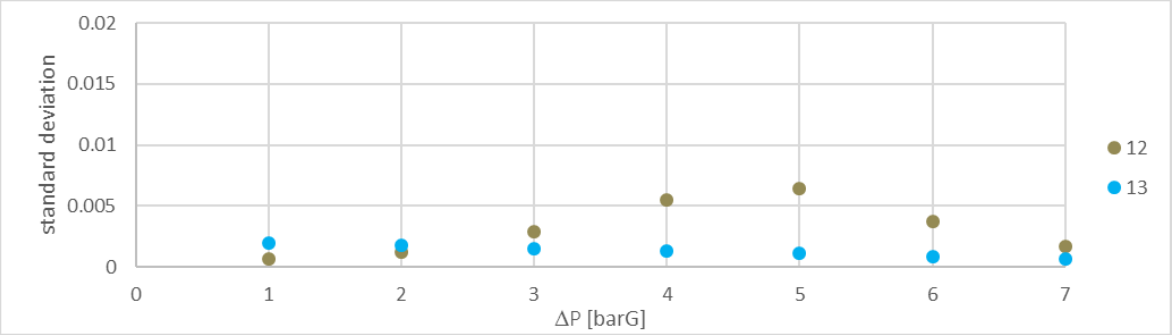

Figure 4.53 - test 12 & 13 - standard deviation

From the chart comparison, it's evident that test 1 is the worst one in terms of repeatability, test 2 has a lower standard deviation at *dp* values greater than 2 [barG]. Test 3 (Figure 4.51) has an high standard deviation in the pressure range characterized by higher differences between the trends obtained in the two repetitions (remind to paragraph 4.2.3, Figure 4.9 and Figure 4.10), but it is still in an acceptable range; no further problems were reveled in test 4 (same chart). Tests 5, 11 and 13 (Figure 4.52 and Figure 4.53) give also good results in terms of dispersion. For what concerns test 12 it happens something different, in fact the standard deviation has a different behavior compared to the other tests analyzed, but can be ascribed to a local oscillation of the fitting functions; anyway, results are still better than test 1.

As it happened many times in different tests, the different repetitions of the same test gave different results that are not in the error tolerance instruments; this kind of things may happen because of the different position that can be assumed by the seal inside the groove. If the groove is big enough for the seal, it can move freely in the lodge assuming different positions. If the seal is clamped or activated, it is forced from the pressure to a particular position. To confirm what just said, the chart related to *current-thick* geometry in misaligned (test 4, Figure 4.51) and aligned configuration (test 1, Figure 4.50) are considered: it can be seen that when the seal has more space to move the standard deviation is higher but if the attention is focused in the misaligned configuration, where the seal has less space to move, the standard deviation is much lower. The same thing can be observed by referring the *upgrade-thin* geometry: in the aligned case (test 2, Figure 4.50) the seal is "free" to move until the activation (after the activation the seal's positions is almost fixed), instead in the misaligned geometry the seal is activated at lower pressure thus the position doesn't vary a lot between the different repetitions as it's evident if Figure 4.52 is observed.

5 Fluid network calculations (SiX update and TCLA savings)

In the present chapter the results obtained in the previous chapter are implemented in the already mentioned Ansaldo Energia's 1D tool, the secondary air system fluid network SiX_o, in order to understand improvement on TCLA saving potentially brought by the use of thinner strip seals. The fitting functions described in paragraph 4.3 are implemented in the model layout and the calculation is performed at Base Load conditions.

5.1 SiX_o fluid network 1D modelization

5.1.1 CalculiX software

The present Ansaldo Energia own software is based on CalculiX, an open-source software developed by MTU Aero Engines, based on finite element analysis. For its adoption in the calculations needed, it is essential to add the elements related to the fluid network which characterize the gas turbine, in this particular case the SAS. MTU had adopted many programming languages to develop the present tool, with aim to describe the different elements behavior and their physics. In order to find the solution of the problem the Newton-Rapson scheme were adopted as solver. Both linear and non-linear calculations can be handled by the software, and, thanks to this, it is able to solve thermal fluid dynamics problems. The main advantage of the solver is related to the possibility of adopting a Multiphysics structural-fluid dynamic approach: it allows, in fact, in gas turbines engines, for example to estimate the clearances and the to make a fluid dynamics analysis together [19].

5.1.2 SiX_o

To evaluate the performance of seals mounted on the engine many ways exist. For what concerns new upgrades, test campaigns using ad-hoc built rigs are usually performed. In order to understand what happens in the real engines, field measurements can be made with traditional instrumentation installed in all the engines or sometimes, during the maintenance operations, additional instruments can be used to analyze a particular problem. If field measurements are not available, CFD is the other option. Since it is not possible to perform the mentioned analysis for all the operating conditions, an Ansaldo Energia's own tool, named SiX_o, is adopted.

SiX_o is developed by the company for internal use; it is a 1D fluid network and, in particular, it is utilized to understand and determine what happens in the SAS lines in the different operating conditions. A representation of a typical fluid network model is reported below:

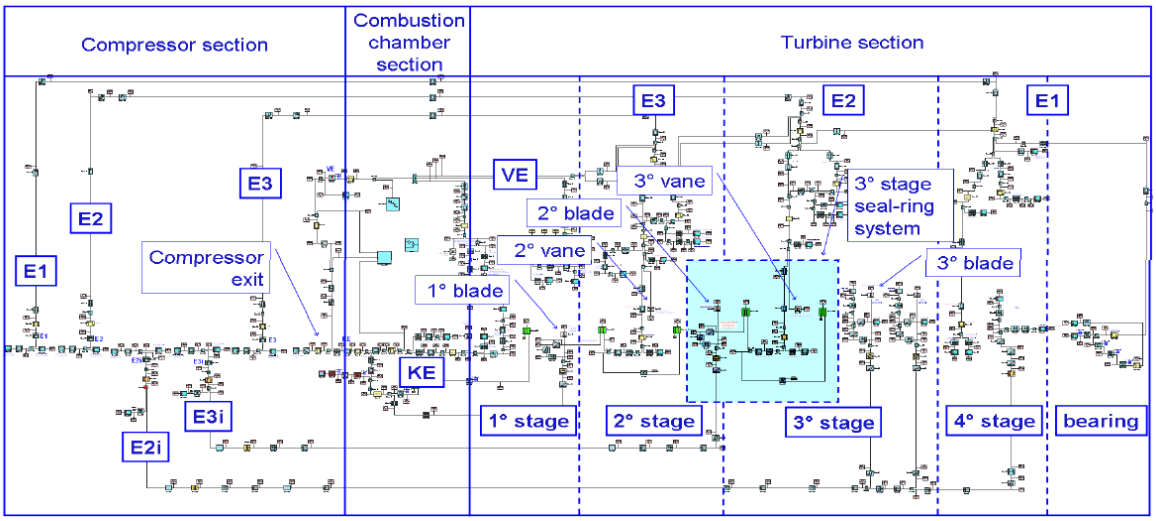

Figure 5.1 – 1D fluid network example [23]

As it was explained in paragraph 5.1.1, SiX_o is based on CalculiX; its main objective consists of estimating the secondary air mass flow rates, pressures and temperatures. Numerous components in the network are represented by an equal number of models, each of which solves the fundamental equations of continuity, momentum, and energy conservation [27]: as said above, it is necessary to model 3D complicated phenomena using laboratory, CFD, or field data and, thanks to the results, it is possible to calibrate the coefficients to use in 1D simplified equations.

At the compressor bleed and turbine main channel for both cooling and leakage flows, the boundary conditions (the working pressure and temperatures) are established for each place in the current software. Every component, or block, adopted in the software is connected to one or more other components via a node that is described by pressure and temperature properties. The bleed lines from the compressor extraction nodes to the hot gas section of the turbine main annulus can be modelled using the modular 1D code.

By linking their input/output ports graphically via a bus data, network components form the full cooling/sealing system of the gas turbine. The thermodynamic conditions at the compressor extraction sites are provided by the inlet boundary components of the network model. Accordingly, outlet boundary elements are:

- modules for stator-rotor cavities
- modules for cooling flows related to vanes and blades
- modules for leakage flows through roots.

By employing the local static pressure derived by the CFD calculation of the turbine rows as the boundary condition, leakage and sealing flows are computed using loss-elements. These elements are described by parameters which consider the real flow conditions and behavior. Their calibration depends by the available data: they can be chosen accordingly with literature knowledge, experimental campaigns or CFD results.

5.1.3 Most relevant connection: “target leakage connection”

In the presented software, many connection types are available.

The most important element of the network for this thesis' work models the strip seal and it is named "*target leakage connection*". It allows to estimate the leakage air through the strip seal, by modelling it as an orifice. In particular, it is described by a correlation for the equivalent iso-entropic orifice for compressible flow. The J_{eq} (defined in paragraph 2.1, equation (2.3)) is provided by a law imposed as input by the user as function of the pressure ratio. This kind if connection is described by many parameters following reported:

- N [-], number of elements in parallel.
- $length$ $[m]$, which is the transversal length of the seal.
- β [-], pressure ratio defined as $\frac{p_{in}}{p_{out}}$;
- J_{eq} $[m]$, equivalent gap at a specified pressure ratio.
- $Npoints$ [-], number of couple of points for the defined J_{eq} law.

In the present connection type, the discharge coefficient C_D is considered as ideal, thus equal to 1, and the J_{eq} value is calculated with the law defined as function of the pressure gradient.

In order to evaluate the leakages across the strip seal, the transversal section is estimated as function of the pressure ratio defined with a preliminary experimental test campaign. The function that allows to calculate the equivalent gap is defined by points and the intermediate values are determined by the solver with a linear interpolation. The transversal section is obtained with the following relation:

$$S = J_{eq} \cdot length \tag{5.1}$$

The total pressure drop is defined as boundary condition with two additional elements, downstream and upstream, and they are selected as consequence of the operating point that it needs to be analyzed.

Finally, the energy balance needs to be imposed; the resultant equation is following reported:

$$T_{t,in} = T_{t,out} \tag{5.2}$$

As it was said some lines above, in this particular case the equivalent gap has to be defined as function of the pressure ratio. In order to do that, since the results shown in paragraph 4.3 are reported as function of the pressure gradient, the correlations obtained needs to be re-defined with the pressure ratio.

The presented connection must have two nodes, one upstream and one another downstream itself, in order to define its boundary conditions. Upstream the analyzed connection there is a node which contains all the flow properties calculated iteratively with all the other network elements (in this case the focus is on the total pressure and total temperature). Downstream the described element there is a node defined as "*plenum*". This particular node contains the hot-gas properties (static pressure) related to the particular turbine main flow location, along the expansion line.

An example of the typical network model is reported as follow:

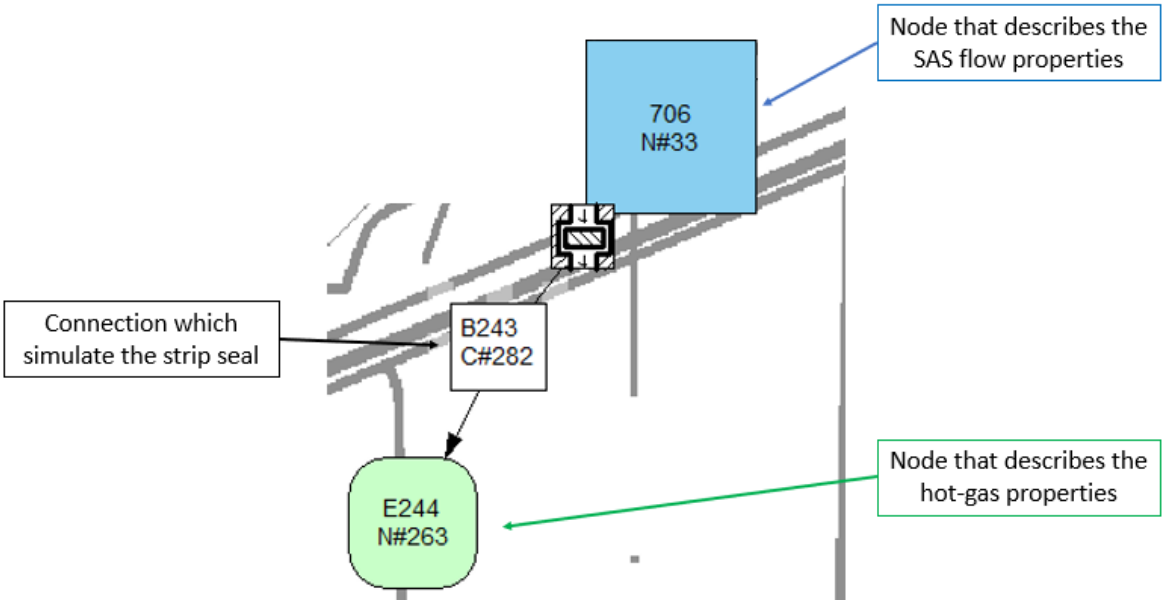

Figure 5.2 – Strip seal modeling example

5.2 SiX_o network refinement

Within this work, the opportunity was taken of improving the current way in which each strip seal is modelled in the SAS network. Therefore, instead of using one single element comprising the full length of the strip and connected to only one pressure as a boundary condition, calculated as the average pressure between the leading edge and the trailing edge side of the stator vane row, a two portions modelling was used.

This was done in order to consider the discharge pressure variation which has an effect on the acting pressure delta for the local portion of the strips and gives place to a different J_{eq} value, also according to the tests done for this work (paragraph 4.2). Therefore, each stator strip seal of the engine was split in two portions: the first one is modelled with the vane leading-edge pressure, the second one with the vane trailing-edge pressure as a boundary condition. As an acceptable approximation against the continuous variation of pressure during the expansion, the strip seal portion upstream the vane aerodynamic throat was linked to the leading-edge pressure, while the strip portion downstream it was modelled with the trailing edge pressure as boundary condition.

The strip seal's splitting was made with the support 3D CAD analysis. The engine CAD is observed in Siemens NX and the throat position was estimated as compared to the strip seal position. The seals are not always longitudinally split equally between leading and trailing edge, in fact the seal is usually unbalanced to one of the two sides. Since the SAS plenum side is at uniform pressure along the seal, it can be expected that there will be a lower pressure gradient at the leading edge and higher at the trailing edge, since the pressure reduces along the turbine axis. Because of this, by remembering the results shown in Chapter 4, a higher equivalent gap is expected at the leading edge.

An example of the splitting operation in the network is shown in the following picture.

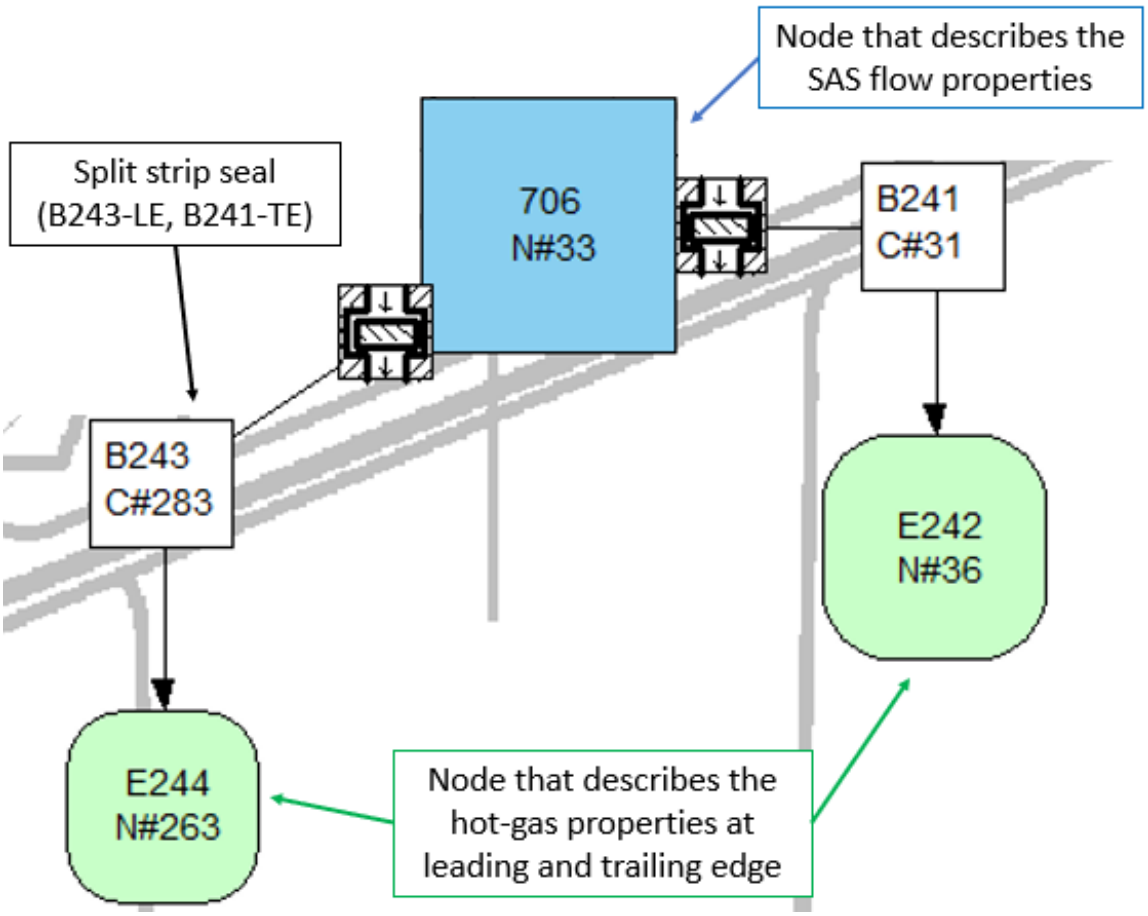

Figure 5.3 – Example of a split strip seal

5.3 Equivalent gap fitting functions

As it was explained in the paragraph 5.1.3, for the SAS calculations the functions which describe the equivalent gap with the pressure ratio are needed for each strip seal configuration: *current-thick*, *thicker*, *upgrade-thin*. Moreover, the results need to be analyzed in both the experimented alignment conditions: *aligned* or *misaligned*. In the paragraph 4.3 the characteristic functions for each case analyzed are reported versus the pressure gradient. The J_{eq} is estimated for each strip location along the turbine, with the further split between leading edge and trailing edge side.

Aligned configuration ensures a univocal equivalent gap law. This gets instead different for what concerns misaligned groove configuration, in fact the triangular gap area mentioned in Chapter 4 has to be considered. In particular, this time it is considered twice for each seal, the first one near leading edge, the second one near trailing edge. In order to obtain the new equivalent gap that includes the mentioned area, involved calculations are reported as follow.

$$A_{eq,exp} = J_{eq,exp} \cdot L_{strip} \tag{5.3}$$

$$A_{eq,SiX} = A_{eq,exp} + 2 \cdot A_{hole} \tag{5.4}$$

$$J_{eq,SiX} = \frac{A_{eq,SiX}}{L_{strip}} \tag{5.5}$$

Where:

- L_{strip} is the length of the particular strip seal analyzed in the engine
- $J_{eq,exp}$ is the equivalent gap obtained during the test campaign
- $A_{eq,exp}$ is the equivalent gap area when the lateral gap area is not considered
- A_{hole} is the lateral gap area introduced in Chapter 4
- $A_{eq,SiX}$ is the equivalent gap area that results if the lateral gap area is considered
- $J_{eq,SiX}$ is the equivalent gap that is imposed in SiX_o.

An example of the equivalent gap trend for a specific turbine vane strip seal in misaligned configuration is reported as follow. As it was done in Chapter 4 the equivalent gap values reported in this section are represented as dimension-less ratio between J_{eq} and a reference value, which is the first equivalent gap value related to *current-thick* strip seal after the activation process.

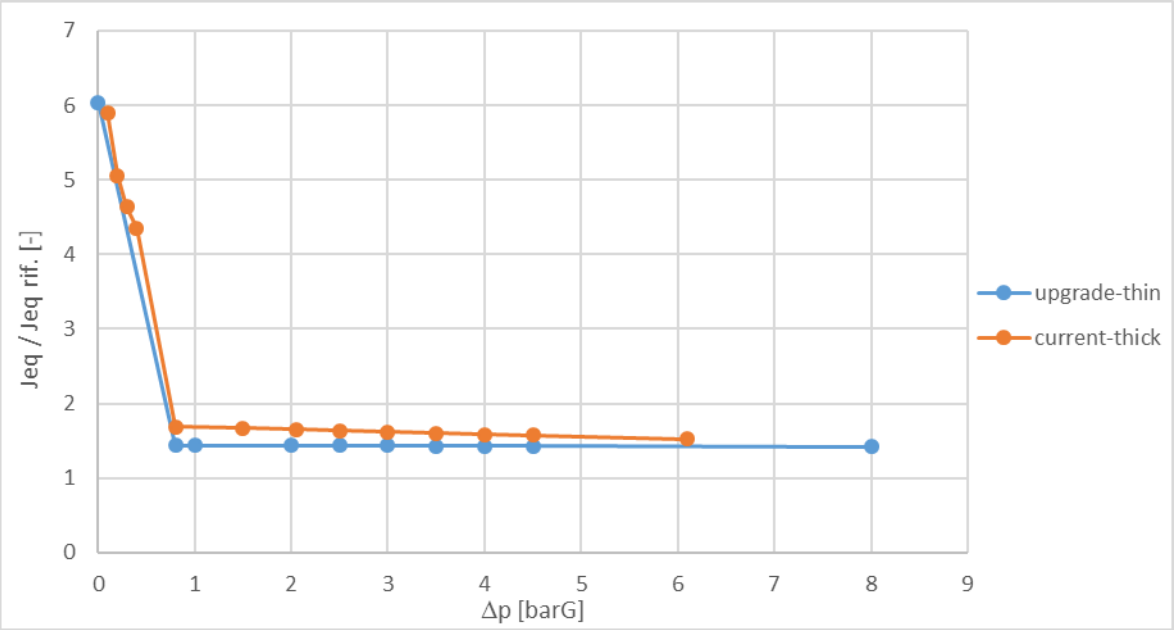

Figure 5.4 – equivalent gap vs. pressure gradient - related to a particular seal in the engine – misaligned configuration

It can be observed that for *upgrade-thin* strip seal, at low pressure ratio the equivalent gap value chosen is the average of experimental data related to the aligned case (any low pressure law was not determined), at high pressure the fitting function obtained in paragraph 4.3 is adopted. The passage between low and high pressure behavior is extrapolated as linear regression by the solver.

Moreover, it can be noticed that *upgrade-thin* strip seal always ensures lower equivalent gap compared to *current-thick* one for the specific vane to which is referred Figure 5.4 but something can change if different vanes are considered; A_{hole} effect has different weight on equivalent gap depending by the seal length (remember equation (5.5)).

5.4 SiX_o results: aligned configuration

In the present section the evaluation of the SAS leakages variation takes place, also with an analysis which concerns the cooling mass flow variations achieved with the sealing performance variation of new strip seals.

In this analysis three different strip seals are considered: *current-thick*, *upgrade-thin*, *thicker* (as it was done for the test campaign). The analysis reported in this chapter is only related to new seals, since the available *upgrade-thin* had not operated long enough to be fairly compared to their analogous *current-thick* ones. After the equivalent gap function update in the solver as well as the above mentioned network refinement via splitting the strips seal element in two sides, the results were obtained. First of all, the leakages variations are analyzed for each vane and the effects on the cooling system is considered; then the global TCLA saving is calculated. Moreover, the strip seals leakage variations are distinguished from the other correlated variations, which include the cooling and other mass flow variations along SAS lines. Below, the charts that describe the leakages variations for each turbine vane are shown.

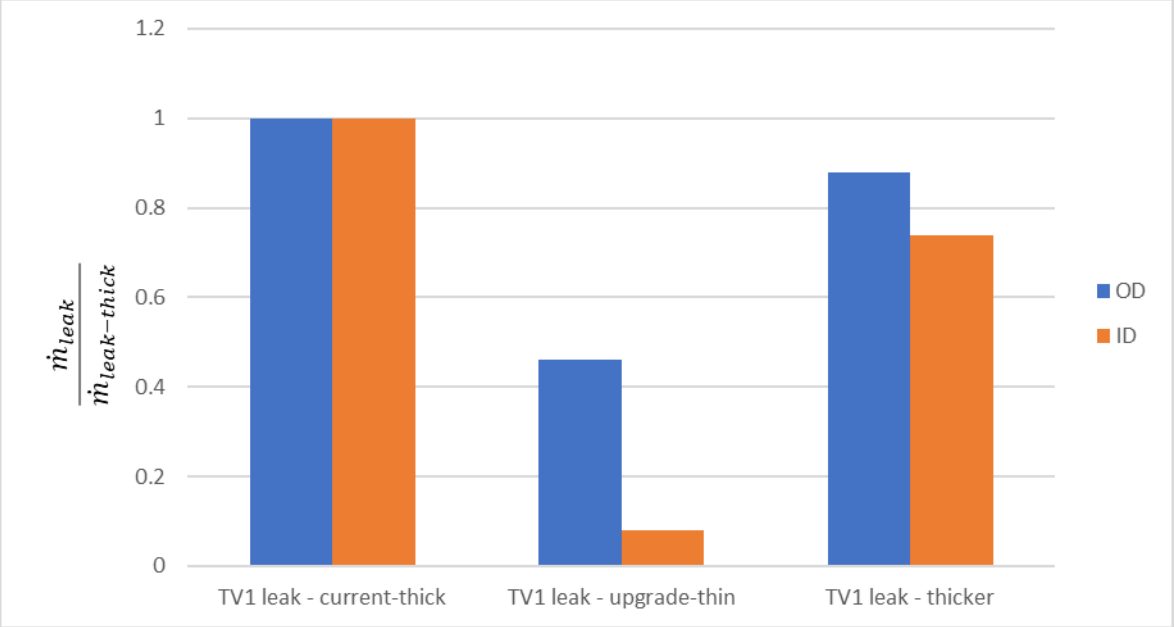

Figure 5.5 – TV1 strip seals leakage compared to current-thick aligned – aligned config.

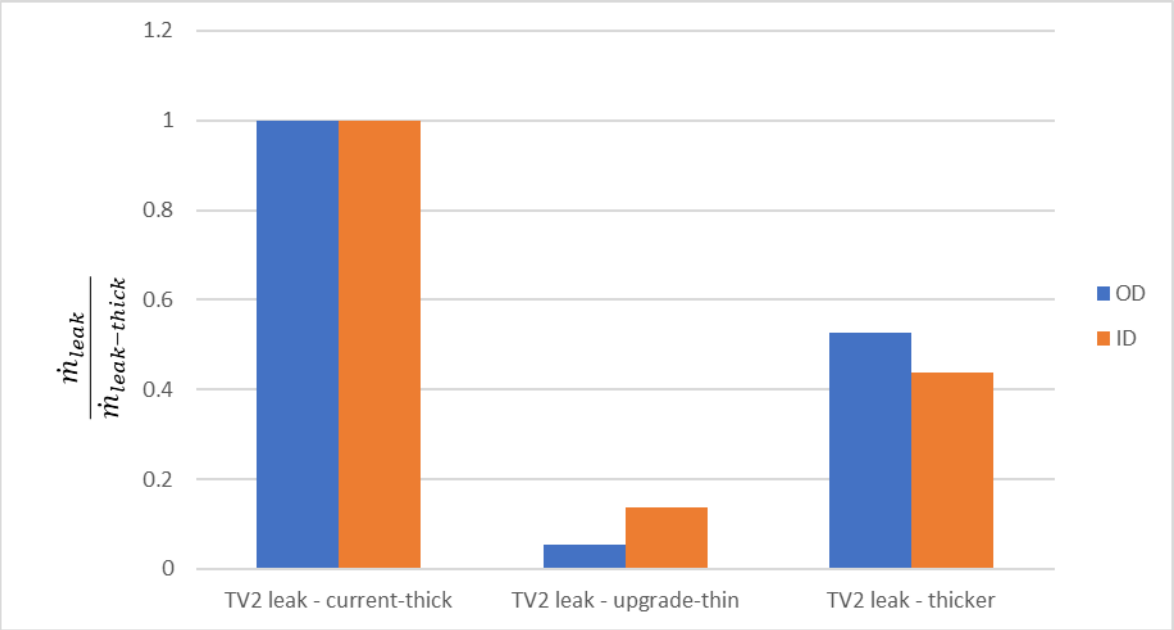

Figure 5.6 – TV2 strip seals leakage compared to current-thick aligned - aligned config.

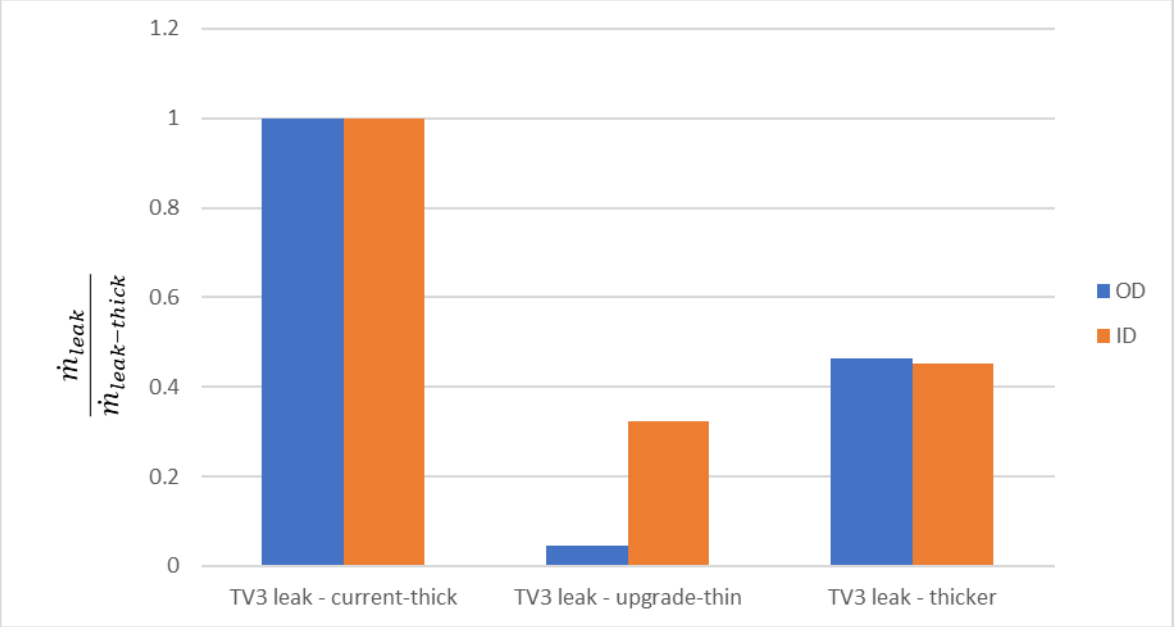

Figure 5.7 – TV3 strip seals leakage compared to current-thick aligned - aligned config.

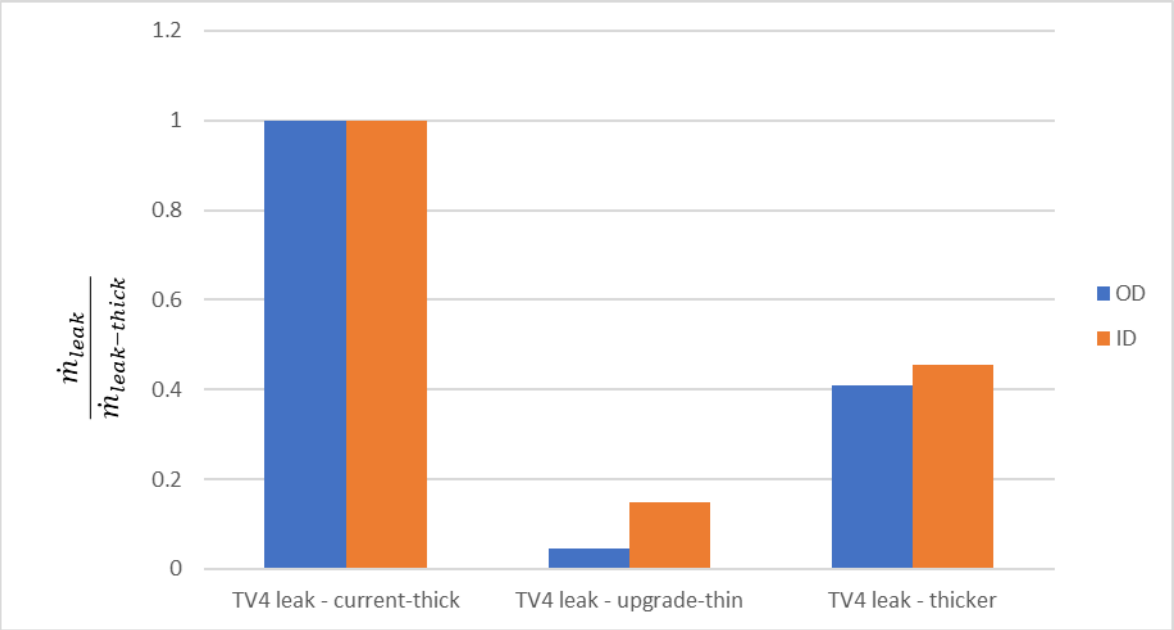

Figure 5.8 – TV4 strip seals leakage compared to current-thick aligned - aligned config.

The plots above reported show leakage flow amount for each turbine vane row axial strip with on the vertical axis the mass flow rate normalized with the one related to *current-thick* strip seal in the aligned configuration. As it can be seen, *upgrade-thin* strip seal always grants a better sealing capability compared to *current-thick*. Moreover, the *current-thick* strip seal performs better if the tolerances allow to fit almost perfectly inside the groove, that is represented by the cases labeled *thicker* strip seal, as compared to when it is subjected to the activation process which only happens over a certain delta pressure (as discussed in paragraph 4.1). Anyway, it can be concluded that for all the turbine vanes *upgrade-thin* strip seal represents the best case with a large leakage reduction in both the radial positions: inner and outer diameter (respectively ID and OD).

After the local leakage variation analysis, it is possible to determine the total leakages variations which distinguish leakages related to the analyzed strip seals and the others due to undirect effects. Below, the chart which shows the mentioned variations is reported.

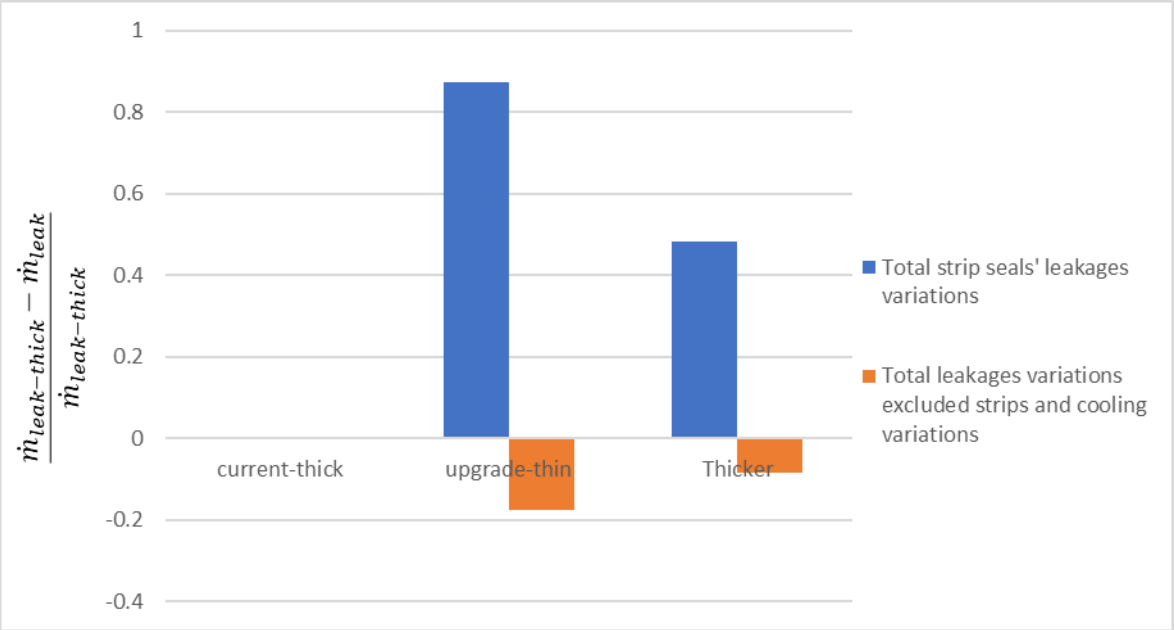

Figure 5.9 – Leakages savings compared to current-thick aligned - aligned config.

The picture above shows the mass flow delta savings related to the different strip seal technology adopted normalized with the total leakage mass flow related to *current-thick* strip seal across properly the strips. Positive values are related to a leakage reduction, negative to leakage rise. It can be observed that the leakage across the seals reduces for both *upgrade-thin* and *thicker* strip seals. Biggest leakage reduction is observed for *upgrade-thin* strip seal (blue column), as it was already clear by looking at the series of plots from Figure 5.5 to Figure 5.8.

In addition, Figure 5.9 shows that strip seals' leakages reduction has a slight impact also for all the other the engine leakages. It can be observed that the leakage reduction across the mentioned seals has, as consequence, leakages rising across SAS lines but much less (orange column). This is due to a slight over pressurization of the SAS plenums which feed all the leakages, which is induced by the relevant reduction of leakage through the axial strip seals object of the upgrade.

Finally, the evidence shows that *upgrade-thin* strip seal ensures lower leakages compared to *current-thick* and *thicker* strips. Below, the chart which shows the cooling air variations linked to the strip seal upgrade for each turbine vane is also reported.

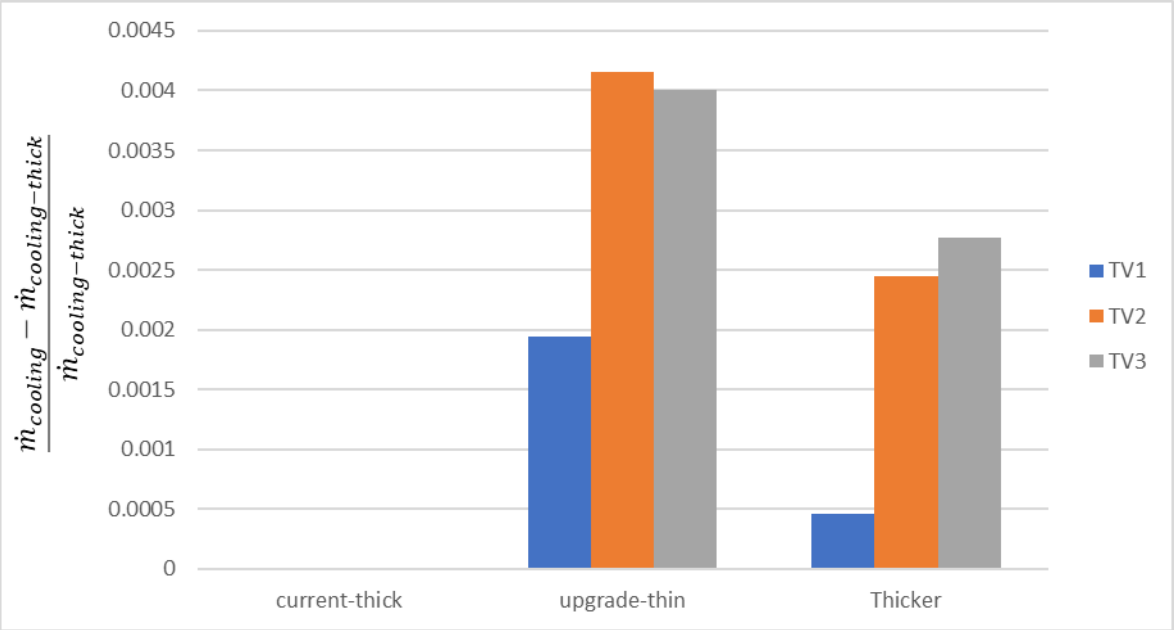

Figure 5.10 - cooling variations compared to current-thick aligned - aligned config.

The plot above shows the cooling air mass flow delta between each seal and *current-thick* one adimensionalized with cooling mass flow for the vane represented by each column and related to the *current-thick* strip seal.

Figure 5.10 shows that cooling air variations are almost negligible, in fact the largest increase is about 0.4% of the original cooling air, found for *upgrade-thin* strip seal in the second turbine vane.

Thanks to the presented calculations, it is then possible to determine the global leakage reduction due to the adoption of different seals. This mentioned variation is shown in the following chart.

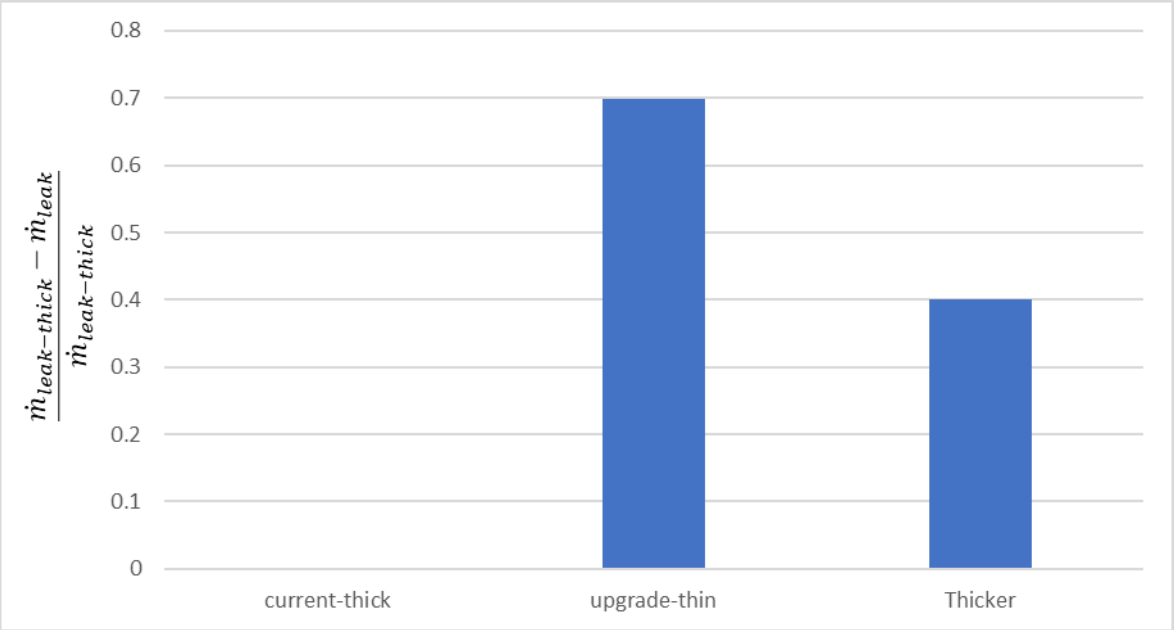

Figure 5.11 - total stator leakage savings compared to current-thick aligned - aligned config.

The chart above shows, on vertical axis, the mass flow variation between each seal and *current-thick* strip seal normalized with total stator leakages related to *current-thick* strip seal. Figure 5.11 shows that, thanks to new sealing geometry, leakages get reduced about 40% when *current-thick* strip seals fits perfectly the groove size. Reduction can be up to 70% if *upgrade-thin* is considered.

The analysis also requires TCLA fluctuation in relation to itself in the current configuration. The graphic that explains it is displayed as follow.

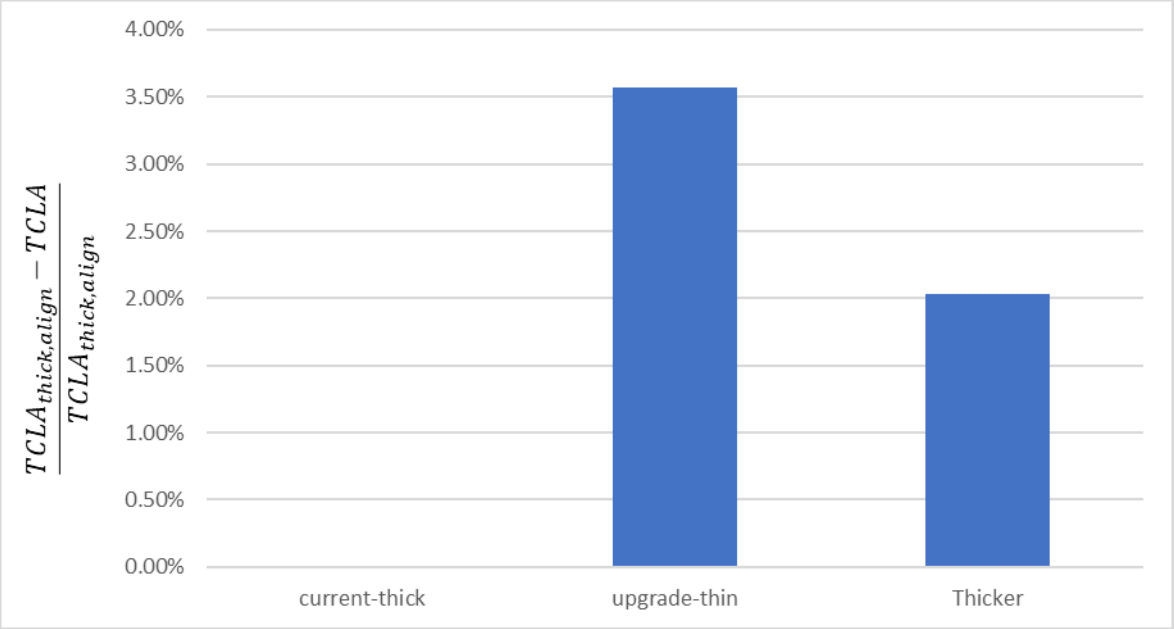

Figure 5.12 – TCLA (% of $TCLA_{current-thick}$) savings compared to current-thick aligned - aligned config.

The image above shows the TCLA variations compared to *current-thick* strip seal adimensionalized with the TCLA related to *current-thick* too. Also in the present plot TCLA saving is observed if *current-thick* strip seal fits perfectly the groove height (about 2.03%), but the most relevant result is detected if *upgrade-thin* one is considered, that reduce TCLA consumption in a more relevant way (about 3.57%).

5.5 SiX_o results: misaligned configuration

As it was done in the previous paragraph, in this section SiX_o results related to the misaligned configuration are analyzed and, also in this case, compared with *current-thick* results in the *aligned* configuration.

In the present analysis only two strip seals (the two types tested in the misaligned groove configuration analyzed in Chapter 4) are analyzed with the solver, in order to understand the behavior of the SAS flows along the whole gas turbine in the misaligned configuration. In order to do that, the fitting laws reported in paragraphs 4.3.1 and 4.3.2 (Figure 4.38 and Figure 4.40) are substituted in the solver. In the present case it is not enough, in fact, as it was explained in the paragraph 4.2.4 and remarked in 5.3, a triangular lateral gap A_{hole} is detected, and it needs to be included in the calculations. In the engine it is probably located at both the seal extremes, leading and trailing edge, thus it is considered two times for each seal analyzed. As a matter of fact, the equivalent gaps imposed in the solver result higher than the ones shown in paragraph 4.3; they include the lateral gap area and its effect on J_{eq} depends by the local strip length, which varies along the gas turbine.

Also in this case, the results will be analyzed for each vane for what concern leakages and cooling variations, then the other leakages variations will be analyzed with the global TCLA saving or rising. Below, the charts that describe the leakages variations for each turbine vane are shown.

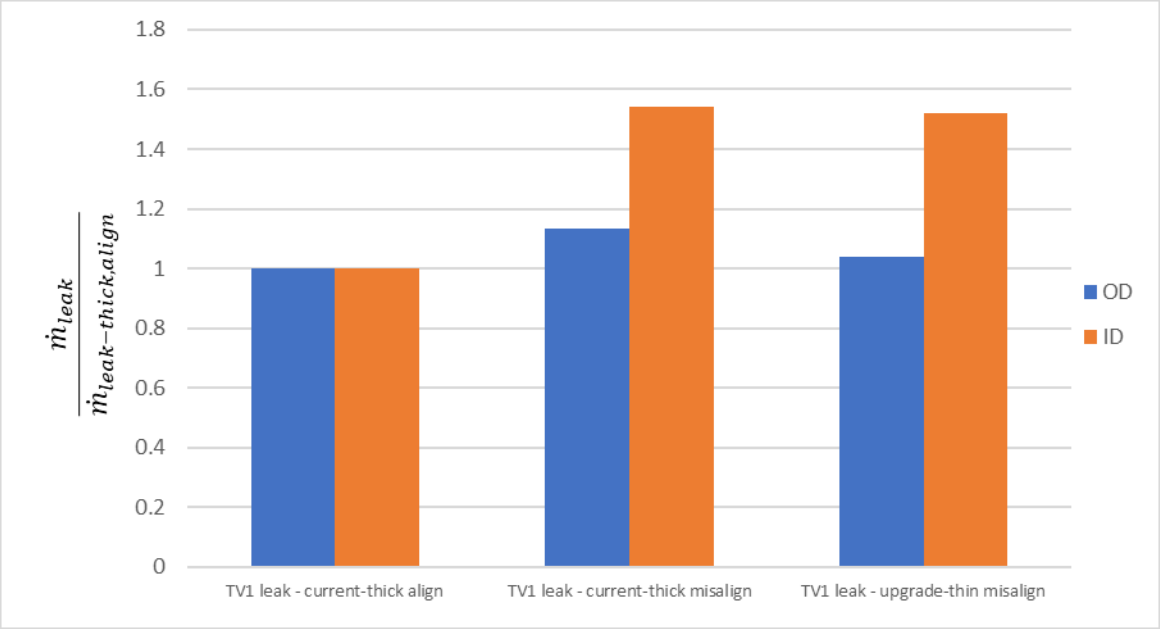

Figure 5.13 – TV1 strip seals leakage compared to current-thick aligned – misaligned config.

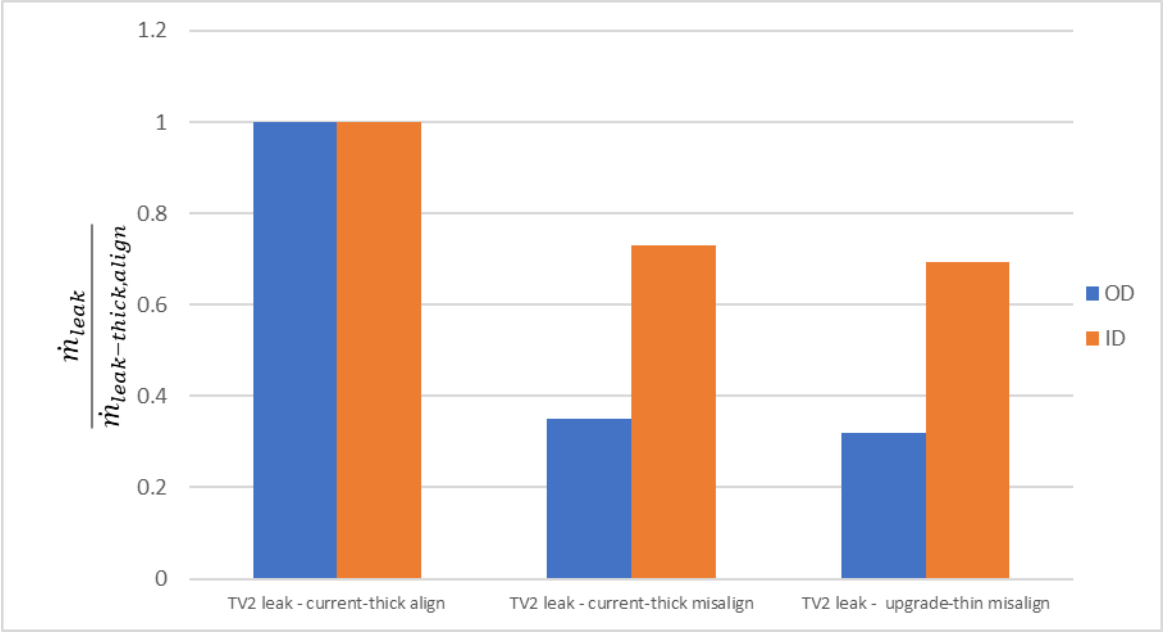

Figure 5.14 – TV2 strip seals leakage compared to current-thick aligned – misaligned config.

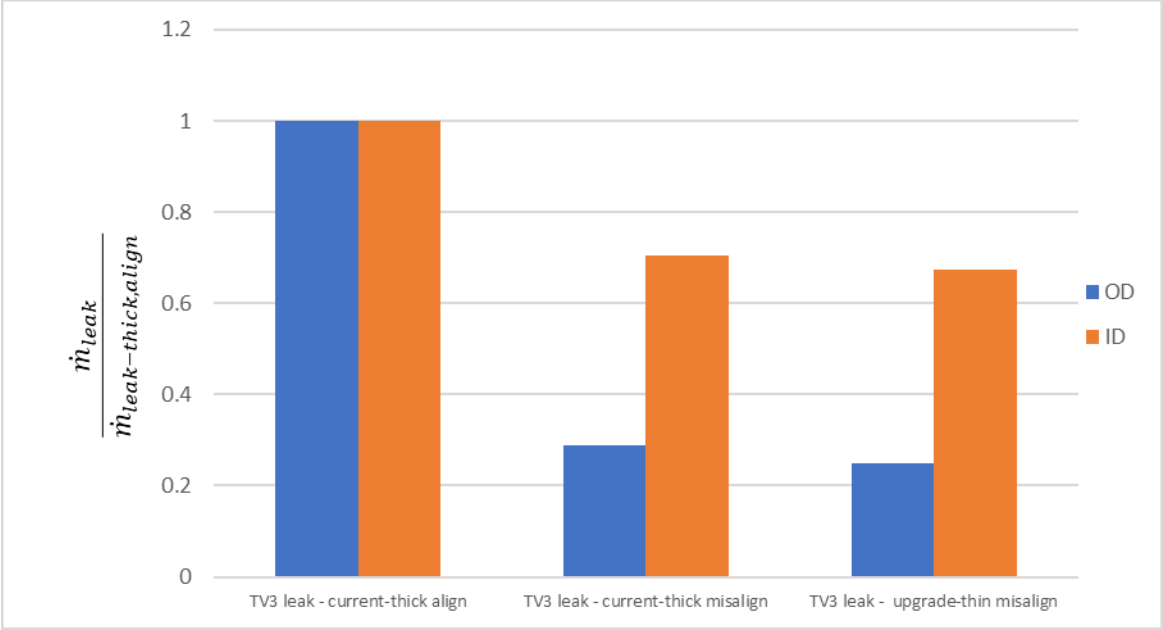

Figure 5.15 – TV3 strip seals leakage compared to current-thick aligned – misaligned config.

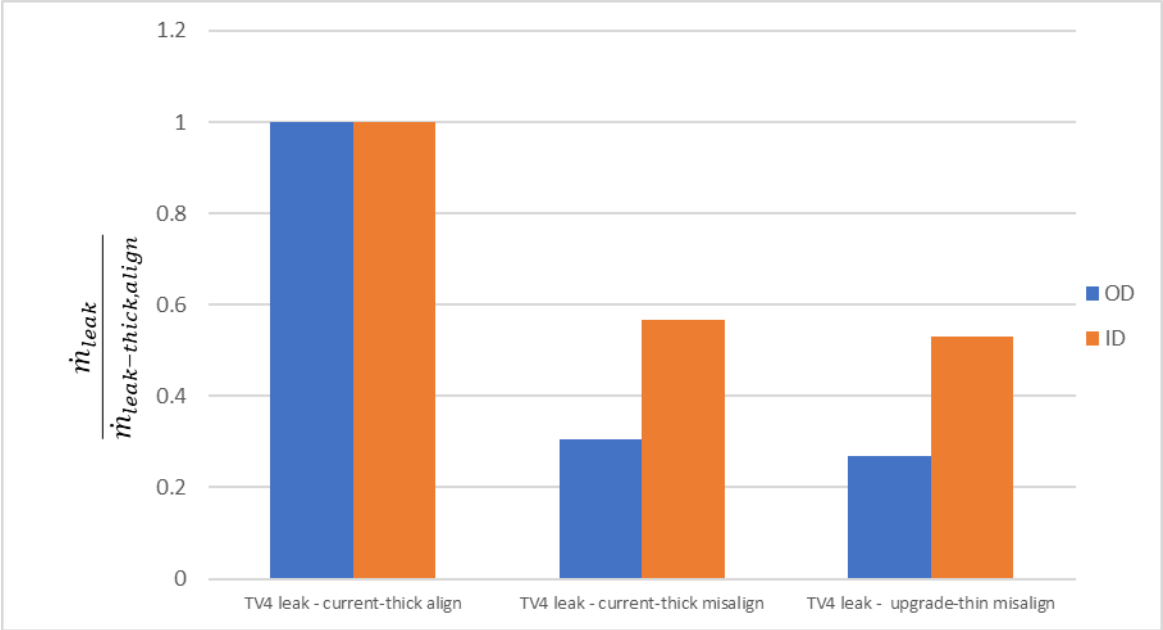

Figure 5.16 – TV4 strip seals leakage compared to current-thick aligned – misaligned config.

The pictures above reported show leakages behavior for each turbine vane with, on the vertical axis, the mass flow rate normalized with the one related to the *current-thick* strip seal in the *aligned* configuration. As it can be seen, the *current-thick* strip seal in misaligned configuration usually ensures a better sealing capability compared to the *aligned* one as it was expected during the discussion in Chapter 4. This does not happen for the shorter strip seals as shown in TV1 (Figure 5.13), because the lateral gap area has a considerable influence on the total gap area modelized with the equivalent gap. Moreover, by comparing results shown in the previous paragraph related to *upgrade-thin* (Figure 5.5 to Figure 5.8), it can be observed that in misaligned configuration it is characterized by higher leakages across the seals for all the vanes.

As it was done for the aligned configuration in previous paragraph, also in this case total leakages are determined. By knowing the ones related to strip seals it is possible to separate the effects between the direct impact of the groove configuration and seal geometry and the ones that indirectly affect the whole engine. Below the chart that describe what just said is reported.

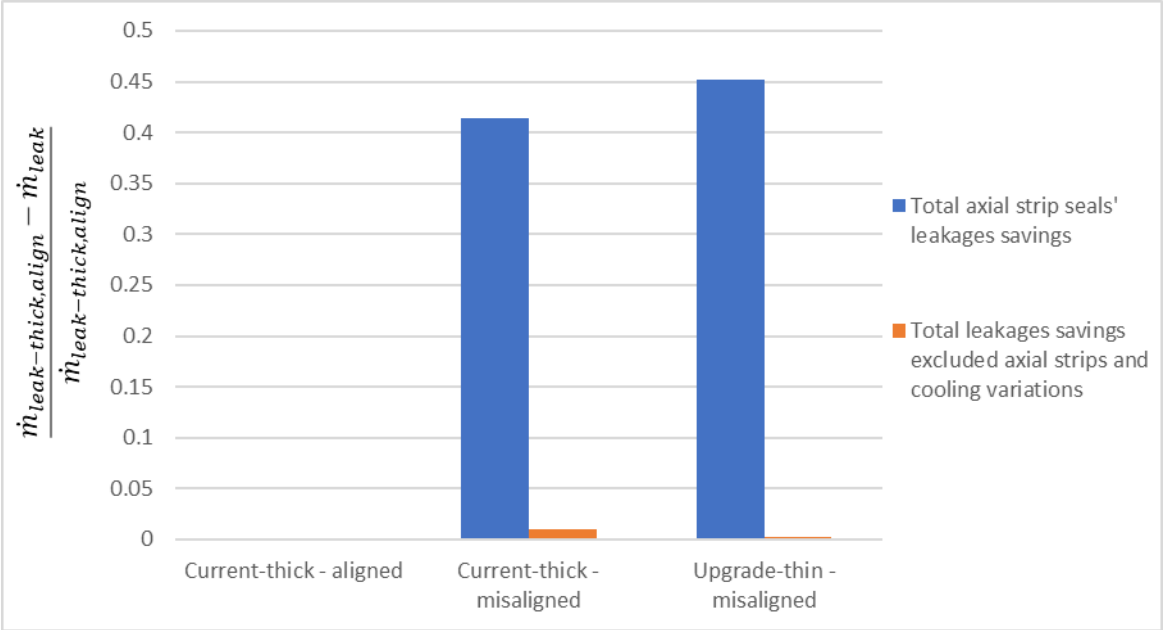

Figure 5.17 - leakages savings compared to current-thick aligned – misaligned config.

The chart shown above describes mass flow savings related to the different strip seal technology adopted and groove alignment adimensionalized with the total leakage mass flow related to *current-thick* strip seal in *aligned* configuration. Positive values are related to a leakage reduction and negative ones to leakage rise, as it happens for the aligned configuration analysis (Figure 5.9). As it can be seen, leakage reduction is observed for all the strip seals leakages (blue columns) and, on the contrary than aligned geometry, leakages across the engine decrease (orange columns have slightly positive values). Probably, the undirect-leakages reduction to TV1 (ascribed to depressurization of the plenum because of high direct-leakages) compensate the other ones' reduction.

In the misaligned groove configuration, *current-thick* strip seal, as it was observed for the greater part of turbine vanes, grants a sealing improvement compared to aligned one. *Upgrade-thin* strip seal (in misaligned configuration) has a slightly better sealing capability compared to *current-thick* strip seal.

Lower leakages across the strip seals mean that there should be slightly more cooling air, but not a significant increase as the leakage reduction as it was said about Figure 5.10 and the chart reported below confirms it.

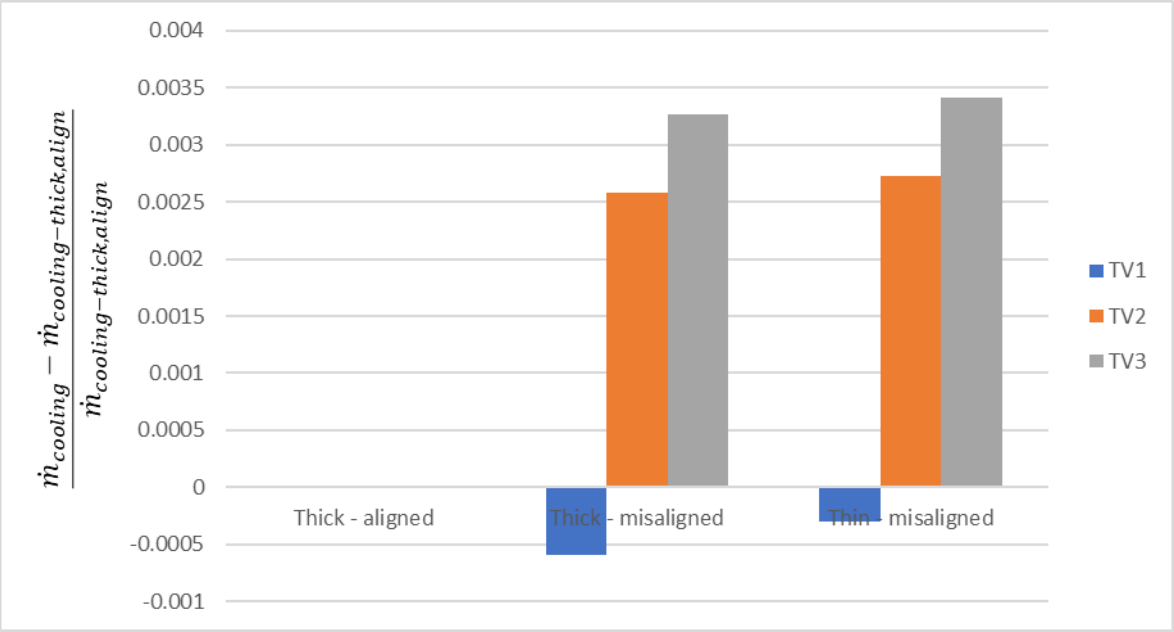

Figure 5.18 - cooling air variations compared to current-thick aligned – misaligned config.

In *misaligned* configuration cooling air variations are even lower compared to aligned case (Figure 5.10), thus presented variations can be neglected too.

As calculations results, the global leakages variation is reported as follow, where it is compared to *current-thick* sealing technology in aligned groove configuration adimensionalized with leakage mass flow related to same strip seal.

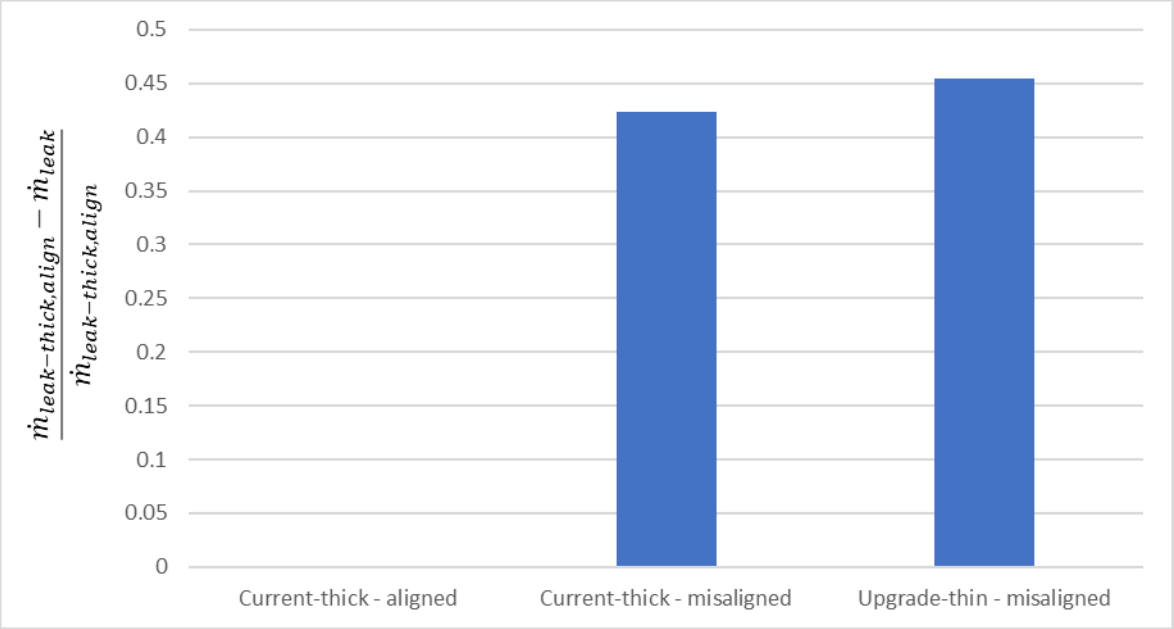

Figure 5.19 – Total stator leakage savings compared to current-thick aligned – misaligned config.

The chart above shows, on vertical axis, the mass flow variation between each seal and *current-thick* strip seal in *aligned* configuration normalized with total stator leakages related

to *current-thick* and *aligned* strip seal too. Figure 5.19 shows that leakages reduce for both the seals analyzed in the *misaligned* configuration; from the picture it can noticed that even in the present case *upgrade-thin* strip seal performs better than *current-thick*, even if the difference between the two seal types reduces respect to *aligned* case (difference about 4% between the two seals).

As it was done in the previous paragraph, the TCLA fluctuation in relation to TCLA which characterizes the current configuration is shown as follow.

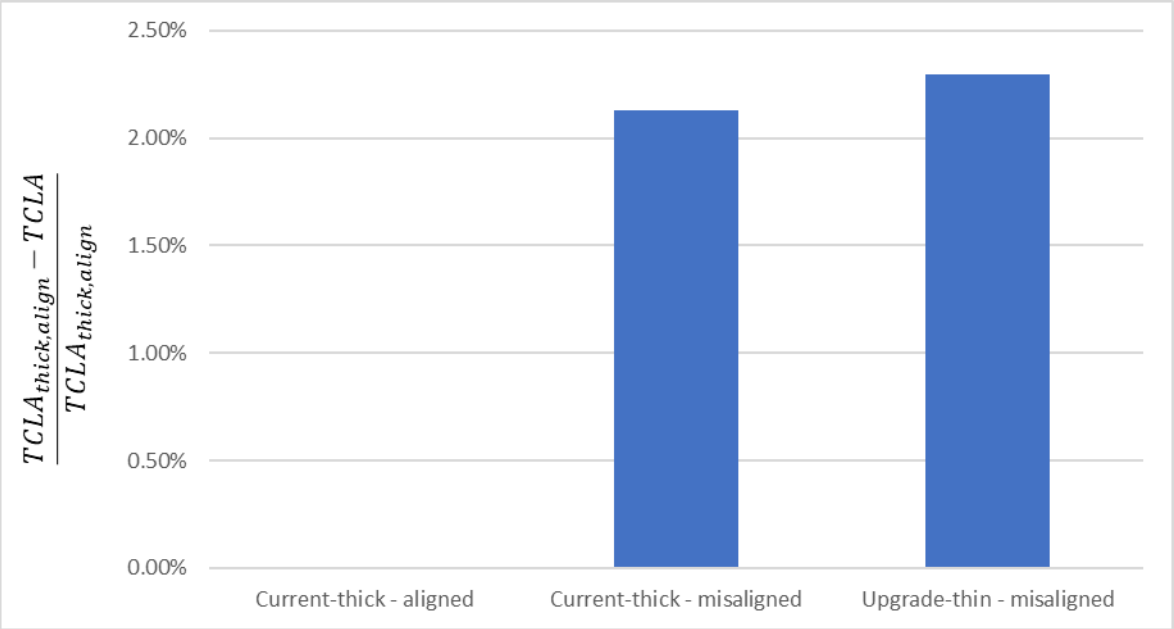

Figure 5.20 – TCLA (% of $TCLA_{current-thick,align}$) savings compared to current-thick aligned – misaligned config.

The image above shows the TCLA savings compared to *current-thick* strip seal in *aligned* groove configuration adimensionalized with the TCLA related to the same seal. The image above confirms that in *misaligned* configuration *current-thick* strip seal ensures better sealing performance than *aligned* one, in particular the relative saving is quite the same of *thicker* strip seal in *aligned* configuration (Figure 5.12). Moreover, Figure 5.20 confirms that also in the present configuration *upgrade-thin* strip seal ensures a better sealing capability compared to *current-thick* one, even if in a slightly way respect to *aligned* configuration. Finally, it can be noticed that *upgrade-thin* strip seal grants a slightly lower sealing capability in *misaligned* configuration (aligned – 3.57% vs. misaligned – 2.29%); the opposite happens for what concerns *current-thick* seal, which improves its sealing performance.

5.6 Potential power and efficiency gain in simple and combined cycle

As result of TCLA reduction, a larger quantity of mass flow can participate to combustion and expand completely in the expander. This ensures a bigger output power and, potentially, an iso-entropic efficiency increase. Performance evaluation is made only considering the aligned groove configuration since the differences between *current-thick* and *upgrade-thin* strip seal in misaligned configuration are neglectable compared to variations related to the aligned groove.

Results related to GT performance are obtained with an Ansaldo Energia tool dedicated to GT performance assessment. The following results takes into account as reference *thicker* strip seal in aligned groove geometry, because it represents the current strip seal-groove matching in real customers' engines (as it was already explained in paragraph 3.2.2, with reference to Figure 3.10). Thanks to variations of compressed air mass flow at external compressor bleeds, an estimation of updated performance is given for both simple and combined cycle.

Output power and efficiency delta are shown in Table 5.1. Negative values mean performance worsening, positive ones are correlated to improvements.

Table 5.1 – performance variations due to the adoption of different kind of strip seal

	Current-thick	*Thicker* (ref.)	*Upgrade-thin*
ΔP sc [MW]	-1.73	0	1.45
Δη sc [%]	0	0	0
ΔP cc [MW]	-2.93	0	2.46
Δη cc [%]	-0.06	0	0.05

Thanks to *upgrade-thin* installation on the GT, power output could increase of about 1.45MW in simple cycle (+0.43% GT Gross Power) while profits are higher in combined cycle with 2.46MW.

Iso-entropic efficiency growth in combined cycle can be translated in a reduction of fuel mass flow needed to obtain the current output power. By supposing the natural gas LHV about 50033.7 [kJ/kg], the fuel saving estimation is about 0.07 [%]. If it is supposed to operate 24 hours per day at BL during the whole year natural gas saving is about 315000 [kg] that are about 470000 [scm[1]]. With reference to 2022 yearly average price of natural gas[2], it can be estimated a saving amount about 600000 [€] if the 2022 yearly average price is considered.

Instead, with the same amount of fuel mass flow, with a power increase of + 2.46MW it is possible to feed electricity to 820 new houses (by supposing 3 [kW] consumption for one single house) without emissions increase.

It can be noticed that *current-thick* strip seal adoption induces the performance decay. This kind of seal in the experimental ambient is subjected to activation process (which is not detected in real GT, thus *thicker* strip seal is taken as reference). Because of this, it can be concluded that if the seal has enough space to move freely inside the groove (in bad tolerances condition, as explained in paragraph 3.2.2) the power output decays.

5.7 Potential future investigations and next steps

In this section the possible next steps in this field of investigation are briefly mentioned. As it was explained in Chapter 4 a worn *upgrade-thin* strip seal is needed; after the experimental tests, also SiX_o calculations will take place. Furthermore, other investigations that are

[1] Standard cubic meter, referred to 1.013[bar] and 15 [°C]
[2] Data given by Amsterdam Exchange Market

under considerations are further investigations of misalignment cases, involving different misalignment step sizes for the groove.

Anyway, before the substitution of all the seals in customers' engines, a last test has to be done: the so called "*rainbow test*". The mentioned test consists of substituting only a few *current-thick* strip seals from many or every engine location with *upgrade-thin* version. The engine will operate until the programmed maintenance outage and when it will be dismounted the strip seals will be analyzed and compared to check the mechanical integrity and durability.

6 Conclusions

In the actual environmental situation, it is crucial to find a way to improve Gas Turbine efficiency; it can be obtained with a more effective Secondary Air System. Aim of this thesis is to analyze the benefits of adoption of thinner strip seals for AE94.3A engine. The main results founded can be distinguished in two kind of considerations: experimental and computational ones.

For what concerns the experimental results, they can be summarized as follow:

- *Current-thick* and *upgrade-thin* strip seals are subjected to a different activation pressure; it is lower for *upgrade-thin* strip seal.
- *Thicker* strip seal ensures lower equivalent gap in the pressure range where *current-thick* strip seal is not activated (in the aligned rig geometry).
- In misaligned configuration, activation pressure shifts to lower pressure for both new and worn strip seals.
- Activation pressure shifts at higher pressure if the strip seal is worn; activation can even disappear in case of extremely damaged seals.
- New *upgrade-thin* strip seal always performs better than *current-thick* in both aligned and misaligned configuration.
- In misaligned configuration *current-thick* strip seal improves its sealing performance, *upgrade-thin* slightly reduces it.
- In misaligned configuration, even worn *current-thick* strip seals improve their sealing performance.
- Worn *upgrade-thin* strip performed similarly to the new one due to the little amount of cumulated operating hours.

For what concerns the computational results obtained from SiX_o calculations, they are recapped below:

- *Upgrade-thin* strip seal reduces the leakages in all the locations where it is inserted.
- *Thicker* strip seal, so when the seal fits almost perfectly the groove size, grants a lower TCLA compared to *current-thick* strip seal analyzed in aligned configuration.
- In the aligned configuration there can be secondary leakages increase because of a little over-pressurization of the plenums generated by lower leakages across the seals.
- Leakages reduction has as consequence the cooling air increase because of the over-pressurization of the plenums.
- In the misaligned groove geometry, approximatively the same results were found for *current-thick* and *upgrade-thin* strip seals.
- It is confirmed that *current-thick* strip seal works better in misaligned configuration than in the aligned one.
- In the aligned configuration, *upgrade-thin* is the best solution for the TCLA reduction.
- *Upgrade-thin* strip seal ensures an output power increase and iso-entropic efficiency gain in combined cycle.

Appendix A: charts legend

The results presented in this document comply with the legend shown below.

Table A.1 - Chart legend 1

Test	Configuration	Thickness	Condition	Color	Filling
1	Aligned	*Current-thick*	New	Red	Full
2	Aligned	*Upgrade-thin*	New	Blue	Full
3	Aligned	*Thicker*	New	Orange	Full
4	Misaligned	*Current-thick*	New	Red	Empty
5	Misaligned	*Upgrade-thin*	New	Blue	Empty
6	Misaligned	*Current-thick* – S3	Worn	Purple	Empty
7	Misaligned	*Current-thick* – S2	Worn	Dark red	Empty
8	Aligned	*Current-thick* – S3	Worn	Purple	Full
9	Aligned	*Current-thick* – S2	Worn	Dark red	Full
10	Misaligned	*Current-thick* – S1	Worn	Dark yellow	Empty
11	Misaligned	*Upgrade-thin* - worn	Worn	Light blue	Empty
12	Aligned	*Current-thick* – S1	Worn	Dark yellow	Full
13	Aligned	*Upgrade-thin* - worn	Worn	Light blue	Full
2019	Aligned	*Current-thick* & u*pgrade-thin*	New	Green	Full

Table A.2 - Chart legend 2

Repetition	symbol
A	rhombus
B	circle
C	triangle
D	square
E	minus

7 Bibliography

[1] Ansaldo Energia, brochure

[2] Lozza G., 2016, “Turbine a Gas e Cicli Combinati”, Esculapio edizioni, Italia

[3] Lanata Valerio, 2019, “Characterization of Secondary Air System circuits in a Gas Turbine engine”

[4] Reid, K., Denton, J., Pullan, G., Curtis, E., and Longley, J., 2005. “The Interaction of Turbine Inter-Platform Leakage Flow With the Mainstream Flow”. Proceedings of ASME Turbo Expo 2005, Reno, Nevada, USA. Paper No. GT2005-68151

[5] Reid, K., Denton, J., Pullan, G., Curtis, E., and Longley, J., 2006. “Reducing the performance penalty due to turbine inter-platform gaps”. Proceedings of ASME Turbo Expo 2006, Barcelona, Spain. Paper No. GT2006-90839

[6] Ranson, W., Thole, K., and Cunha, F., 2005. “Adiabatic Effectiveness Measurements and Predictions of Leakage Flows Along a Blade Endwall”. Journal of Turbomachinery, **127**, July, pp. 609–618.

[7] Farahani, A., Childs, P., 2006, “Nozzle guide vane static strip seals”. Proceedings of ASME Turbo Expo 2006, Barcelona, Spain. Paper No. GT2006-90185

[8] Farahani, A., Childs, P., 2007, “Characterization of static strip seal flow”. Proceedings of ASME Turbo Expo 2007, Montreal, Canada. Paper No. GT2007-27469.

[9] Huber, T., Bricaud, C., Zierer, T., 2017, “Investigation of strip seal leakage with special focus on seal groove design and relative displacement of sealing”. Proceedings of ASME Turbo Expo 2017, Charlotte, NC, USA. Paper No. GT2017-64440.

[10] Rathbun, F. O., 1964, “Experimental leakage rate experiments”, Proceedings of Conference on Design of Leak-tight separate fluid connector.

[11] Armand, G., Lapujoulade, J., Paigne, J., 1964, “A theoretical and experimental relationship between the leakage of gases through the interface of two metals in contact and their superficial micro-geometry”, Vacuum, 14, 53-57.

[12] Roth, A., Inbar, A., 1968, “An analysis of the vacuum sealing process between turned surfaces”, Vacuum, 18, 309-317.

[13] Roth, A., 1970, “The influence of the surface roughness on the specific leak rate of gasket seals”, Vacuum, 20, 431–435.

[14] Matsuzaki, Y., and Kazamaki, T., “Effect of Surface Roughness on Compressive Stress of Static Seals”, JSME international journal. Ser. 3, Vibration, control.

[15] Murtagian, Fanelli, V., Villasante, J. A., Johnson, D. H., and Ernst, H. A., 2004, “Sealability of Stationary Metal-to-Metal Seals”, Journal of Tribology, Volume 126, Issue 3.

[16] Bricaud, C., Schulz, O., Zierer, T., Peltier, V., Schwitzke, C., Bauer, H.J., 2021, “Experimental investigations into the effect of surface roughness and contact force on leakage between two rigid metallic surfaces”**,** Proceedings of ASME Turbo Expo 2021, Virtual, Online. Paper No. GT2021-59163.

[17] Rafols, F. P., Larsson, R., Almqvist, A., 2016, “Modelling of leakage on metal-to-metal seals”, Tribology Intl. 94, 421-427.

[18] Chupp, R. E., Hendricks, R. C., Lattime, S. B., Steinetz, B. M., 2006, “Sealing in turbomachinery”, NASA, NASA/TM-2006-214341.

[19] Dhondt G., CalculiX CrunchiX user's manual
[20] Massardo A., Sistemi Energetici, Slide del corso
[21] Feijia Yin, 2016, "Modelling and Characteristics of a Novel Multi-fuel Hybrid Engine for Future Aircraft", Delft University of Technology
[22] Mustafizur Rahman, Thamir K. Ibrahim, Kumaran Kadirgama, Rizalman Mamat, Rosli Abu Bakar, 2011, "Influence of Operation Conditions and Ambient Temperature on Performance of Gas Turbine Power Plant"
[23] Bozzi Luca, D'Angelo Enrico, "Numerical and experimental investigation of secondary flows and influence of air system design on heavy-duty gas turbine performance" Proceedings of ASME Turbo Expo 2012, Paper No. GT2012-68392
[24] Carl M Sangan, Oliver J Pountney, James A Scobie, Mike Wilson, J Michael Owen, Gary D Lock, 2012, "Experimental measurements of ingestion through turbine rim seals. Part 3: single and double seals". Proceedings of ASME Turbo Expo 2012, Paper No. GT2012-68493
[25] Carl M Sangan, Oliver J Pountney, James A Scobie, Mike Wilson, J Michael Owen, Gary D Lock, 2012, "Experimental measurements of ingestion through turbine rim seals. Part 1: externally-induced ingress". Proceedings of ASME Turbo Expo 2011, Paper No. GT2011-45310
[26] Marchitto A., Scambio Termico, Slide del corso
[27] Reichert A.W., Janssen M., 1996, "Cooling and sealing air system in industrial gas turbine engines", ASME International Gas Turbine and Aeroengine Congress and Exhibition, England

8 Nomenclature

Notations

k	specific heat ratio
C_p	constant pressure specific heat capacity
p	pressure
T	temperature
η	efficiency
β	pressure ratio
L_n	useful/net work
L_c	compressor work
L_t	turbine work
η_c	compressor iso-entropic efficiency
η_t	turbine iso-entropic efficiency
h	enthalpy
$\dot{m}$	mass flow rate

Subscripts

conv	convective
cond	conductive
opt	optimal
max	maximum
eq	equivalent
ref	reference
crit	critical
amb	ambient
exp	experimental
leak	leakage
exh	exhaust
align	aligned

Definitions and acronyms

SAS	Secondary Air System
TCLA	Turbine Cooling Leakage Air
HRSG	Heat Recovery Steam Generator
BL	Base Load
MEL	Minimum Environmental Load
TIT	Turbine Inlet Temperature
LP	Low Pressure
HP	High Pressure
SS	Suction Side
PS	Pressure Side
LE	Leading Edge
TE	Trailing Edge
EDM	Electrical Discharge Machining
FS	Full Scale

mfr	mass flow ratio
TV	Turbine Vane
GT	Gas Turbine
IC	Internal Circuit
EC	External Circuit
sc	Simple Cycle
cc	Combined Cycle